Enhancing Risk Analysis Capacities for Flood, Tropical Cyclone Severe Wind and Earthquake for the Greater Metro Manila Area

Component 5 – Earthquake Risk Analysis

PHILIPPINE INSTITUTE OF VOLCANOLOGY AND SEISMOLOGY
GEOSCIENCE AUSTRALIA

Trevor Allen[1], Hyeuk Ryu[1], Bartolome Bautista[2], Ma. Leonila Bautista[2], Ishmael Narag[2], Winchelle Ian Sevilla[2], Ma. Lyn P. Melosantos[2], Kathleen Papiona[2], Jun Bonita[2]

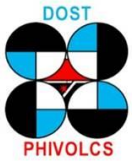

1. Geoscience Australia
2. Philippine Institute of Volcanology and Seismology

Contents

Executive Summary

The Philippines experiences some of the world's worst natural hazards, being exposed to frequent earthquakes, floods, tsunami, landslides, volcanic eruptions, cyclones and annual monsoons. The Greater Metro Manila Area (GMMA), which includes Metro Manila, is particularly vulnerable to the devastating effects of natural disasters, with a population of over 20 million residing on land that is cut by active earthquake faults and subject to intense riverine flooding. The GMMA is also frequently affected by typhoons, which can result in severe wind damage, storm surge and intense flooding. Landslides, tsunamis and volcanic eruptions also pose a risk to residents within the GMMA. The risk from these natural hazards is further exacerbated as poverty often results in populations residing in buildings that are not built to withstand these hazards or in areas that are frequently affected by flooding, such as along flood drainages.

This report summarised the activities and outputs of Component 5 of the 'Enhancing Risk Analysis Capacities for Flood, Tropical Cyclone Severe Wind and Earthquake for the Greater Metro Manila Area' Project. The goal of this project is to analyse the risk from flood, severe wind and earthquake in the GMMA through the development of fundamental datasets and information on hazard, exposure and vulnerability. Component 5 focussed on the development of earthquake hazard modelling and risk analysis for the Greater Metro Manila Area. Earthquake scenarios triggered by rupturing of the West Valley Fault were the basis for the seismic hazard modelling. Exposure information available in the exposure database for the Greater Metro Manila Area, together with vulnerability models developed by the University of the Philippines Diliman – Institute of Civil Engineering (UPD-ICE) were combined with the hazard modelling to calculate the expected physical damage to buildings and the resultant economic loss. Expected injuries and fatalities for the residential population were also calculated.

1 Introduction

The Greater Metro Manila Area (GMMA) is a global megacity with an estimated population of up to 20 million. According to Asia Development Bank (ADB) reports (ADB, 2009), it is estimated that as many as 35% of the population within the GMMA live in informal settlements, many of whom live below the poverty line. This makes the city and its people vulnerable to the impacts of natural disasters, such as earthquakes.

The Philippine archipelago represents a complex system of microplates that are being compressed between two convergent plate margins that bound the nation: the Philippine Sea to the east and Eurasian plates to the west. Between the convergent subduction zones, oblique tectonic motion is accommodated by numerous crustal faults that traverse the archipelago; in particular, the 1,600 km-long Philippine Fault Zone, which runs from northern Luzon in the north through to the island of Mindanao in the southern Philippines (e.g. Aurelio, 2000, Barrier et al., 1991). Because of its tectonic setting, the Philippines experiences frequent damaging earthquakes (e.g. Bautista and Oike, 2000).

The 90–135 km-long Marikina Valley Fault System (Daligdig et al., 1997, Papiona and Abigania, 2013, Papiona et al., 2013, PHIVOLCS, 1999, 2008a, Rimando and Knuepfer, 2006) belongs to the aforementioned system of faults that accommodate oblique convergence (e.g. Daligdig et al., 1997, Rimando and Knuepfer, 2006) (Figure 1.1). The MVFS is comprised of the East and West Valley Faults (EVF and WVF, respectively). The WVF transects the eastern part of Metro Manila and posed the most significant earthquake threat to Metro Manila and nearby provinces (Figure 1.2). Understanding the frequency of large earthquakes on the WVF and the potential magnitudes are of critical importance to emergency managers to prepare for and mitigate against the impact of these infrequent, high consequence events. The recurrence of large earthquakes on the WVF has previously been estimated at between 400 to 600 years, with considerable uncertainty (Nelson *et al.*, 2000). Given the length of the fault, it is believed that it could accommodate an earthquake of up to moment magnitude M_W 7.5 base on published fault-scaling relationships (Wells and Coppersmith, 1994).

The Philippine Institute of Volcanology and Seismology (PHIVOLCS) and Geoscience Australia (GA) have developed a long-term partnership to better understand and reduce the risks associated with earthquake hazards in the Philippines. Herein, we extend upon methodologies developed through the Quick Unified Inventory of Vulnerability and Exposure for REDAS (QuiveR) Project; an earthquake impact pilot study for Iloilo City, Western Visayas (Bautista *et al.*, 2012), designed to enhance the damage estimation capabilities of the Rapid Earthquake Damage Assessment System (REDAS) (Bautista *et al.*, 2011). The GMMA Risk Assessment Project (RAP) builds upon QuiveR methods through:

1. the development and population of a digital geotechnical database schema from paper records
2. improved site class models based upon a combination of geotechnical measurements and topographic slope
3. the review of ground-motion prediction equations (GMPEs) based on measured strong ground motions from the Philippines
4. the addition of modern ground-motion to intensity conversion equations (GMICEs) in REDAS

5. the use of a more detailed building and population exposure database (GMMA-RAP Exposure Team, 2013)
6. the use of updated fragility curves supplied by the University of the Philippines Diliman Institute of Civil Engineering (UPD-ICE, 2013)
7. the revision and optimization of REDAS impact software to:
    a. accommodate impact calculations for wider suite of building types
    b. accommodate building fragilities for different building code compliance periods (e.g. pre-code, low-code and high-code)
    c. read exposure data and calculate directly from shapefiles rather than first converting to Generic Mapping Tools grid files
    d. calculate humanitarian impacts at four casualty levels (e.g. minor injuries, …, fatalities) based on different collapse rates of buildings

In addition to the provision of earthquake impact information from improved ground-shaking, exposure and vulnerability models, this project included a paleoseismic trenching activity to attempt to better constrain both the potential frequency and magnitude of large earthquakes on the WVF. This represented a major component in the RAP Earthquake Component in terms of logistics and potential impact to this and future studies. In total, three trenches along the extent of the WVF were excavated and the subsequent analysis is outlines herein. Such is the importance of these contributions to the hazard and risk in the GMMA, the excavation of a fourth trench is planned beyond the delivery timetable of the RAP. Improved knowledge of earthquake recurrence on the WVF can vastly improve the accuracy of probabilistic seismic hazard and risk assessments (PSHA and PSRA, respectively).

The work undertaken through the GMMA RAP also leverages off and complements the previous Metro Manila Earthquake Impact Reduction Study (MMEIRS, 2004). While the MMEIRS study was, in some ways, more comprehensive in its outputs than what was attempted in the GMMA RAP, it is based upon previous generation hazard models, which can now be better quantified owing to improved hazard calculation techniques and the collection of more earthquake data. Furthermore, an important limitation of the MMEIRS was that PHIVOLCS was not left with a capability or process to repeat these kinds of studies. Through the GMMA RAP, we have leveraged off the PHIVOLCS-developed REDAS software to develop tools that can be incorporated into PHIVOLCS standard operating procedures for earthquake impact assessments throughout the Philippines. Nevertheless, the MMEIRS study provides an important benchmark for earthquake impact assessments in Metro Manila. Consequently, where possible, the results from the current study are compared to the MMEIRS.

To help PHIVOLCS prepare for the development of future PSHAs and PSRAs for the Philippines, this Project also included training in the Global Earthquake Model's OpenQuake software (Pagani *et al.*, 2010; Crowley *et al.*, 2011; Horspool and Ghasemi, 2012). This training facilitated the development of first-order hazard assessments for the GMMA. The process of this training will be outlined. However, the outputs of this activity are too preliminary to be released publically.

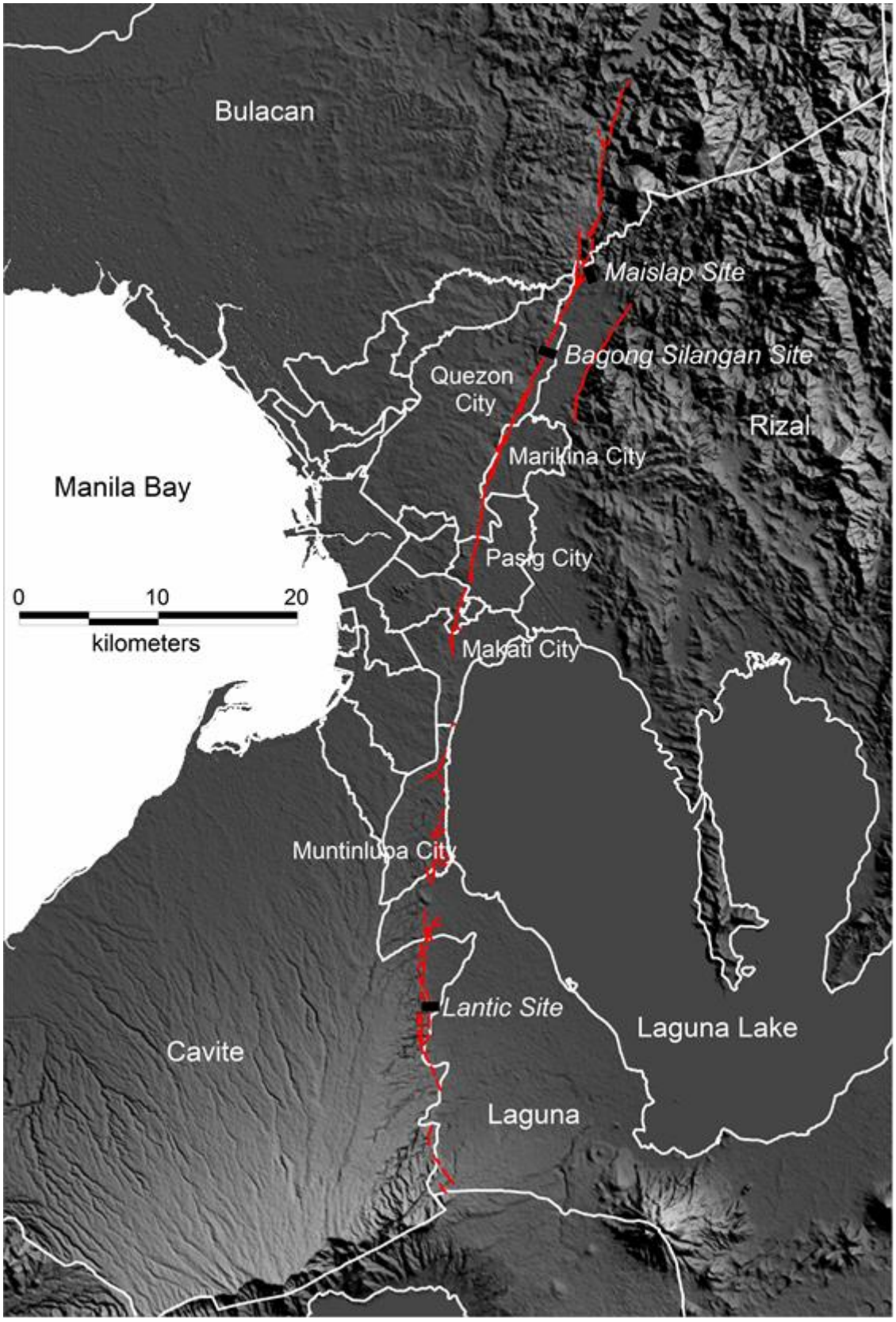

Figure 1.1. Map of the Valley Fault System and location of the trench sites. Red lines are the traces of the West and East Valley Fault. White lines are the boundaries of local government units and black rectangles are the location of the trench sites.

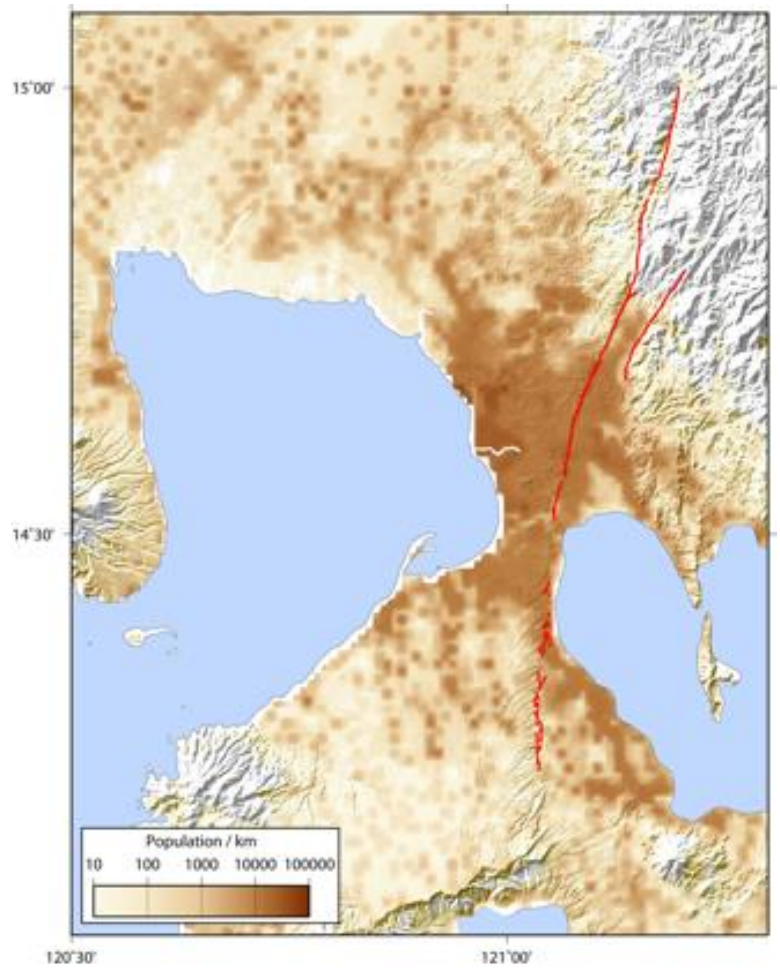

Figure 1.2. The MVFS (heavy red lines) relative to the 2008 Landscan global population dataset (Bhaduri et al., 2002).

2 Previous work

2.1 Paleoseismic Studies of the West Valley Fault

PHIVOLCS has employed paleoseismic studies since 1990's and established earthquake parameters along the segments of Philippine Fault in Nueva Vizcaya, Guinyangan-Ragay Gulf, Masbate and Mindanao areas (Daligdig, 1996; Papiona and Kinugasa, 2008; Tsutsumi et al., 2006; and Perez et al., 2010). The Greater Metro Manila area has been affected many times by earthquakes from different sources (or faults) based on the Philippine earthquake catalog (SEASEE, 1985; Bautista, 1996; Bautista and Oike, 2000; PHIVOLCS earthquake catalog). The earthquake sources that would have the greatest impact on Metro Manila and nearby provinces is the movement of the VFS specifically the WVF (MMEIRS, 2004).

Previous work by Rimando and Knuepfer (2006) has mapped the different geometric segments of the WVF and estimated their magnitude potential using length and magnitude scaling relations by Wells and Coppersmith (1994). They estimated that the WVF is capable of M 7.3 for the length of 87.5 km while the EVF is capable of maximum M7.5 for the length of 115 km. In terms of paleoseismology, Nelson et al. (2000) conducted paleoseismic studies of the WVF in Sitio Maislap, Brgy. San Isidro, Rodriguez, Rizal (Figure 1.1). They use vertical displacement measured from the trench and Wells and Coppersmith (1994) scaling relations to estimate magnitude 6 to 7 for the WVF. They also used C14 dates to constrain the frequency of M 7.2 earthquake and suggest a conservative range of 300 to 1000 years return interval for the northern half of the WVF, but favor a range of 400 to 600 years. These results have 100 to 400-year uncertainties. Additionally, the Maislap trench site is located on a splay that connects the EVF and WVF thus, posing doubt of its validity as representing the main WVF or EVF.

2.2 Site Class Model

Several studies investigating the response of strong ground-motion in the GMMA now exist (e.g. Abeki et al., 1993; Bautista et al., 1994; Iwatate and Dy, 2000; Narag et al., 2000). One of the first studies was based on a large-scale microtremor study intended to measure the fundamental period of at multiple locations throughout Metro Manila across a regular grid (Narag et al., 2000). Key observation from this study was the good correlations among the predominant periods of microtremor, the derived amplification factors, and the shallow-surface geology.

Many hazard studies now rely on proxy site-conditions information determined from maps of geology and other geomorphic and geotechnical indicators (Wills et al., 2000; Matsuoka et al., 2005; Wald and Allen, 2007). Wald and Allen (2007) presented a method for mapping uniform global seismic site conditions, or the time-averaged shear velocity to 30 m depth (VS30), from the Shuttle Radar Topography Mission (SRTM) 30 arc-second (approximately 1 km resolution at the equator) digital elevation model (Farr and Kobrick, 2000). The basic premise of Wald and Allen's (2007) technique is that topographic gradient can be diagnostic of seismic site-conditions, or VS30, because more competent (high-velocity) materials are more likely to maintain a steep slope, whereas deep (low-velocity) basin sediments are deposited primarily in environments with low gradients. Allen and Wald

(2009) later evaluated the use of higher-resolution topographic data for estimating VS30. While higher resolution data did not offer a significant improvement in the estimation of VS30, it did provide some improvements in the transition regions between sedimentary basins and steep hill-slopes. Consequently, the LiDAR data collected through the GMMA RAP was employed to estimate VS30 across the GMMA using the 9 arc-second coefficients recommended by Allen and Wald (2009). Figure 2.1 shows a mosaic of VS30 across the study area, which incorporates both the low-resolution SRTM data and the LiDAR data.

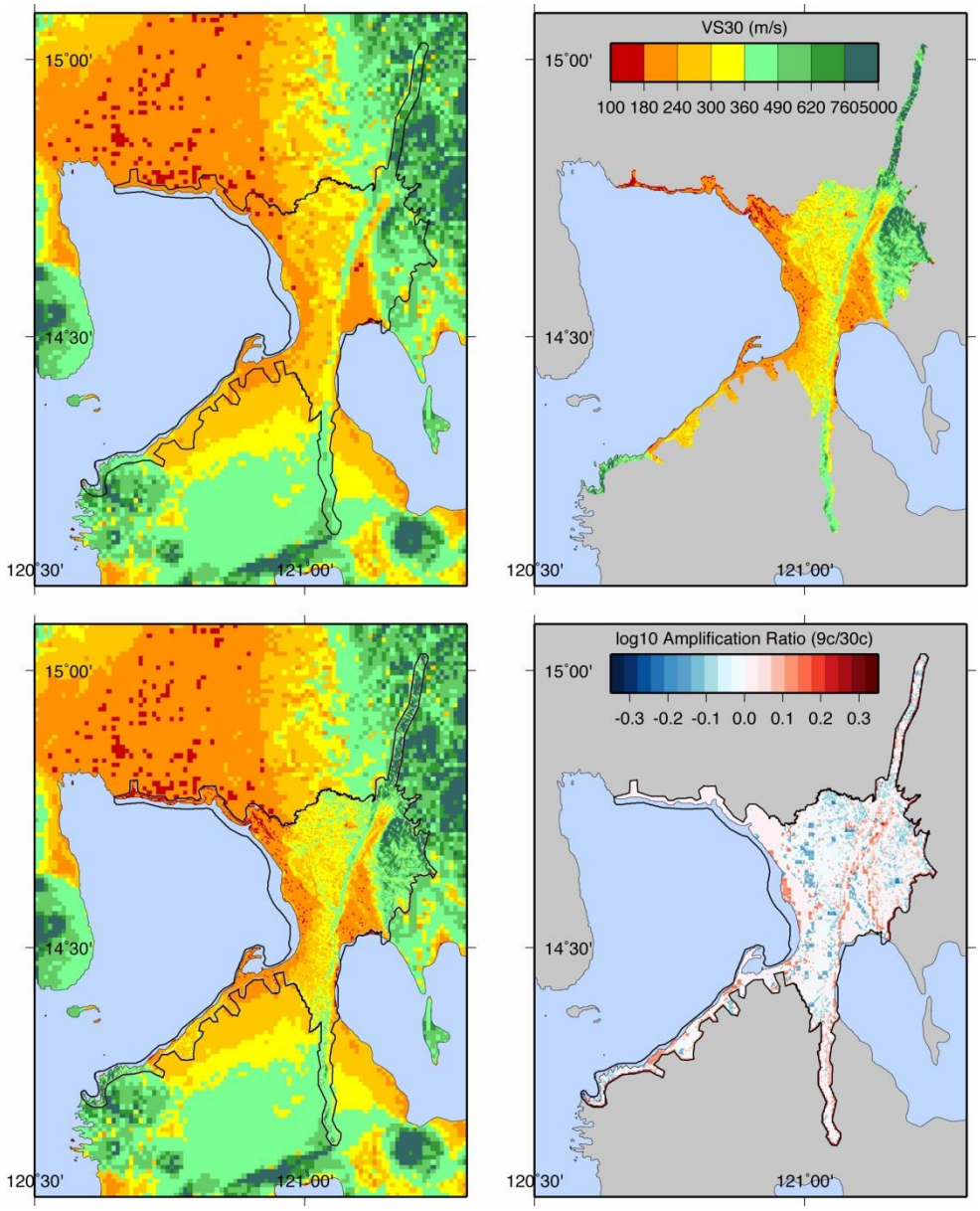

Figure 2.1. Time-averaged shear-wave velocity estimated from topographic gradient; VS30 model estimated from 30 arc-second SRTM (top left) and LiDAR (top right) data down-sampled to 9 arc-seconds, respectively. A mosaic of SRTM and LiDAR (bottom left). In all sub-plots, the solid black line indicates the extent of the LiDAR data. The bottom-right figure indicates the amplification ratio between the SRTM and LiDAR datasets assuming uniform peak ground acceleration across the spatial area using the Allen and Wald (2009) slope- VS30 coefficients. The higher-resolution LiDAR data tends to better resolve the site class factors for the slope-basin transition regions of the Marikina Valley.

Grutas and Yamanaka (2012) developed a site class model for the Metro Manila area (Figure 2.2). Their model combined measured VS30 data and topographic gradient, together with geomorphic and fundamental period obtained from microtremor recordings. Unfortunately the spatial extent of the Grutas and Yamanaka (2012) site class model was not large enough to accommodate the full GMMA study area. Furthermore, the spatial extent was difficult to modify without more detailed information on the geomorphology of the region.

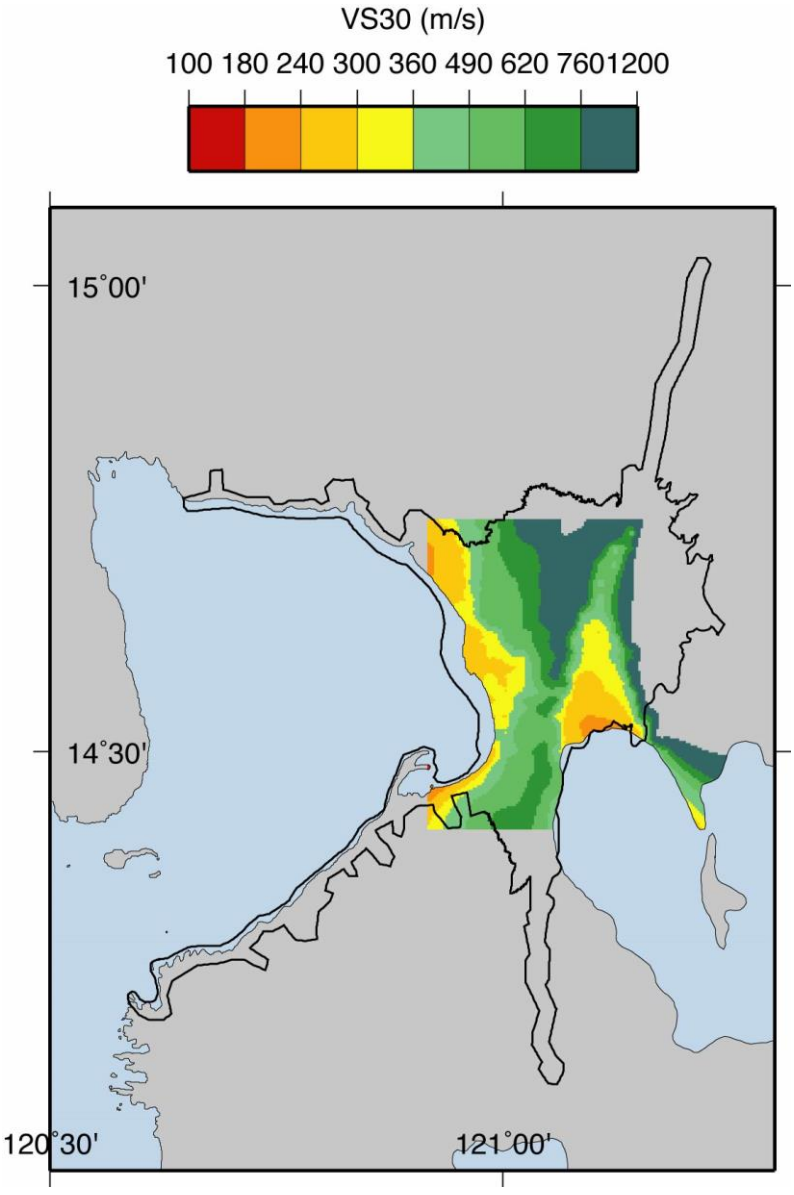

Figure 2.2. Reproduction of the Grutas and Yamanaka (2012) site class model plotted for the spatial extent covered by the GMMA-RAP. Solid black line indicates the extent of the LiDAR data capture.

3 Data

3.1 Paleoseismic Study of the West Valley Fault

3.1.1 Introduction

Paleoseismology, the study of past earthquakes, is important in acquiring fault parameters that will be used as input in generating earthquake scenarios for probabilistic seismic hazard and risk assessments in an area. It involves trenching or excavation of trench across the fault trace to expose evidence of past earthquakes that occurred even beyond the written history or catalog. Trenching attempts to understand:

1. the detailed location of the fault
2. the time of occurrence of past earthquakes and their frequency; and
3. the potential size of an earthquake that a fault can generate.

By trenching, the subsurface traces of the fault will be exposed, therefore allowing verification of the location of the major fault that repeatedly moves and identification of splays that form the deformation zone. The time of occurrence of a past earthquake may be inferred by knowing the age of sediments that were displaced by the fault. The widely used method to determine the age of the sediments in paleoseismic studies is by correlating the C14 age of embedded charcoal or organic materials within the sediment. In C14 or radiocarbon dating method, buried pieces of wood that became charcoal through time were collected and subject to laboratory procedures and measurements (i.e. pre-treatment, accelerator mass spectrometry technique, and calendar calibration) for C14 decay measurements.

To estimate the potential size of an earthquake that can be generated, trenching is required in different sections of the fault to determine whether the timing of past earthquakes identified in each trench can be correlated. Sections of the fault that moved at the same time leads to an estimate of the total length of fault rupture, which may then be used as input in estimating the potential earthquake magnitude. In some cases, the amount of displacement measured from the trench and from geomorphic features produced by the movement of the fault is used if the length of the fault cannot be inferred.

The Valley Fault System (VFS) is a 90 to 135 km long (Daligdig et al., 1997; PHIVOLCS, 2000; Rimando and Knuepfer, 2006; Papiona and Abigania, 2013; Papiona et al., 2013) right-lateral strike-slip fault system that bounds the Marikina Valley. It is composed of West Valley Fault (WVF) that transects the eastern part of Metro Manila and parts of the provinces of Bulacan, Laguna, Cavite and Rizal and of East Valley Fault (EVF) that transects several towns in the province of Rizal (Figure 1.1). Based on Bautista (1996) and Bautista and Oike (2000), the most recent earthquake that could probably be ascribed to the VFS is the 1658 earthquake. The 1658 earthquake reportedly caused death and injuries and caused damage to several churches in Manila and Antipolo (SEASEE, 1988). Bautista (1996) assigned a magnitude 5.7 for this earthquake and attributed its epicenter with WVF. This earthquake was not widely felt and reports provide no indication of surface faulting anywhere in

the vicinity of the WVF. Consequently, any surface-rupturing earthquake along the WVF may have happened beyond the Philippines written history (before year 1500 AD).

This study aims to reassess and validate these existing results by excavating trenches on different sections of the WVF. Trenches were excavated in Brgy. Bagong Silangan, Quezon City to represent the northern section of WVF. Another trench was excavated in Brgy. Lantic, Carmona Cavite for the southern section and one more trenching activity is planned on the north-south trending splay of WVF in Rodriguez, Rizal. The results of these trenches will be integrated and correlated with the existing studies of the WVF to determine a better understanding of the frequency of earthquake occurrence, the length of the fault or segments of the fault that ruptured, and the magnitude of potential earthquakes along the WVF.

3.1.2 Methodology

During previous mapping activities, (Daligdig et al., 1997; PHIVOLCS, 2008b; Rimando and Knuepfer, 2006; Papiona and Abigania, 2013; Papiona et al., 2013) landforms associated with faulting along the West Valley Fault have been identified using mainly 1966 and 1982 aerial photographs. Additionally, DEM derived from high resolution LiDAR data was also used to identify the surface expressions of the fault with respect to current built environment. The fault scarp is the most prominent surface expression of the WVF. Side hill ridges, incised spurs, gully and streams were also observed in aerial photographs and field visits.

The group visited several candidate sites for trenching. We targeted sites along the main trace of the WVF in the north around Rodriguez and San Mateo, Rizal, Quezon City and Marikina City, and in the south beyond the creeping area in Laguna and Cavite (Figure 1.1). The purpose of selecting these widely-spaced sites was to be able to characterize whether the WVF fault ruptured all throughout its length at any time in its historic or recent pre-historic past. The basic considerations in selecting the trench sites includes: 1) a clear and simple geomorphic expression of the fault. If possible, a scarp with small vertical offset to allow identification of offset layer piercing points and to maximize exposure of faulting events; and 2) depositional areas which allow layers of sedimentation and preservation of charcoal materials.

We excavated trench perpendicular to the trace of the fault, exposed the layers of sediment and fault structures on the trench walls, and logged and documented those features on 1:20 scale stitched photographs. Embedded charcoals were collected, dried and directly sent to Beta Analytic Carbon Laboratory in Florida, U.S.A. for C14 radiocarbon dating. In some cases charcoal are scarce or not always present even in areas where it is expected to be preserved. In cases where charcoal material was absent in the trench wall, we collected sediments containing quartz and feldspar mineral for Optically Stimulated Luminescence (OSL) dating. In OSL dating, the time elapsed since the last exposure of these minerals to sunlight is measured. Consequently, this provides an estimation of the time of burial of those minerals during sediment accumulation (Murray and Olley, 2002). The collected sediments were sent to Luminescence Dating Laboratory in Oxford University.

3.1.3 Trenching results

In the following sections, the words lithologic unit or simply unit is defined as a layer or a group of layer of sediments with same mode of deposition or age. While layer is individual set of sediments that is part of a unit. In the figures relating to the following sections, each unit is represented by different color

while layer and other geologic features within the unit are depicted by dashed lines. We use number to name each unit. Fault traces are shown as red bold (clearly evident fault traces) or dashed line (inferred fault traces). We use the word “Event” to refer to past surface rupturing earthquake inferred from the evidence observed in the trench. Event numbers for each trench indicates relative chronology of past earthquakes in that particular trench but it does not necessary relate or follow other events in other trench sites. Age of the charcoal materials are labelled as calendar years in the figures but in the text the equivalent BP (year before 1950) is also given.

3.1.3.1 Bagong Silangan Trench

The Bagong Silangan trench is located in Brgy. Bagong Silangan, Quezon City. The WVF is manifested here as a prominent fault scarp (Figure 3.1). It is also relatively confined into a simple trace indicating a narrow deformation zone. The adjacent stream provides sediment supply and charcoal materials. Two trenches 20 meters apart were excavated in the area. The north trench was excavated on a scarp that crosses a ~50 m stream channel while the south trench is on the front of lava flow deposits. The area is relatively well preserved and has only been disturbed by years of cultivating rice.

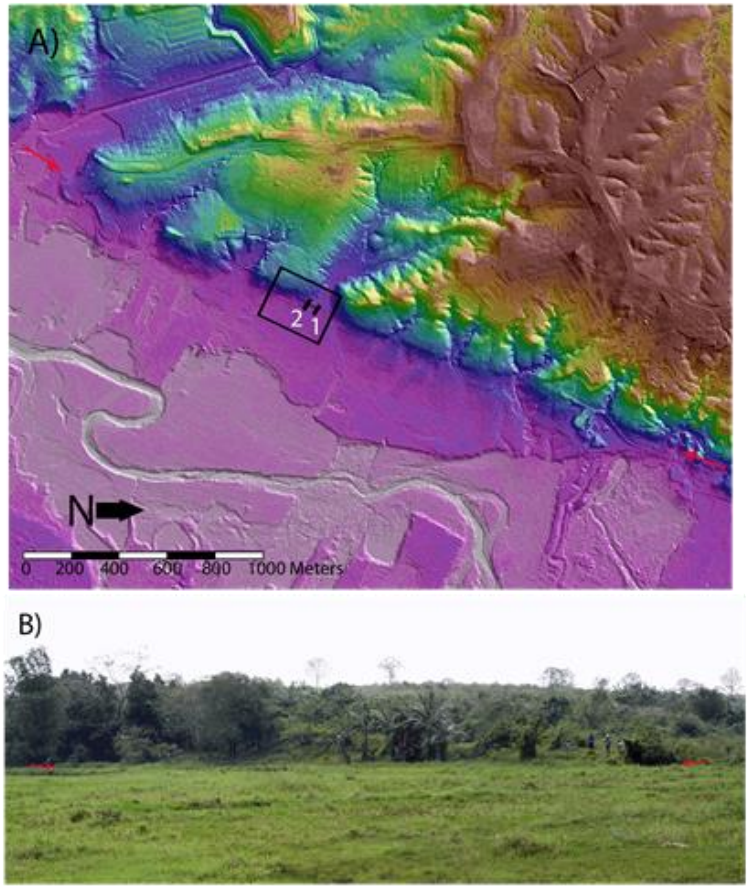

Figure 3.1. A) Location of the Bagong Silangan trench overlaid on Light Detection and Ranging -derived digital elevation model (LiDAR-DEM). Red arrows show the trend of the trace of the WVF. Solid black rectangles are location of the (1) north and (2) south trenches. Black hollow rectangle indicates the location of the photograph in (B). B) Photograph of the site showing fault scarp on the front of topographic high.

3.1.3.2 Bagong Silangan North Trench

3.1.3.2.1 Stratigraphy

The stratigraphy in Bagong Silangan North Trench is composed mainly of stream and flood deposits of brown silt to clay sediments. Contacts between layers are not distinct. Five major lithologic units were identified (Figure 3.2). Unit 5, the oldest unit in the trench is a loose gravelly stream deposit overlain by Unit 4, which is composed of sand to clay layers of reworked tuff. Unit 4 has a coarse to very coarse bottommost sand that grades from medium to fine sand and becomes progressively finer (silty to clayey) towards the upper part of the unit. The upper two units (Unit 3 and Unit 2) are flood deposits of silty clay composition with lenses or basal lag of coarse-grained sediments. Unit 1 is modern man-made fill fifty years old or less.

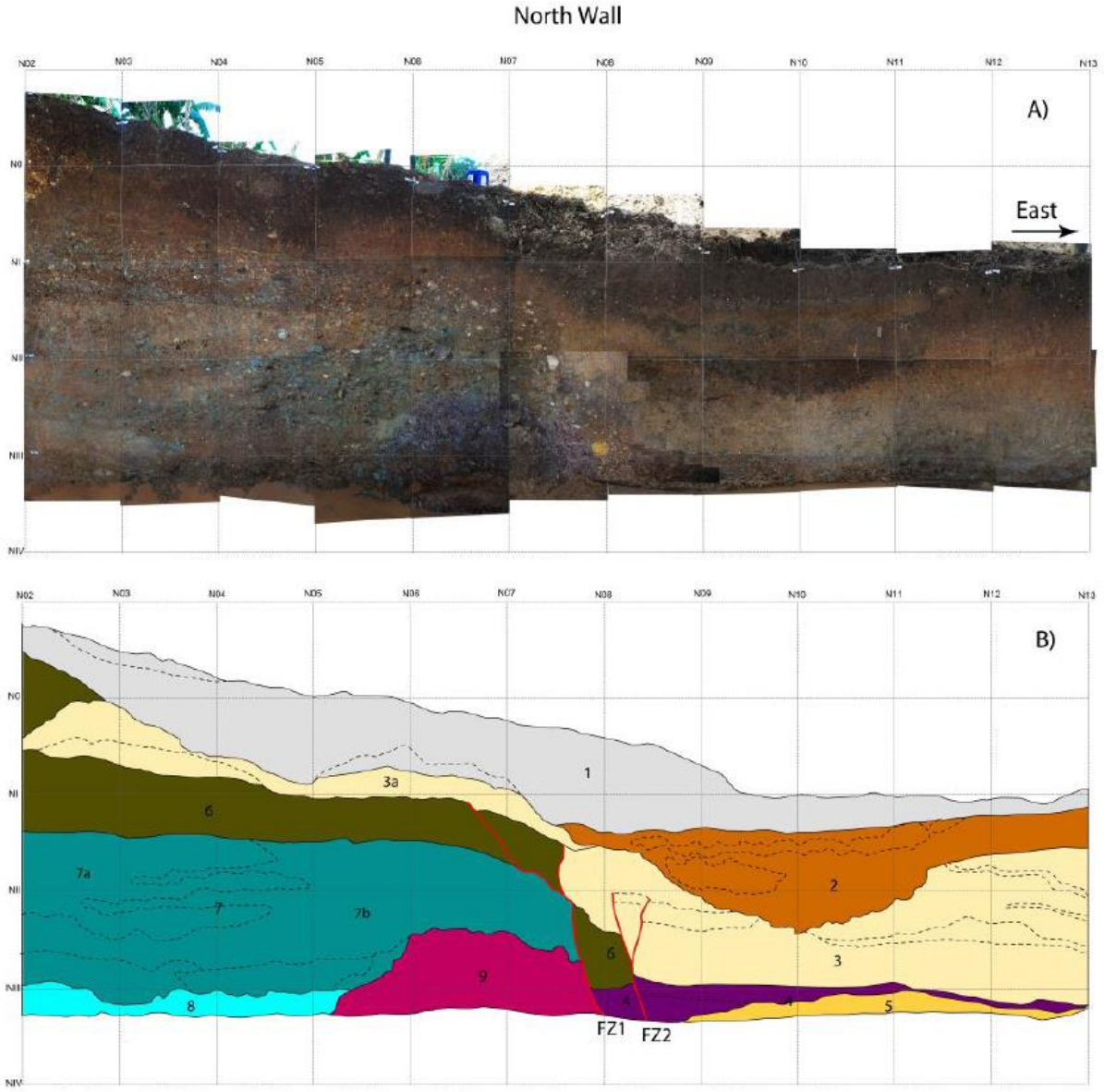

Figure 3.2. A) and C) Stitched photographs of Bagong Silangan North Trench north wall and south wall, respectively. B) and D) Drawing of Bagong Silangan North trench north wall and south wall, respectively. Vertical

and horizontal lines are 1x1 meter grid. Labels on top and on left of the figure are grid numbers. Lithologic unit is separated by solid lines while layers and other sediment feature observed in the wall are depicted as dashed lines. Labels within the unit are unit numbers. Red line is the strand of the fault. Solid triangles with labels are location of the embedded charcoal and its calendar age.

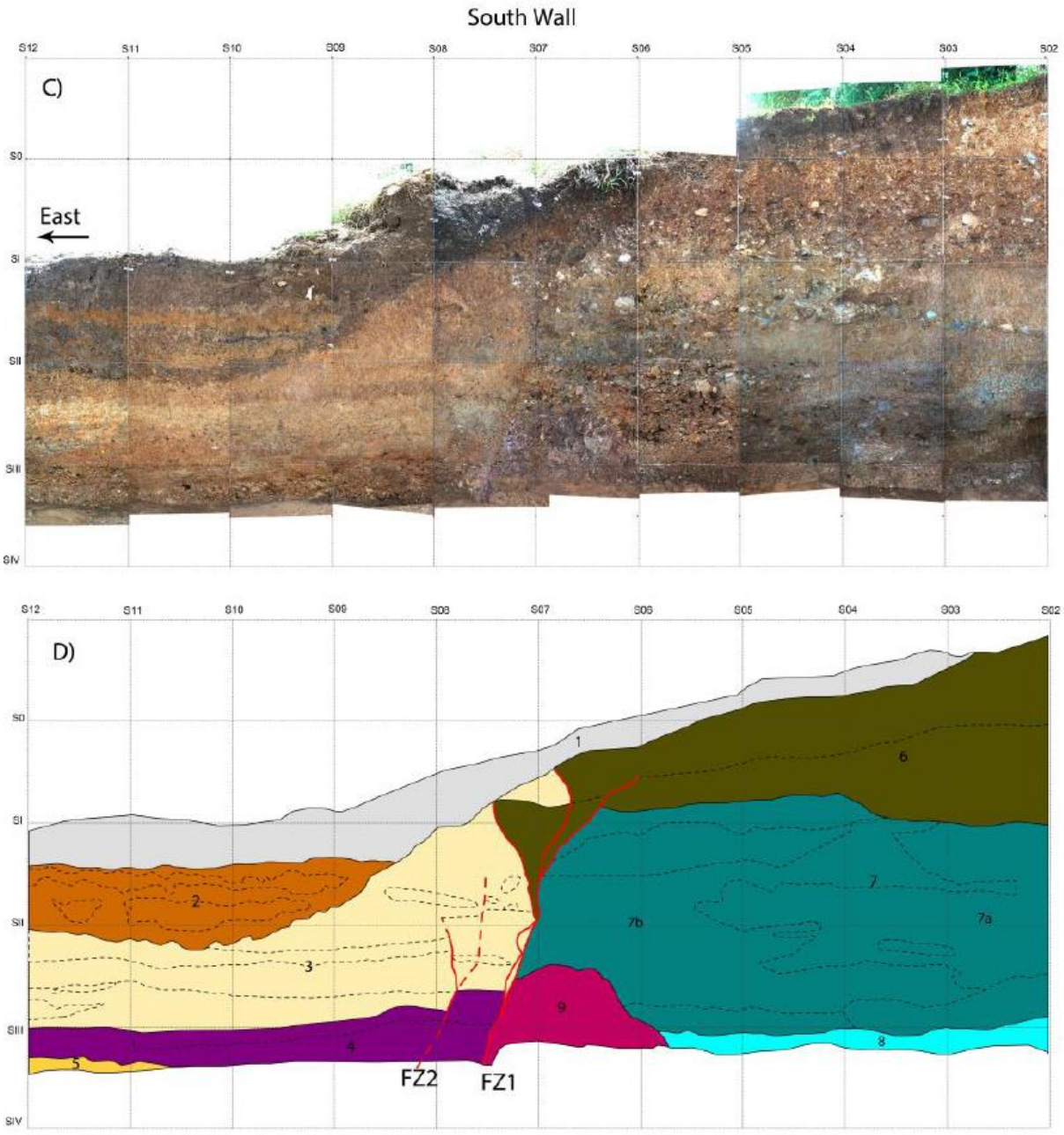

Figure 3.2 continued.

3.1.3.2.2 Surface Faulting Events

Unit 5 is vertically separated downward by 50 cm on the north wall of the trench along grid N9 (Part B of Figure 3.2). This sharp displacement may suggest displacement by surface faulting (Event 1). Rotated or vertically inclined pebbles in Unit 5 were also observed in grid N9 which could mean that these pebbles were dragged downwards along the fault. No similar feature however, was seen in

south wall. Although in grid S9 to S7 (Part D in Figure 3.2), a U-shaped structure with a hanging lens of Unit 4 and Unit 5 above was observed. Unit 2 is discontinuous towards the east (before grid N10 and S10). Although the discontinuity of Unit 2 and the changes in thickness of Unit 3 and Unit 2 towards the east may indicate faulting, this evidence is insufficient since we did not find fault strands transecting these upper units. Thus, for this trench we assume only one surface rupturing event.

3.1.3.2.3 Timing of the Surface Faulting Events

Charcoal is abundant within the units in the trench except for Unit 5 and 1. Sample taken from the sandy layer at the bottom of Unit 4 between grid N10 and N11 (Part B in Figure 3.2) has an age range of 1280 to 1390 AD (BP 670±30) while sample from the silty layer above the aforementioned sandy layer has an age range of 1420 to 1450 Ad (BP 460±30). This indicates that Event 1 in this trench happened within the years 1280 to 1450 AD.

3.1.3.3 Bagong Silangan South Trench

3.1.3.3.1 Stratigraphy

South trench was excavated only 20 meters south from north trench yet it exhibits very different stratigraphy. Evidence of faulting is also striking and more pronounce here than in the north trench.

At least nine major lithologic units were identified in the south trench (Figure 3.3). In both north and south walls, relatively older units observed on the west side of the trench are discontinuous to the east. The sharp contact between these discontinuous units is clearly defined by fault traces. Unit 6 and layer 7a are debris flows or landslide-type deposits. Unit 7 is composed of interfingering colluvium (7a) and an alluvial deposit of massive clay with highly weathered clast (7b). Unit 8 is gravelly stream channel deposit while Unit 9 is a reddish basement, or possibly a transported mass of rock of volcanic origin. Unit 6, 7 and 9 have sharp vertical contact with the units east of the fault zone. Unit 6 are vertically separated along the fault zone 1 (FZ1) by 120 cm (Figure 5B). Parts of Unit 6 and Unit 7 may have shed during faulting forming a deposit of colluvium mixed with the separated portion of Unit 4.

The bottommost unit at the east of the fault zone is a gravelly stream channel deposit (Unit 4) that banks on massive yellow clay (Unit 5) topped by sandy deposits. These units are overlain by flood deposits (Unit 3) of reworked volcanic sediment. Each episode of flood is either marked by the sandy lag or lens at the bottom of each layer. The stream channel-shaped Unit 2 on the east side are modern deposit (~50 years old or less) based on the observed embedded plastic materials at its bottom, while Unit 1 is modern man-made fill similar to Unit 1 in north trench. Unit 3 is also present on the west of the fault zone. We identified Layer 3a based on its similarity with the sediments in Unit 3 in the east of the fault zone but we did not see this layer on the south wall of the trench.

3.1.3.3.2 Surface Faulting Events

We identify at least three events in this trench. The continuity of some units on the west side from the fault zone (Figure 5) might be found below the exposed units in the east side of the trench implying that multiple events may have displaced these units along the same fault. Only three of these events were identified. The fault strands in FZ1 terminates at the top of Unit 6 suggesting the occurrence of Event A before the deposition of Layer 3a (Part B of Figure 3.3). The evidence of another possible event (Event B) includes the hanging strata of Unit 7 within Unit 3 in the along the easternmost fault in

FZ1 in the south wall (Part D of Figure 3.3). This feature implies that Event B occurred when Unit 3 was deposited, hence preserving the hanging face of a layer along the fault. These two events might have partly displaced Unit 6 in grid N08. Event C is manifested by the fault strands in FZ2 that terminate within Unit 3. In the south trench, a vertical separation of about 20 cm was measured in Unit 4. If we assume this as produced by a single event, the 120 cm cumulative displacement of Unit 6 could be caused by six surface faulting events.

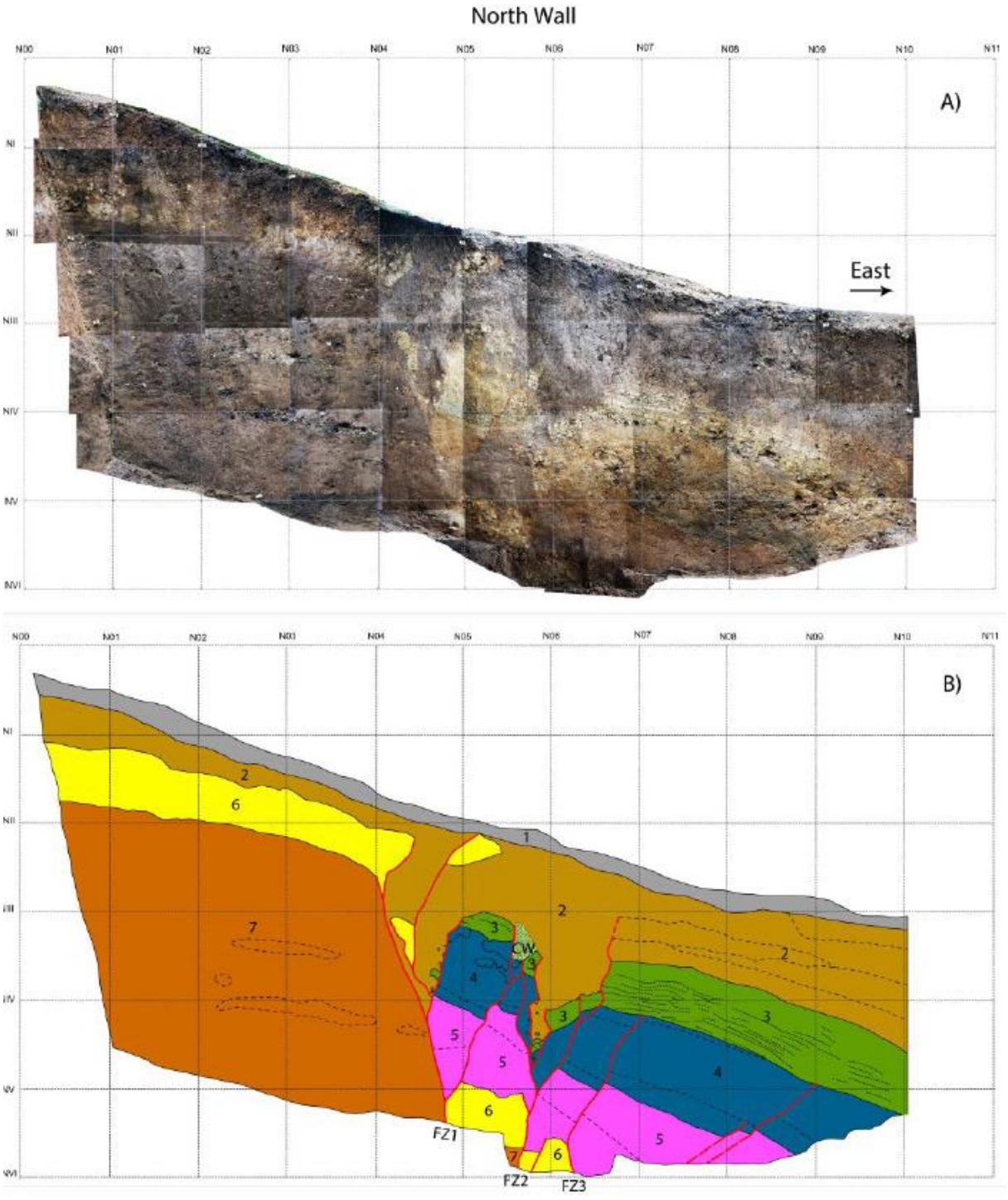

Figure 3.3. A) and C) Stitched photographs of Bagong Silangan South Trench north wall and south wall, respectively. B) and D) Drawing of Bagong Silangan south trench north wall and south wall, respectively. Vertical

and horizontal lines are 1x1 meter grid. Labels on top and on left of the figure are grid numbers. Lithologic unit is separated by solid lines while layers and other sediment feature observed in the wall are depicted as dashed lines. Labels within the unit are unit numbers. Red line is the strand of the fault. Labels FZ are fault zone number.

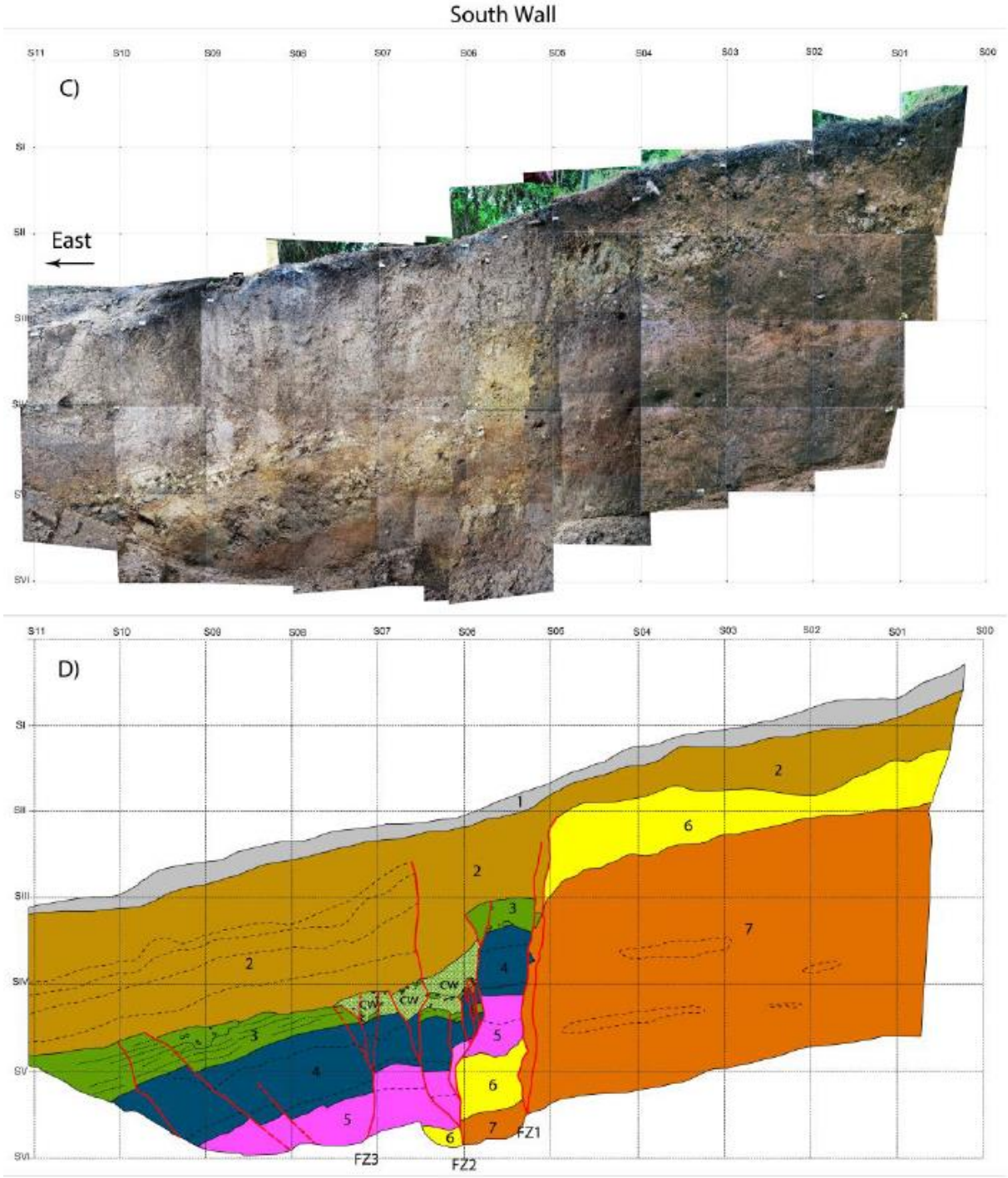

Figure 3.3 continued.

3.1.3.3.3 Timing of the Surface Faulting Events

Charcoal is scarce in the trench. We find one sample in Unit 3 on the far east part of the trench but the result yielded a post-1950 age. We collected sediment samples for OSL dating method instead for this trench. As of the writing of this report, we still do not receive the results of the OSL dating to constrain the timing of the events for this trench.

3.1.3.4 Lantic Trench

The Lantic Trench site is located in Calayugan area, Brgy. Lantic, Carmona, Cavite (Figure 3.4). The WVF in the area is characterized by prominent fault scarp as high as 6 m on a hill front. The trench was excavated on small alluvial fan with a scarp of less than one meter. Alluvial sediments and charcoal are deposited at the site from a creek which flows through a small valley

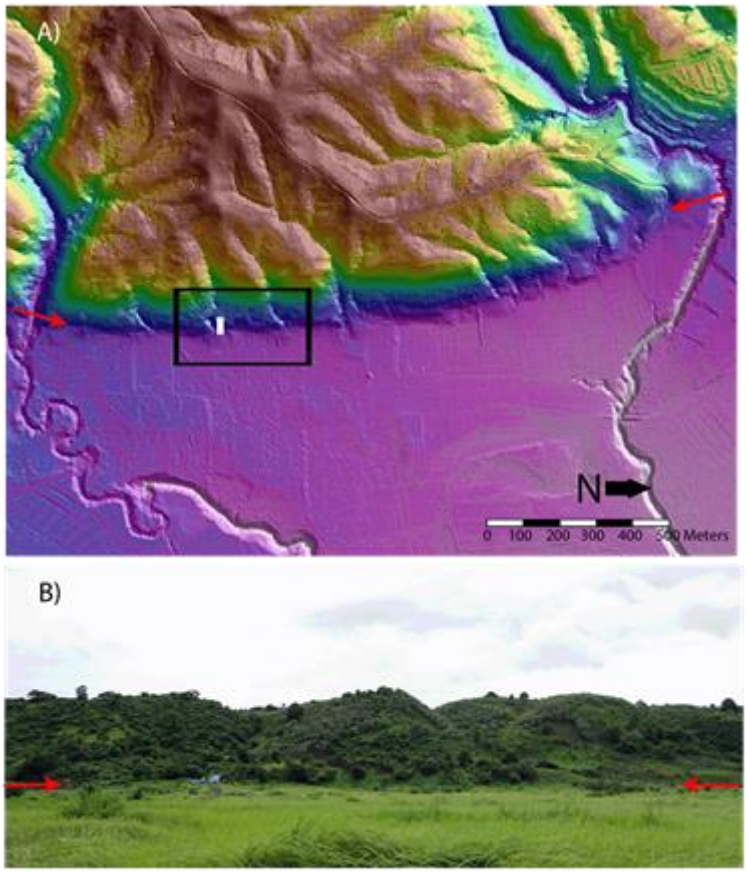

Figure 3.4. A) Location of the Lantic trench overlaid on Light Detection and Ranging -derived digital elevation model (LiDAR-DEM). Red arrows show the trend of the trace of the WVF. Solid white rectangle is the location of the trench. Black hollow rectangle indicates the location of the photograph in (B). B) Photograph of the site showing prominent fault scarp on the mountain front transecting small alluvial fan. Blue object on the left of the photograph is the location of the trench.

3.1.3.4.1 Stratigraphy

At least seven stratigraphic units were clearly discernible in the Lantic trench walls (Figure 3.5). The deeper four units (Unit 3 to 7) were similar to the sequence of scoria pyroclastic flow sequence from Taal Caldera eruption identified by Martinez and Williams (1999) while the upper units are alluvial fan

deposited from adjacent stream. The traces of the fault cutting through sediments and other features related to faulting were clearly identified on both trench walls.

The oldest unit in the trench is Unit 7, which is lithologically similar to the main body of pyroclastic flow sequence described by Martinez and Williams (1999). It is 3m thick, dominates most of the west part of the trench, and is composed of dark brown silty clay with clast of cream- and reddish scoria (<3cm size). It is overlain by Unit 6; a scoria-rich ash deposit. These two units are vertically separated along the main fault zone by 3.0 to 2.4 m similar to the observed height of scarp on the surface nearby the trench site. On the west side from the fault zone Unit 6 is directly overlain by Unit 2, which is a much younger alluvial fan deposit. This indicates that a period of erosion has removed the sequence of overlying unit that is similar to what is seen in the east side of the fault zones.

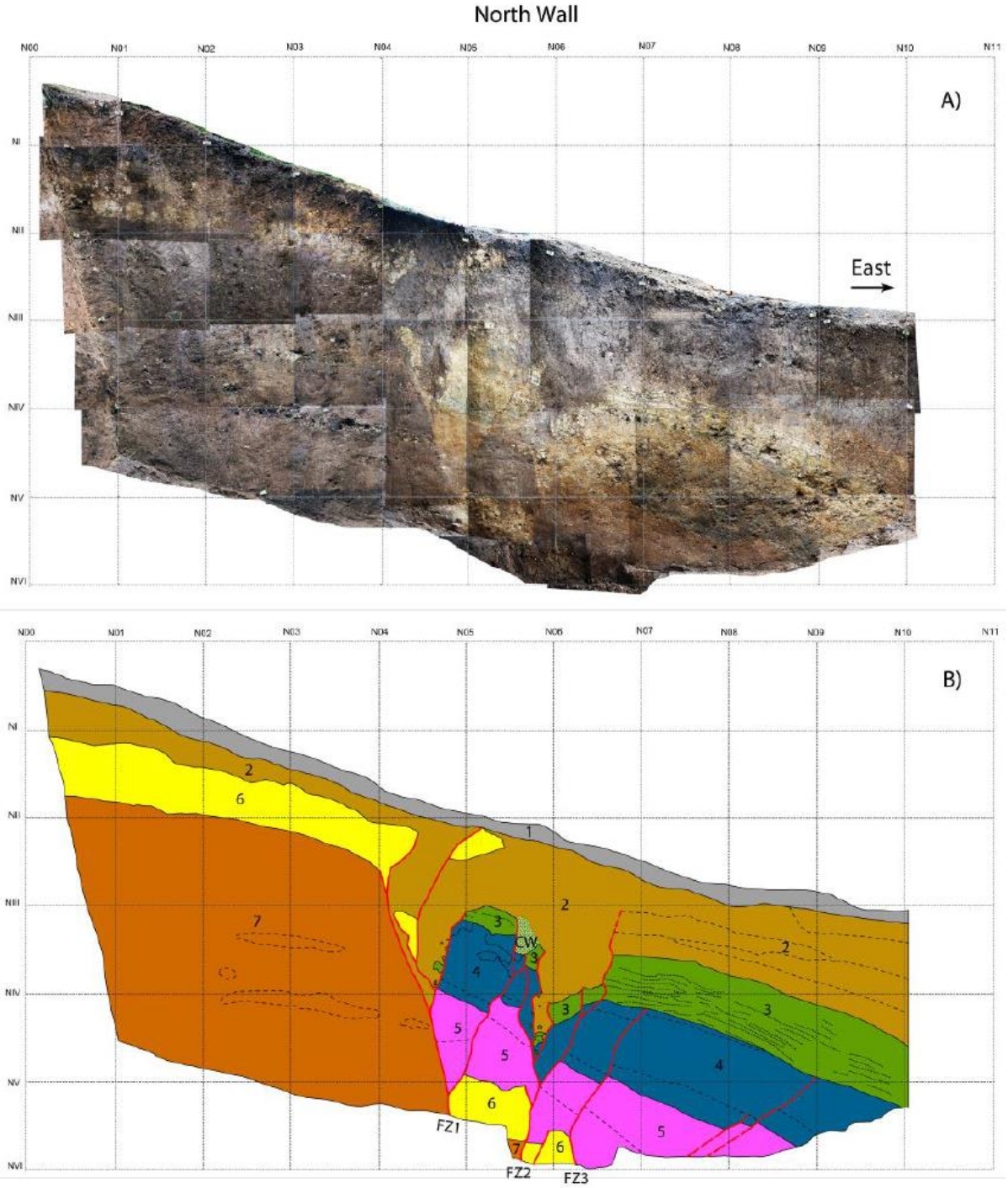

Figure 3.5. A) and C) Stitched photographs of Lantic Trench north wall and south wall, respectively. B) and D) Drawing of Lantic south trench north wall and south wall, respectively. Vertical and horizontal lines are 1x1 meter grid. Labels on top and on left of the figure are grid numbers. Lithologic unit is separated by solid lines while layers and other sediment feature observed in the wall are depicted as dashed lines. Labels within the unit are unit numbers. Red line is the strand of the fault. Labels FZ are fault zone number. CW is colluvial wedge.

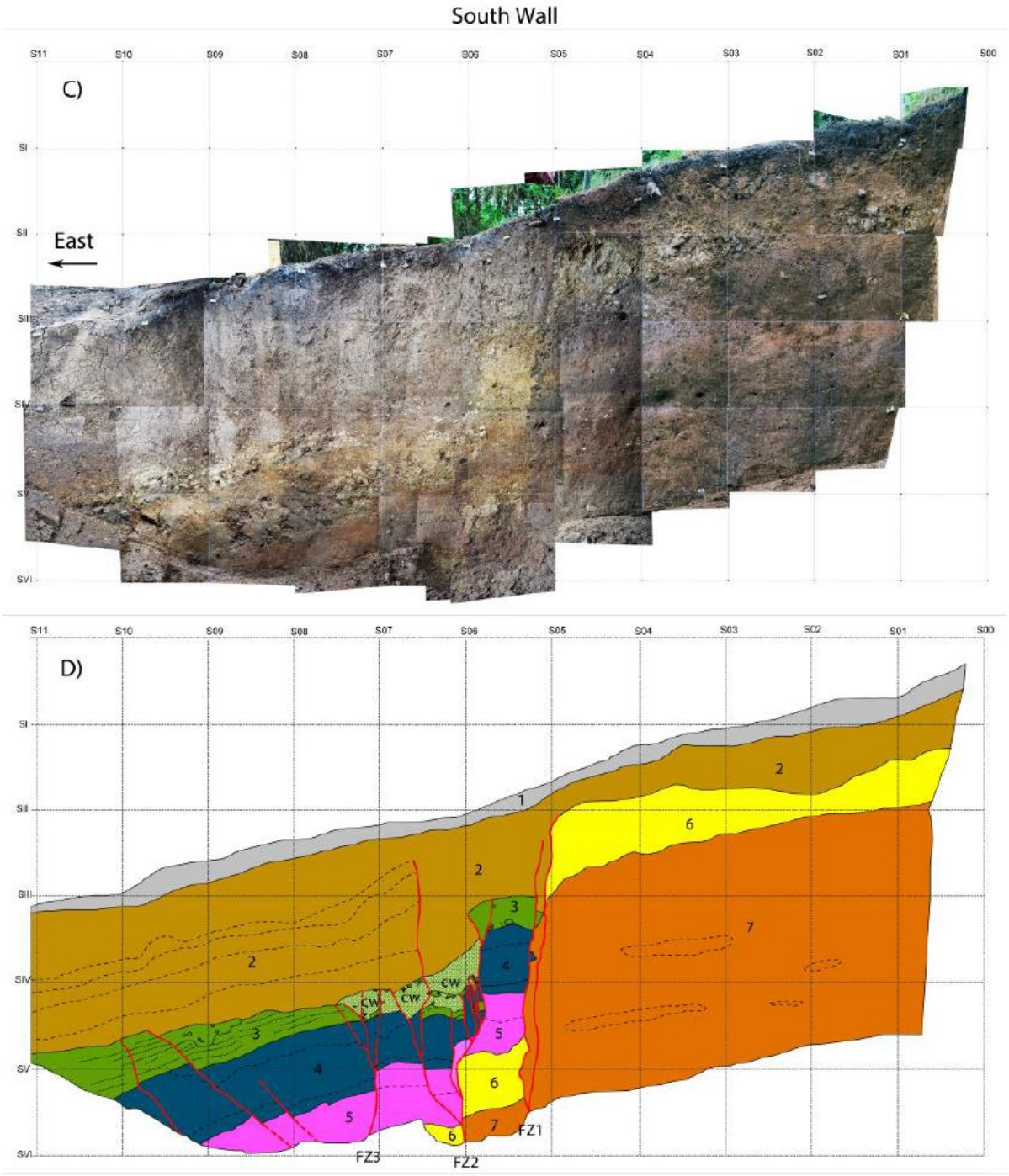

Figure 3.5 continued.

On the east side and along the fault zones, Unit 6 is overlain by another unit of pyroclastic flow deposit (Unit 5) which has smaller clasts and more silty matrix compared to Unit 7. Overlying this is Unit 4, a grayish- to cream-colored accretionary lapilli–rich unit. Above it is a unit of ash fall (Unit 3) characterized by interbeds of silt and cream-colored clay deposits. Unit 5, Unit 4 and Unit 3 are transected by near vertical fault along FZ1, FZ2 and FZ3 and by westerly dipping minor faults on the east of the trench.

Unit 2 is the alluvial fan deposit composed mainly of brown clay. Layers observed within the units are difficult to identify and in some areas it is not clearly visible due to the mixing of sediment layers along the fault zone. Mostly, these layers were defined from the train of pebbles at its bottom.

3.1.3.4.2 Surface Faulting Events

Strong evidence of surface faulting was observed in the trench, such as discontinuous units, filled cracks, vertical displaced units, overhanging strata, abrupt termination of fault traces and colluvial wedges (Figure 3.5). However, we cannot lucidly associate and describe all individual events inferred in the trench since most of the events ruptured along the same fault zone and transected the same units repeatedly. We were only able to separate clearly at least two events in the trench. The termination of fault traces on top of Unit 3 and the deposition of colluvial wedge (CW in Figure 7B and 7D) above Unit 3 clearly indicate surface faulting (Event J) before the deposition of Unit 2. Additional evidence of an event – possibly the most recent – is the horizontal separation of Unit 6 between grid N04 and N05 (Part B of Figure 3.5). The dropped materials from Unit 2 within the crack it produced suggest an event during or after the deposition of Unit 2 (Event K). Possibly associated with this event is the overhanging feature of Unit 3 near grid S06 (Part D of Figure 3.5), which also suggests that Unit 2 existed when faulting occurred. Other events were inferred based on the cumulative displacement measured from relatively young to older units.

The cumulative vertical separation of Unit 6 and Unit 7 along the main fault zone FZ1 is 240 to 300 cm. If we consider the 65 cm and 80 cm vertical separation between Unit 6 and 7 in grid S06 (Part D of Figure 3.5) and near grid N06 (Part B of Figure 3.5), respectively, as maximum vertical displacement in one event, we infer at least three events and possibly five have displaced Unit 6 and 7. Conversely, if the 29 cm displacement in Unit 3 along the easternmost strand in FZ2 (Figure 7B) is one event, the 65 to 80cm displacement of Unit 6 and 7 along FZ2 would mean at least two events have ruptured this fault, hence along the main fault zone, at least three and maximum of ten events may be inferred.

3.1.3.4.3 Timing of Surface Faulting Events

Martinez and Williams (1999) estimated the age of the scoria pyroclastic flow sequence to about 5,000 years old (5,600 to 6,800 BP) based on the embedded charcoal samples collected from its bounding sediments. Charcoal is also scarce in this trench. We found charcoal in Unit 6 but its age of 680 to 880 AD (1240±30BP) appeared to be too young for this pyroclastic flow sequence. Consequently, we can only infer that in this trench, at least three events and maximum of ten events post-dating the 5,000 year old pyroclastic flow deposit.

3.1.4 Discussion and conclusion

In Bagong Silangan North trench we were able to measure a 50 cm single-event vertical displacement while in the south trench 20 to 40 cm was estimated. These values are consistent with the vertical displacement measured by Nelson et al. (2000) in Maislap trench site and the minimum of 55 cm scarp height measured by Rimando and Knuepfer (2006). Nelson et al. (2000) computed a M 6 to 7 for the northern part of the West Valley Fault. They however, concluded that it might be too small considering the length of the WVF. Rimando and Knuepfer (2006) on the other hand, using their computed 0.26 to 0.56 vertical to horizontal displacement ratio (V:H), estimated a M 7.6 to 7.7 for the northern segment of the WVF, but favors the 6.4 to 7.4 magnitude based on length. Using Rimando and Knuepfer's (2006) V:H ratio and Wells and Coppersmith's (1994) empirical equation, we

estimated a range of 6.4 to 7.0 magnitude earthquake consistent with the previous computations of Nelson et al. (2000)

Similarly, with the Lantic trench, using V:H ratio (0.26) computed by Rimando and Knuepfer (2006) in the area, we estimate a magnitude range of 6.5 to 7.2, smaller than Rimando and Knuepfer's (2006) computation of M 7.6.

We still cannot estimate the total length of fault rupture based on our current paleoseismic data since we cannot correlate the timing of the past earthquakes from the Bagong Silangan and Lantic trenches. Based on the V:H ratio alone, a conservative range of magnitude 6.4 to 7.3 might be in order for WVF. This is consistent with the results based on length computed by Rimando and Knuepfer (2006) and by the total length of WVF based on the current mapping activities (Papiona et al., 2013) .

For the timing of the events we can only conclude based on our current data that in Bagong Silangan north trench, one and possibly the most recent surface rupturing event was inferred before year 1450 AD. While in Lantic trench, we can only estimate that three to ten surface rupturing events post-date 5000 years.

Our data on the age of sediments is insufficient and should be used with care in estimating the frequency of surface rupturing earthquakes. Moreover, it should also be noted that the WVF is a right-lateral strike-slip fault. Thus magnitude estimates based on vertical displacement alone may not be conclusive. Additionally, based solely on the current trenching data, we cannot distinguish whether the segments comprising Lantic area ruptured at the same time with the northern segment including the splay where the trench of Nelson et al. (2000) were excavated. Follow-up trenching activities should be conducted along the WVF to solve these issues. Moreover, the rupture characteristics of EVF are still unknown. Its proximity to Metro Manila also poses threat in terms of earthquake hazard. Therefore, paleoseismic studies should also be conducted along EVF in order to understand its potential earthquake magnitude and frequency and how it relates to the movement of WVF.

3.2 Geotechnical Database

The amplification of earthquake ground motions are highly influenced by the presence of loosely consolidated near-surface sediments. To better understand the potential impacts of near-surface sediments, the collection and synthesis of geotechnical information is necessary. This information includes, but is not limited to, the thickness of lithological units, grainsize, Cone Penetrometers Test (CPT) blow count, and occasionally, direct shear-wave measurements. Owing to the ever-increasing urban and infrastructure development throughout the GMMA, a natural by-product is a collection of large volumes of geotechnical data required to guide the civil works. A database schema was designed and a tool for encoding the data was developed by PHIVOLCS. The development and the painstaking population of this database are discussed below.

3.2.1 Design of database schema

Following several discussions between PHIVOLCS and GA staff, a relational database structure was developed to encode the borehole logs for which PHIVOLCS is the custodian. The schema allows for the capture of comprehensive information regarding borehole lithology, CPT measurements, or direct velocity measurements. Its creation also improved the rudimentary geotechnical database earlier used to digitally archive and systematize the borehole dataset holdings of PHIVOLCS collected from earlier

initiatives by various researchers. PHIVOLCS possesses a large archive of paper borehole descriptions, which often provide valuable information from which to garner seismic site classifications. In order to use these data effectively, the paper records were scanned and encoded such that digital data could be made available to manipulate.

The geotechnical database schema was designed based on information found on borehole logs usually required for geotechnical evaluation. The database also allows for more specialised information that may become available in the future, for example from down-hole velocity measurements. The schema divides the borehole information into three tiers (see Appendix E). The first tier corresponds to the metadata and provides a unique identification to each borehole dataset. The second tier divides the borehole dataset information into groups corresponding to its sedimentary and velocity characteristics. The third tier provides the details for the sedimentary characteristics.

The database was created using SQLite and embedded into REDAS as a specialized module. The database outputs spreadsheets, which can be imported into Microsoft EXCEL to allow simplified data analysis. Population of the database is has been underway since it was created in December 2011. At the end of 2012, researchers and research assistants have populated it with nearly 1,000 datasets from Metro Manila, which is more than half of the holdings of PHIVOLCS for the area. In 2013, the geotechnical database also began to be populated by datasets from Greater Metro Manila.

3.3 A Site Class Model for the GMMA

3.3.1 Evaluation of site class existing models

Significant local amplification of ground motion during earthquakes may arise on areas underlain by thick sediment layers. Therefore the evaluation of site effects or the effects of local geology is an utmost importance in seismic hazard analysis. In this study, we used shear wave velocity information to characterize site effects in GMMA.

Metropolitan Manila features diverse lithologic units. Previous workers divided its landforms into three major regions: the Central Plateau, the Coastal Lowland, and the Marikina Plain (Figure 3.6) (Gervasio, 1968; Matsuda et al., 2000; MMEIRS, 2004). The Central Plateau is a rolling landform with an elevation of about 15-40 m in the Metropolitan area (e.g. Matsuda et al., 2000; MMEIRS, 2004). It consists of the Pleistocene Guadalupe formation, which is divided into the older Early to Middle Pleistocene conglomerate, silty mudstone, and tuffaceous sandstone and the younger Late Pleistocene tuffaceous clastic rocks and well-bedded tuff, also known as adobe (Gervacio, 1968; BMGS, 1982; Matsuda et al., 2000). West of the Central Plateau lies the Coastal Lowland consisting of sand bars, backmarsh, and the Pasig River delta as well as the reclaimed land in the Manila Bay area. The soil deposit thickens gradually towards the Manila Bay to about 60 m thick at the Pasig River delta (Matsuda et al., 2000; MMEIRS, 2004). Sandwiched between the Central Plateau in the west and the mountainous area of Rizal Province in the east is the Marikina Plain. It consists of mixtures of unconsolidated gravel, silt, and clay. On its upper reaches (north part of Marikina Plain), the river terraces and natural levees are well developed while on its lower reaches (south part of Marikina Plain) are mostly composed of delta deposits (e.g. Matsuda et al., 2000; MMEIRS, 2004). These diverse lithologic features of Metropolitan Manila present variations in shear wave velocity, hence different site amplification.

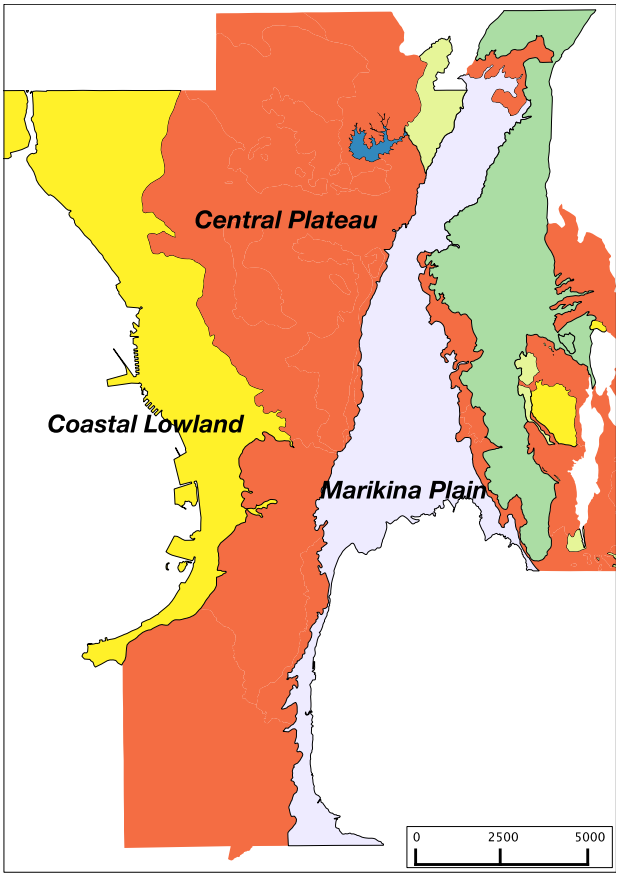

Figure 3.6. Map showing the three major geomophologic (labelled) regions in GMMA modified from MMEIRS (2004).

In this study, we used VS30 as proxy for site amplification. Amplification is proportional to shear wave velocity through,

$$\frac{1}{\sqrt{V_s.r}}$$

where V_S is the shear wave velocity and ρ is the density (Aki and Richards, 1980). Density is about constant along the depth of interest. What varies is the shear wave velocity. The VS30 is estimated from borehole data using the equation below:

$$V_{s30} = \frac{30}{\sum_{i=1}^{N} (h_i / v_i)}$$

where h and v are the thickness and shear wave velocity of layer, i and N is the total number of layers in the top 30 m.

We analysed a total of 373 borehole paper logs located in 10 cities and one municipality in Metro Manila (Figure 3.7) to obtain VS30 estimates. The logs are from MMEIRS (2004) database. We

compared these values with VS30 derived from existing model (Grutas and Yamanaka, 2012) and topographic-sloped based methodology (Wald and Allen 2007) to evaluate the site-class models for GMMA. Although the distribution of boreholes in GMMA is biased by locations, we still proceeded with the comparison since the boreholes sampled the major geologic units in GMMA. As will be discussed in the next section, this study applied a hybrid approach using geotechnical and geological data to estimate VS30 at locations not sampled by the boreholes.

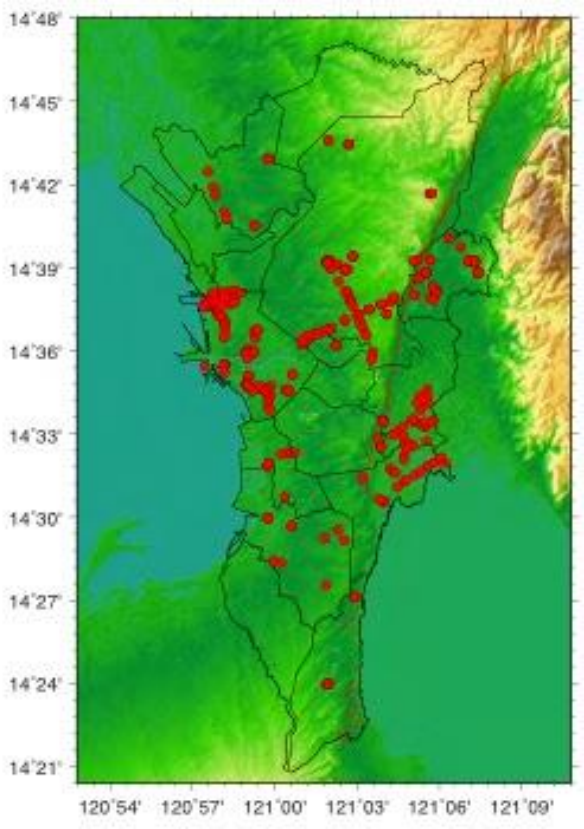

Figure 3.7. Map showing the location of boreholes (red circle) used in the estimation of VS30. Also shown are the political boundaries in Metro Manila (black lines) as well as the trace of the Valley Fault System (red lines).

The VS30 was estimated from the stratum code and the standard penetration test blow count (SPT-N) entries of the logs. The stratum code refers to the different rock types in Metro Manila based on the Japanese soil classification scheme (Matsuda et al., 2000; MMEIRS, 2004). Matsuda et al. (1998) used this scheme to classify the soil types in Metro Manila that was later adapted in the MMEIRS (2004) report. In general, the rocks are grouped into seismic engineering bedrock and soil deposits. The pyroclastic rock and tuff layers comprise the seismic bedrock commonly exposed in Central Plateau area while buried as deep as 120 m in the Coastal Lowland and Marikina Plain. These layers are characterized by having shear wave velocity exceeding 700 m/s or a SPT-N value exceeding 50 (Matsuda et al., 2000; MMEIRS, 2004). Overlying the basement rocks are the soil deposits composed of Quaternary Alluvium and soils derived from the weathered products of the basement rocks. The corresponding shear wave velocity of each soil type varies depending on the location following the Regional Classification of Lowland Area of MMEIRS study. This classification scheme was devised in

MMEIRS to account for the variation of soil properties and subsequently velocity based on depositional environment.

To obtain VS30 using the SPT-N value, we used Imai et al. (1975) empirical relations,

$$Vs = 89.8 \cdot N^{0.341}$$

where Vs is the shear wave velocity and N is the blow counts, so as to be consistent with the MMEIRS report. Although several empirical relations (e.g. Akin et al., 2011 and references therein) exists today in the literature, these relationships have significant differences and resolving these differences is beyond the scope of this work.

Only those boreholes deeper than 22 m were used in VS30 estimation following Boore (2004). Exceptions are those boreholes that reached the basement rock at shallower depth. Most of these boreholes are located in the Central Plateau area, which only have few meters of soil cover. In all, we were able to estimate VS30 from 267 out of 373 available borehole data based on this depth criterion.

Figure 3.8 shows the histogram plot from which VS30 could be estimated from either Stratum Code or SPT-N. Estimates from each technique are grouped into site class definition of the National Earthquake Hazard Program (NEHRP) classification (Building Seismic Safety Council, BSSC, 2004). Here we showed that sites in Metro Manila fall from Site class C (very dense soil and soft rock) to Site class E (soft soil) classifications. While several of the boreholes are in Site class C the reader should keep in mind the boreholes are not evenly distributed throughout the study area.

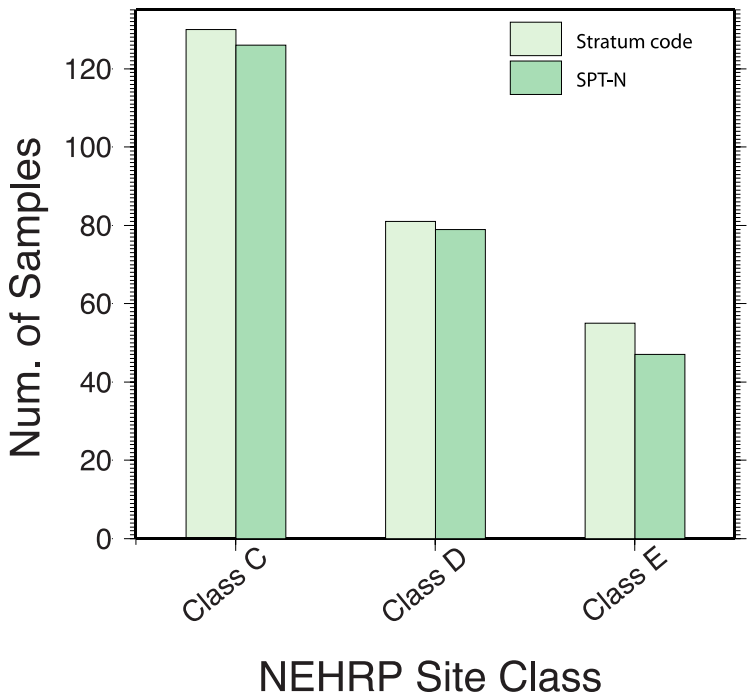

Figure 3.8. Histogram of Vs30 grouped based on site class definition of NEHRP. While majority of boreholes fall under site Class C, the observation only reflects the non-uniform distribution of the boreholes. Nevertheless, the plot suggests that the lithologies in Metropolitan Manila fall under site Class C to E.

The consistency in the VS30 values obtained from stratum code and SPT-N is demonstrated in Figure 3.9. The general trend suggests that boreholes located in Central Plateau fall under Site Class C reflecting the stiffness of the tuff and relatively thin sediments cover. Those boreholes located in the south part of Marikina plain cluster under Site Class E consistent with the observed thick sediments in the area (Matsuda et al., 2000). The VS30 values from the topographic-sloped based methodology are in general comparable with the borehole-derived values specifically in the Marikina Plains (Figure 3.10). However, this method predicts significantly lower values compared with the boreholes located in the Central Plateau. Because the plateau has low overall slope, the slope-based methodology assigned this region as soft rock or soils instead of hard rock, hence the underestimation in the VS30 values (e.g. Wald and Allen, 2007). The Grutas and Yamanaka (2012) model agrees better with boreholes located in the plateau although in some boreholes the model predicts higher values. This discrepancy is due to the 700 m/s velocity (based on PS logging) used in boreholes for the whole basement rock while the Grutas and Yamanaka (2012) model velocity varies across the region. The Grutas and Yamanaka model also predicts higher VS30 values in Marikina Plains.

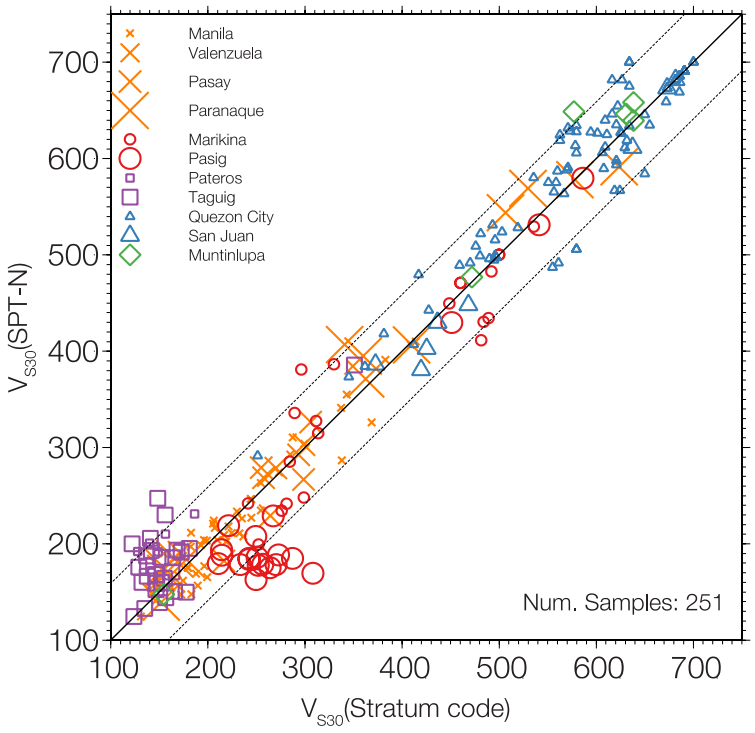

Figure 3.9. Plot showing a good correlation of Vs30 values derived from the stratum code and from the SPT-N value. Different symbols represent the grouping of Metro Manila cities based on the regional classification of lowland areas in MMEIRS (2004). The dashed lines are the ±1 standard deviation in the Vs30 differences of the two data sources. The solid line is the 1-to-1 line.

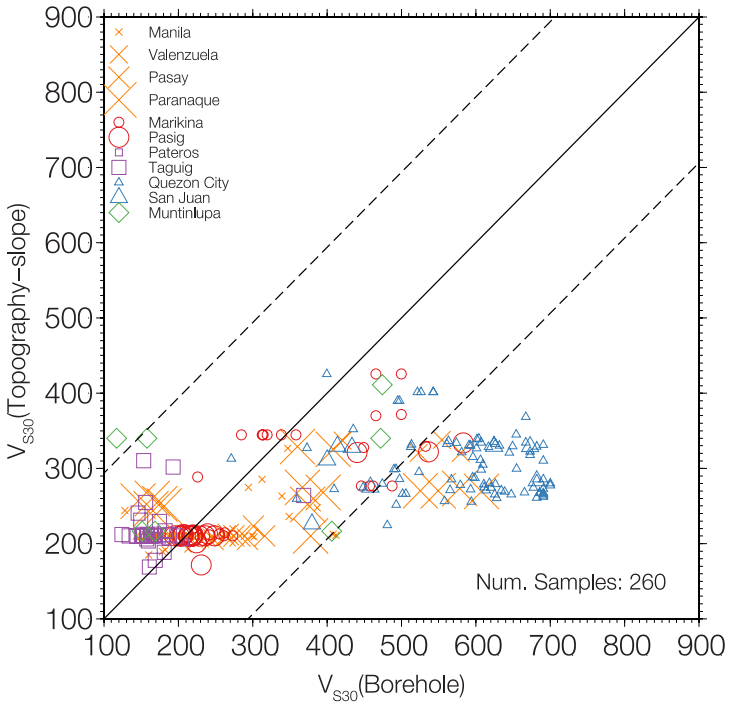

Figure 3.10. Plot showing the correlation of Vs30 values derived from the borehole and from the topography-slope methodology. Different symbols represent the grouping of Metro Manila cities based on the regional classification of lowland areas in MMEIRS (2004). The dashed lines are the ±1 standard deviation in the Vs30 differences of the two data sources. The solid line is the 1-to-1 line.

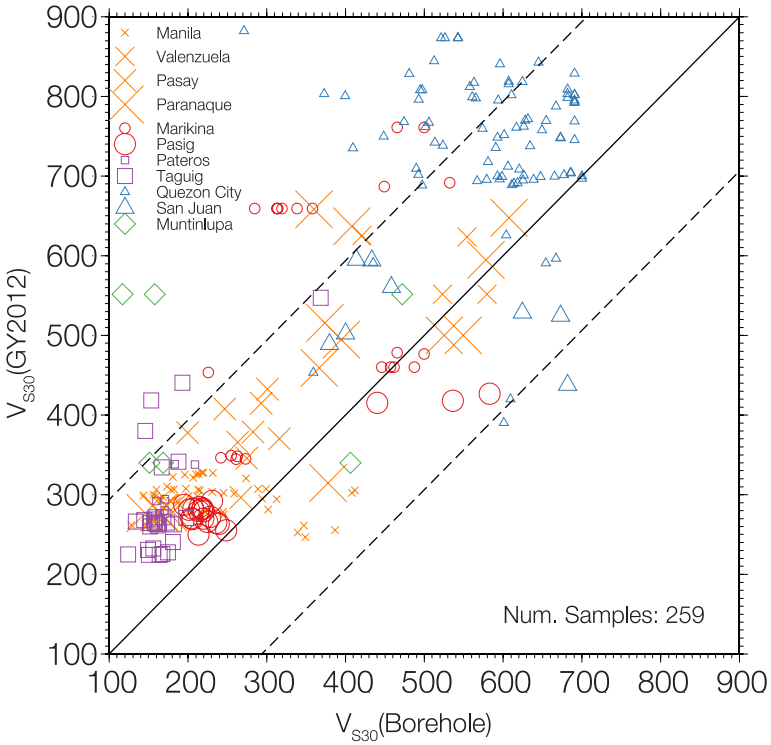

Figure 3.11. Plot showing the correlation of Vs30 values derived from the borehole and from the Grutas and Yamanaka (2012) model. Different symbols represent the grouping of Metro Manila cities based on the regional classification of lowland areas in MMEIRS (2004). The dashed lines are the ±1 standard deviation in the Vs30 differences of the two data sources. The solid line is the 1-to-1 line.

3.3.2 Hybrid Topographic Gradient Model

Based on the analyses above, no one site classification model performs adequately when compared to VS30 values estimated from borehole data. For example, the Grutas and Yamanaka (2012) model estimates seismic velocities well across the Central Plateau, but tends to overestimate VS30 in the Marikina Valley. In contrast, the topographic gradient method performs relatively well in the Marikina Valley. However, it performs poorly in the Manila Plateau, where the flat-lying Taal volcanic deposits are characterised by relatively high seismic velocities.

The Grutas and Yamanaka (2012) model requires several input variables in order to be applied. Unfortunately, these input variables were not uniformly available throughout the GMMA study area. In contrast, the topographic slope model can be applied anywhere a digital elevation model exists. Because the site class model of Grutas and Yamanaka (2012) did not cover the full study area, a hybrid topographic approach was implemented to take advantage of the borehole data collected through the geotechnical sub-component of this study to bias topographic gradient proxies of VS30 based on the mapped extents of surficial geological units. A digital shapefile of mapped surficial units was obtained from PHIVOLCS. The mapped geological units were subdivided into three key units: Quaternary sedimentary deposits, Taal Volcanics, and basement rock. Measured VS30 values were extracted for each of these units, VS30 observations. In each case, the data were compared to the site class model from the combined SRTM-LiDAR (Figure 2.1). The median differences between the topographic gradient model and the measured VS30 data are given in Table 3.1. The areas enclosed within the different geological units were subsequently biased by the median differences in Table 3.1 (Figure 3.12).

Table 3.1. Bias VS30 factors applied to the topographic gradient site class model for the primary geological units in the GMMA area.

GEOLOGICAL UNIT	MEDIAN VS30 BIAS (m/s)
Taal Volcanics	+280
Quaternary Sediments	-11

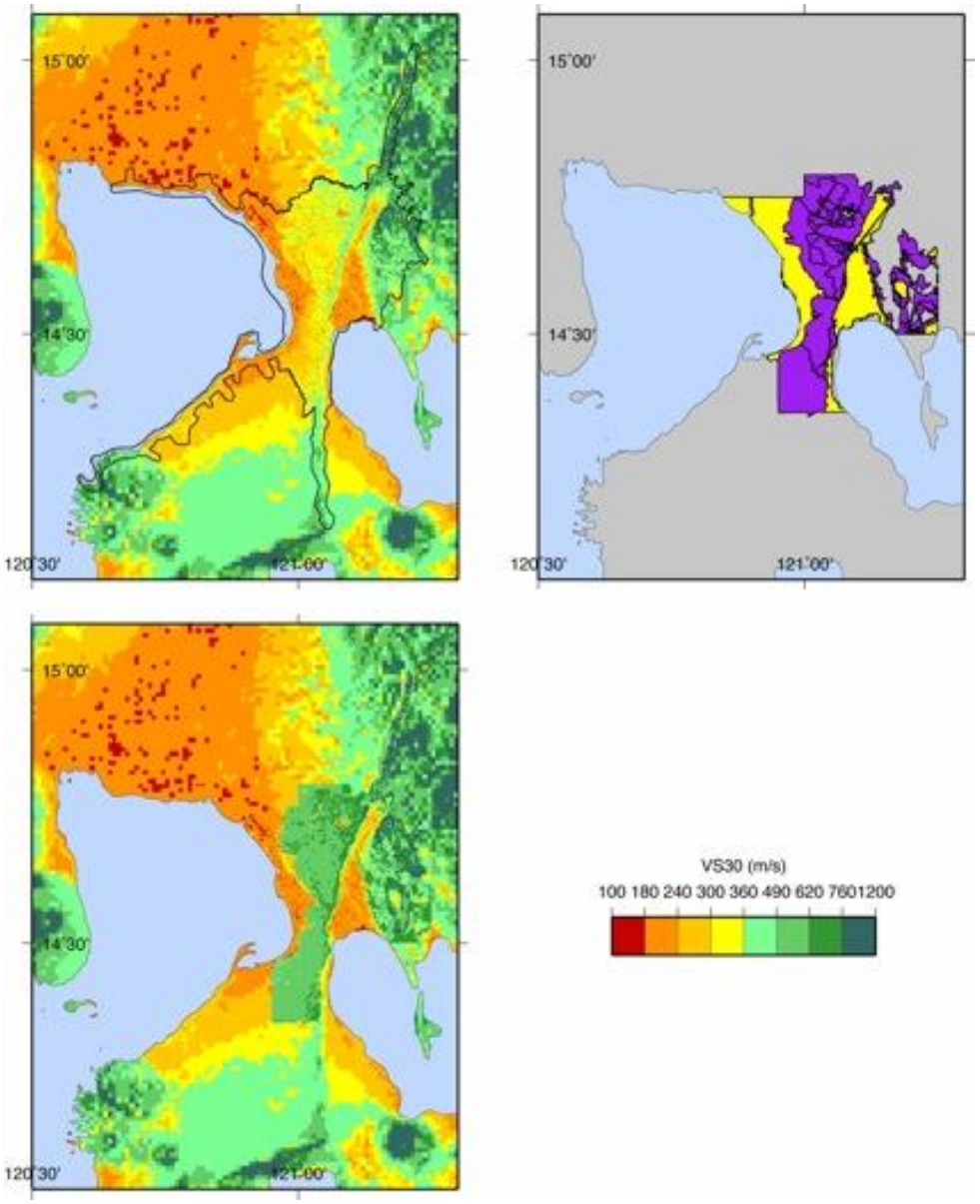

Figure 3.12. Modified site class model based on topographic gradient. (Top-left) Combined SRTM-LiDAR mosaic (same as Figure 5 bottom-left). (Middle) Mapped geological units. Yellow units are classified as Quaternary sediments (bias of -11 m/s) and purple units indicate the extent of the Taal volcanics (bias of +280 m/s). (Bottom) Resulting site class model biased by VS30 estimates.

3.4 Evaluation of Philippine Ground-Motion Data

The rapid augmentation of existing digital earthquake monitoring networks in the Philippines has resulted in more earthquake data being recorded than ever before. While seismic monitoring networks in the Philippines are relatively sparse in comparison to Japan, Taiwan or California, for example, they are still capable of capturing useful data that can be used to evaluate the intensity of ground-motions in the Philippines. However, with relatively few strong-motion data available in the Philippines, a ground-motion prediction equation (GMPE) specific for this region cannot be developed at the moment. Until this is realized, hazard analysts may use GMPEs derived from regions with similar tectonic setting as the Philippines. In this section, relevant ground-motion data of Philippine

earthquakes recorded by the Philippine Seismic Network (PSN) were gathered and consolidated in order to analyse and statistically compare their maximum values against several published GMPEs. These analyses aim to determine and recommend an appropriate GMPE for earthquake hazard and risk assessment in the Philippines.

3.4.1 Data processing tools

Today, PHIVOLCS is running a state-of-the-art seismic network using modern Nanometrics instruments. Several software tools exist to read these data. However, PHIVOLCS also continue to run a legacy digital seismic network that was installed in 2000. This Kelunji network has collected valuable data since its installation. However, until now, PHIVOLCS did not have a means of using these data for ground-motion attenuation studies. Consequently, a suite of software tools was developed to perform several functions that are useful for ground-motion attenuation studies. These tools can currently perform the following functions:

- Read earthquake time history data in several text and binary formats
- Poles and zeros instrument correction (Scherbaum, 1996) and write output time history in acceleration, velocity and displacement
- Calculates instrument corrected Fast Fourier Transform (FFT) and write output spectrum
- Calculates and outputs 5% damped pseudo response spectrum (PSA)
- Convert to Wood-Anderson (Anderson and Wood, 1925) displacement time history and calculate local magnitude (Richter, 1935; 1958)
- Exports to Seismic Analysis Code (SAC) format
- Plots frequency, amplitude and phase instrument response

The tools were developed in the Python programming language and leverage of modules developed from the ObsPy Project (Beyreuther et al., 2010). A preliminary manual for the codes is provided in Appendix G.

3.4.2 Data

For this study, a total of 173 waveforms of 18 Philippine earthquake events recorded by velocity- and acceleration-type seismographs were chosen from the waveform database of PSN. The magnitude of these earthquakes range from 4.9 to 7.6 with reported intensity ratings of V and above in the PHIVOLCS Earthquake Intensity Scale (PEIS), a ten-point intensity scale currently used in the Philippines. Depths of the earthquake dataset were constrained to crustal events (<50 km) with epicentral distances less than 800 km from the recording stations. Earthquake event descriptions are summarized in Table 3.2. From the magnitude-distance plot of the dataset shown in Figure 3.13, it clearly shows that there are few near-field data (<10 km), due to limitations of the network as shown by the present station density and inter-station distance of PSN.

Prior to the comparative analyses, ground motion data were made uniform by converting records from velocity-type seismographs to acceleration. Pseudo response spectra were subsequently computed from the acceleration time-histories.

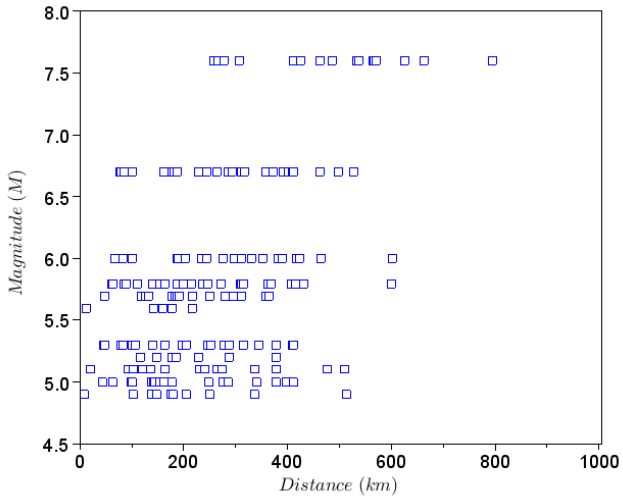

Figure 3.13. Summary of data used in this study.

Table 3.2. Summary of Earthquakes used in this study

Sequence number	DateTime (UTC) (YYYY-MM-DD-hh:mm)	Magnitude	Longitude	Latitude	Depth	Number of Records
1	2007-06-14-14:49	5.5	125.168	10.347	12	11
2	2007-07-19-15:09	5.3	125.190	10.366	2	12
3	2008-01-13-12:15	5.7	120.726	17.252	13	7
4	2009-01-29-22:43	5.1	124.753	10.956	4	7
5	2009-11-11-13:48	5.7	125.584	9.367	16	9
6	2009-12-21-19:59	5.3	121.425	17.509	16	8
7	2010-03-02-02:51	5.8	122.565	18.404	19	8
8	2010-03-22-19:57	5.8	120.751	18.429	17	7
9	2010-11-05-16:40	5.8	122.897	12.825	19	8
10	2011-02-17-22:20	5.0	120.480	16.452	14	7
11	2011-05-21-13:08	5.1	121.891	17.186	13	7
12	2011-11-07-09:43	4.9	125.000	7.900	1	6

Sequence number	DateTime (UTC) (YYYY-MM-DD-hh:mm)	Magnitude	Longitude	Latitude	Depth	Number of Records
13	2012-02-06-03:49	6.7	123.260	10.030	12	25
14	2012-03-05-23:05	5.2	123.630	12.400	23	20
15	2012-02-06-10:10	6.0	123.150	9.930	12	7
16	2012-08-31-12:45	7.6	127.000	11.020	45	14
17	2012-09-03-19:44	5.6	124.960	7.890	3	5
18	2012-09-03-19:52	4.9	125.000	7.750	3	5

Total Records: 173

3.4.3 Computing True Ground Motion and Response Spectra

Seismic instrumentation of PSN is mostly composed of three-component velocity sensors with their digitized raw data traditionally archived in digital counts; a sample of raw waveform is shown in Figure 3.14. The equivalent true ground motion can be derived by data transformation together with the appropriate instrument response. Figure 3.15 shows the combined magnification and phase angle response of the Teledyne Geotech SS-1short-period velocity-type sensor and Kelunji digitizer.

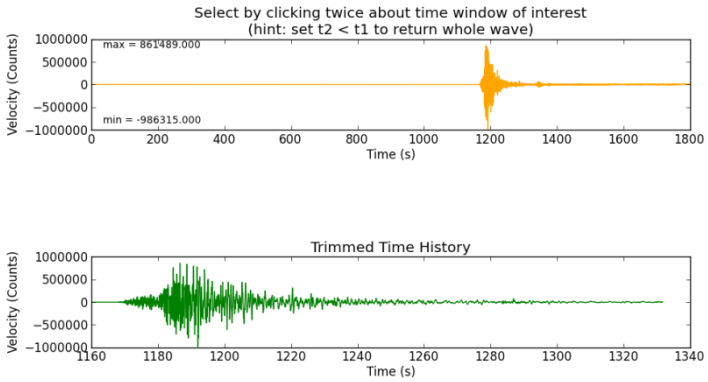

Figure 3.14. Raw velocity waveform from one of PSN seismic station.

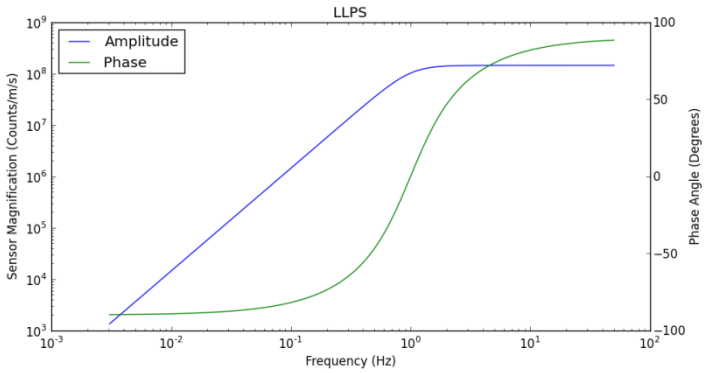

Figure 3.15. Instrument response for short-period velocity-type sensor of PSN seismic station.

Using Fast Fourier Transform (FFT), the recorded time-series is transformed to its equivalent spectral form in the frequency domain. True ground motion can then be computed by deconvolving the instrument response from the recorded time history:

$$G(f) = \frac{R(f)}{I(f)}$$

where **I(f)** is the instrument response function, **R(f)** is the recorded waveform, and **G(f)** is the true ground motion (e.g. displacement or velocity or acceleration spectral amplitude) as a function of frequency, f, respectively. The geometric mean of the two horizontal components was then calculated in the spectral domain. Displacement, velocity and acceleration spectral amplitudes can be computed from each other by differentiation and integration in frequency domain given by

$$A(f) = 2\pi f V(f)$$
$$D(f) = V(f)/2\pi f$$

where **A(f), V(f), D(f)** are acceleration, velocity, and displacement, respectively. The instrument-corrected spectra were transformed back to the displacement, velocity and acceleration time histories using Inverse Fast Fourier Transform (IFFT). Absolute maximum values were directly obtained to get the peak ground displacement (PGD), peak ground velocity (PGV), and peak ground acceleration (PGA) from each time series. Pseudo-response spectral acceleration (PSA) shows the maximum motion of a single degree of freedom structure with various damping when subjected to ground accelerations at the base. The PSA with 5% damping was calculated for selected vibration periods. The whole process is summarized in Figure 3.16.

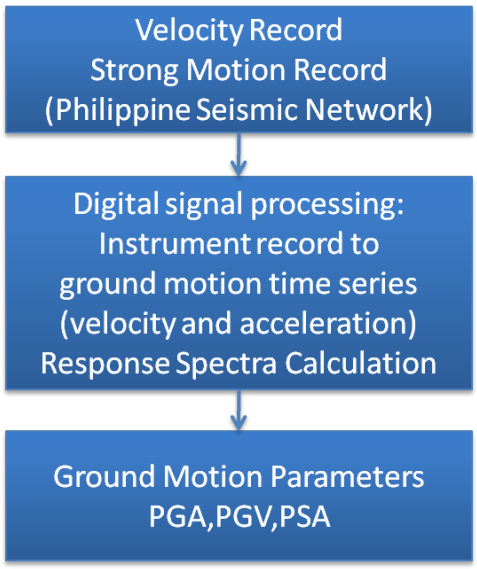

Figure 3.16. Computation flow for the calculation of ground-motion intensities.

3.4.4 Comparison of Data to GMPEs

A Ground Motion Prediction Equation (GMPE) mathematically depicts the attenuation of the median level of ground shaking generated by an earthquake as it propagates away from its source. It generally relates the ground-motion parameter of interest to one or more parameters of earthquake source, wave propagation path and local site conditions. Most of the established GMPEs were empirically derived from records of strong ground motion resulting from natural earthquakes in specific regions or tectonic regimes. Depending on the datasets used to derive a particular GMPE, each equation has its own limitations and applicability. This report investigated several GMPEs with particular attention to those whose datasets were derived from areas having a similar tectonic setting as the Philippines. This study used GMPEs published by Akkar & Bommer (2010), Ambraseys et al.(2005), Boore & Atkinson (2008), Chiou & Youngs (2008), Fukushima & Tanaka (1990), Kanno et al. (2006), Sadigh et al. (1997), and Zhao et al. (2006).

Table 3.3. Summary of GMPE evaluated in this study.

Study Authors	Abbreviation	Supported Outputs (Ground Motion Parameters)
Akkar & Bommer (2010)	Akkbom10	PGA,PGV, RSA (0.05 s, 0.10 s, 0.15 s, …, 3.00 s)
Ambraseys et. al. (2005)	Amb05	PGA, RSA (0.050 s, 0.055 s, 0.060 s, …, 1.100 s)
Boore & Atkinson (2008)	Booatk08	PGA, PGV, RSA(0.010 s, 0.020 s, 0.030 s, …, 10.000s)
Chiou & Youngs (2008)	Chiyou08	PGA, PGV, RSA (0.01 s, 0.02 s, 0.03 s, …, 10 s)
Kanno et. al.(2006)	Kan06	PGA, PGV, RSA (0.05 s, 0.06 s, 0.07 s, …, 5.00 s)
Sadigh et. al. (1997)	Sadigh97	PGA, RSA (0.07 s, 0.10 s, 0.20 s, …, 4.00 s)
Zhao et. al. (2006)	zha06	PGA, RSA (0.05 s, 0.10 s, 0.015 s, …, 5.00 s)
Fukushima and Tanaka (1990)	fuktan90	PGA

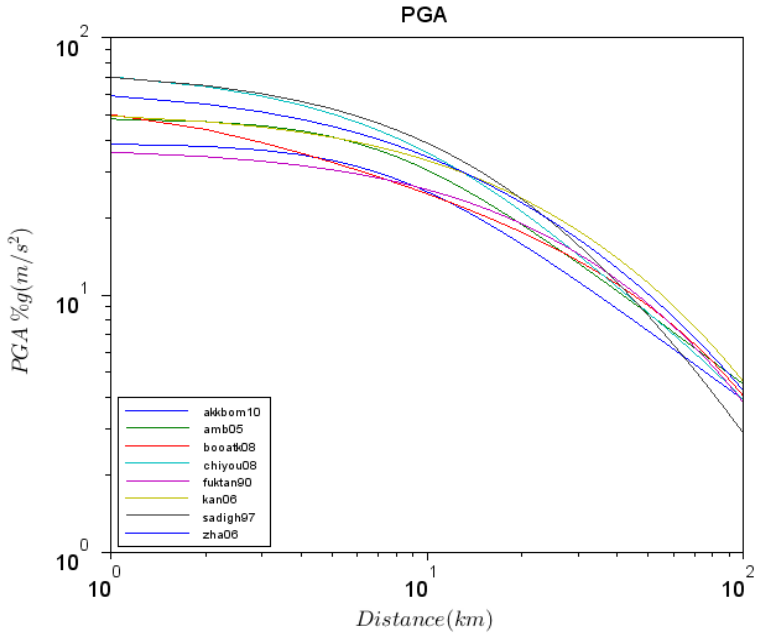

Figure 3.17. Ground Prediction Equations used in this study.

Ground motion models listed in Table 3 are coded up based on their published functional form and coefficients. Ground motion levels such as PGV, PGA and SA can then be computed using the following as input values: (1) earthquake parameters of the recorded event: that is the earthquake magnitude and mechanism, (2) site-to-rupture distance, which is assumed to be the distance from the epicentre to the recording site, and (3) the site class, in this case, assumed to be a rock site (VS30 = 750 m/s) for which most of the stations of PSN are situated. Then the residuals of each computed ground motion level to the actual data is computed as:

$$r = \log \frac{Y_{observed}}{Y_{predicted}}$$

where **Y** could be PGV, PGA or PSA at different natural vibration periods. Sample residual plots of PGA for each GMPE model are shown in Figure 3.18. Other plots for different natural vibration periods are available in Appendix H.

Residual data were binned into classes of 20-km distance intervals and the median was derived from each class interval and compared with the GMPEs in Figure 3.19. Data points falling beyond 200 km from the epicentre were not included in the analysis given that most of the GMPEs are valid only up to this distance. Results suggest that Philippine short-period ground-motions appear to attenuate at faster rates (at distances > 100 km) than is predicted by global models used commonly in hazard assessments. Furthermore, despite much larger variability among models the attenuation of Philippine ground motions at longer periods shows no obvious bias with distance (to at least 200 km).

For the GMMA-RAP, we are mostly concerned with near-source sites within 60 km of the earthquake source. Because the fragility curves in the engineering vulnerability component are tied to PGA, we chose to determine which of the candidate GMPEs are most appropriate to this ground-motion

parameter. Hence, in order to rank the candidate models, the median residuals for each GMPE are computed for a 60-km distance interval and are shown in Table 4.

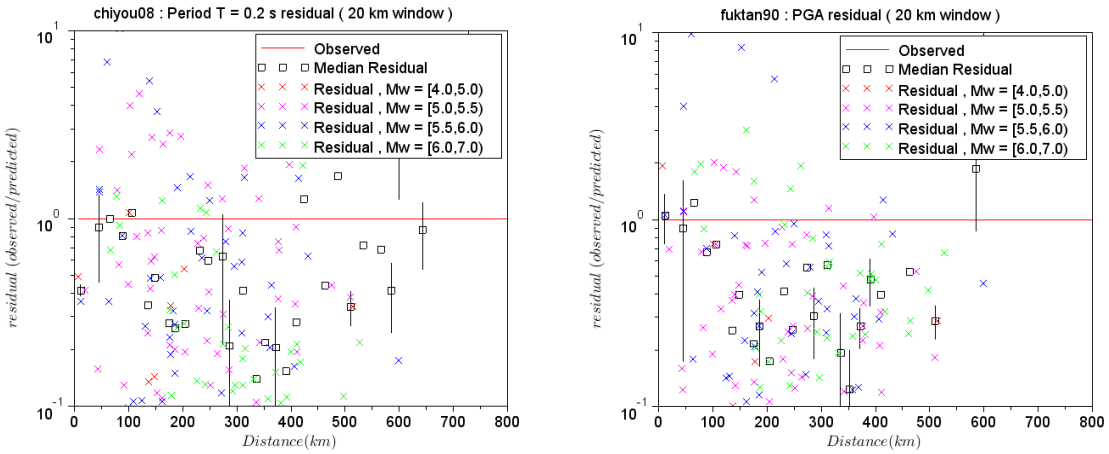

Figure 3.18. Residual plots for PGA computed using Fukushima& Tanaka (1990) (right) and Chiou & Youngs (2008) (left). Median residual are also plotted with corresponding error bars.

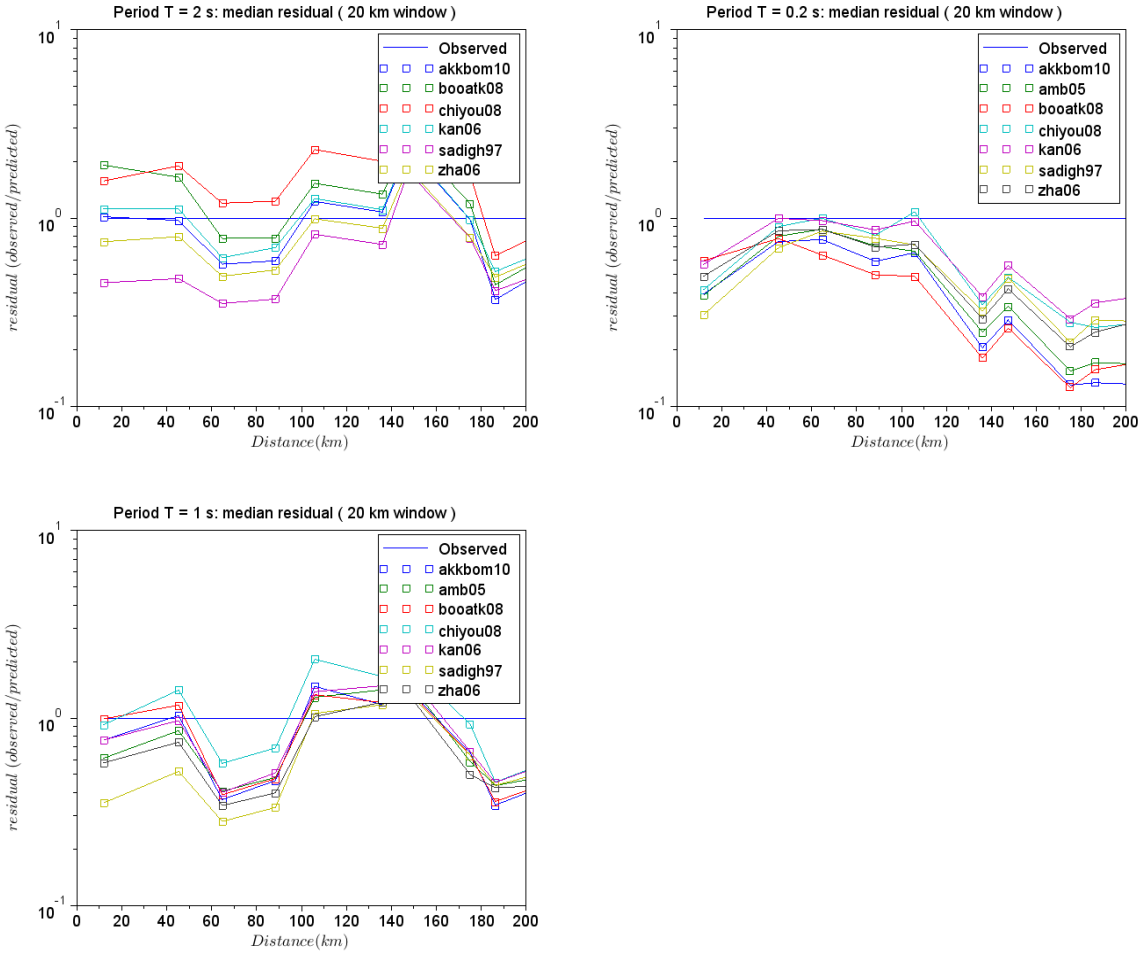

Figure 3.19. Median residual for PGA and PSA (periods 0.2 s, 1 s, 2 s) at 20 km intervals.

Table 3.4. GMPEs ranked based on residual analysis of observed and predicted PGA. Mean and median values are calculated based on 25 earthquake time histories with a source-to-site distance of less than 60 km. Those GMPEs highlighted in bold are Boore & Atkinson (2008), Chiou & Youngs (2008), Fukushima & Tanaka (1990) and Sadigh et al. (1997).

GMPE	mean log10 residual	median log10 residual	Standard Deviation	abs(median log10 residual)
fuktan90	**-0.108**	**0.032**	**0.514**	**0.032**
sadigh97	**-0.075**	**0.038**	**0.497**	**0.038**
chiyou08	**-0.019**	**0.067**	**0.474**	**0.067**
booatk08	**-0.005**	**0.096**	**0.523**	**0.096**
akkbom10	0.033	0.121	0.479	0.121
amb05	0.019	0.140	0.491	0.140
zha06	0.040	0.145	0.495	0.145
kan06	0.098	0.181	0.489	0.181

4 Methods

4.1 Hazard calculation

4.1.1 Peak Ground-Motion to Intensity conversions

While the GMPEs discussed above model the attenuation of recorded instrumental ground-motions, macroseismic scales fundamentally simplify communicating earthquake hazard and risk, especially in comparison with standard seismological or engineering metrics. Furthermore, the advantage of using macroseismic ground-shaking metrics in earthquake impact assessments is that earthquake damage functions derived from physical properties of structures and experimental data are not uniformly available for all global structure types, particularly in the developing world (Allen et al., 2012).

The above statement is also true of the GMMA RAP. The UPD-ICE team charged with the development of the earthquake fragility curves was able to develop so-called analytical fragility curves based on peak ground motions for many common engineered structures. However, for older and non-engineered structure types, the UPD-ICE team was limited to developing fragility curves using macroseismic intensity.

Output intensities from model predictions can be very sensitive to the GMPE and ground-motion to intensity conversion equation (GMICE) combination (Allen and Wald, 2009). Consequently, it is important that the earthquake fragility curves used in the RAP are developed using the same GMICE as is used to calculate the hazard calculation. For this study, the Worden et al. (2012) GMICE was employed. This relationship is based on several thousand ground-motion-intensity pairs and has been found to work well when compared to global data.

To generate the ground shaking intensity for GMMA, we used the West Valley Fault as the causative fault for the ground shaking simulations. The MMEIRS (2004) report suggests that this fault will cause the greatest damage in Metro Manila should it generate an earthquake of M7.2, the estimated maximum size. We also considered the most probable earthquake, which is a M6.5, based on the disaggregation study by PHIVOLCS to identify events that impact GMMA significantly. These two scenario events will allow us to evaluate their relative impacts to GMMA, hence providing critical guides for emergency response and mitigation planning. We used REDAS to model the ground shaking intensity. Inputs to the modeling processes include VS30 for the amplification factor and the faulting parameters of scenario earthquakes. Table 4.1 lists the faulting parameters based on the August 19, 1658 event, which has been suggested to occur on the West Valley Fault (Bautista, 2000).

Table 4.1. Earthquake parameters used in ground shaking modelling.

Epicenter	Depth (km)	Magnitude	Style of faulting
14.65N, 121.087E	5	M7.2 and M6.5	Strike Slip

Figure 4.1 shows the ground shaking intensities in PEIS for both scenario earthquakes. Both simulation results show maximum intensity of high VIII, specifically in the Marikina plain regions

adjacent to the West Valley Fault and on the coastal plain in the west underlying Pasig. The intensity distribution clearly reflects the effect of the underlying geology on the amplification of seismic motion.

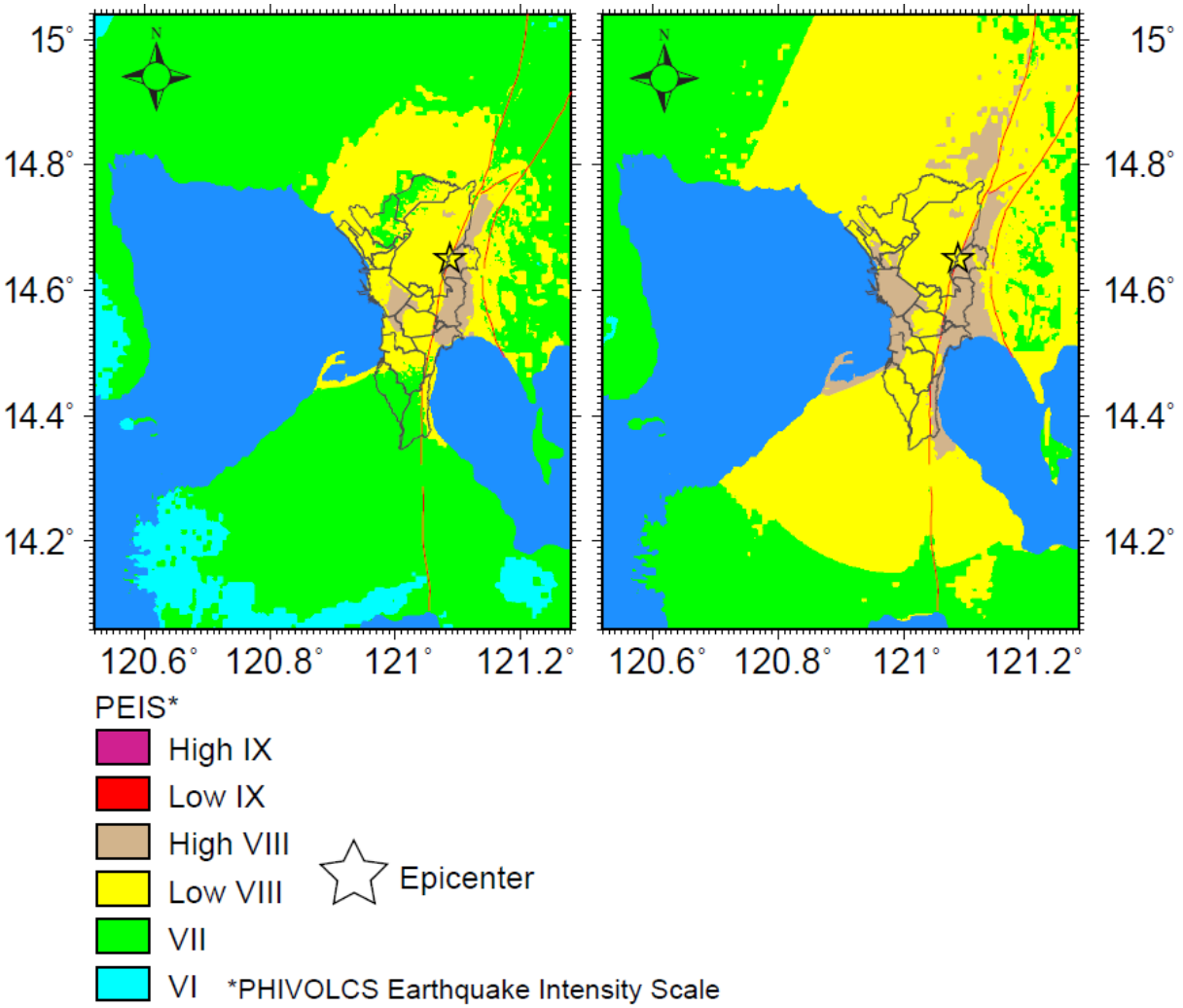

Figure 4.1. Ground shaking model for a M6.5 (left) and M7.2 (right) West Valley Fault Scenario earthquakes. Intensities are expressed in PEIS.

4.2 Earthquake Impact Assessments

4.2.1 Damage assessment of the built environment

The GMMA-RAP Exposure Component has developed a database of building floor areas per building types for over 85,000 different land use polygons (refer to Exposure Information Development report). The floor areas for the different building types are further subdivided by building height subclasses. Unlike the grid-based approach used in the QuiveR study (Bautista et al., 2012), the aggregate floor area for each building type is collapsed to the polygon centroid. Subsequently, the reference ground-motion intensity calculated by REDAS for each scenario damage assessment is taken at the centroid of the polygon. Because the land-use polygons described in the exposure report are generally quite

small, it not expected that ground-motions would vary significantly across any given polygon. Therefore, we do not expect that this decision will affect loss estimates for the GMMA-RAP.

Building fragilities for the GMMA-RAP were developed through a combination of analytical and expert judgment processes. Seismic vulnerability and fragility curves are used to assess the performance of a structure subjected to an earthquake. Seismic fragility curves are used to describe the performance of an engineering component or system subjected to earthquake excitations in probabilistic terms. They represent the probability of exceeding different damage states given the ground shaking intensity. Damage is usually categorised into discrete damage states: namely, Slight, Moderate, Extensive and Complete (NIBS-FEMA, 2011).

The seismic fragility curve is approximated by a lognormal cumulative distribution function shown in equation:

$$P\left[ds \mid S_d\right] = \Phi\left[\frac{1}{\beta_{ds}} \ln\left(\frac{S_d}{\bar{S}_{d,ds}}\right)\right]$$

where:

- $P\left[ds \mid S_d\right]$ is the probability that a damage state ds is reached or exceeded for a given spectral displacement Sd;
- Φ is the standard normal cumulative distribution function;
- β_{ds} is the standard deviation of the natural logarithm of damage state, ds; and
- $S_{d,ds}$ is the median value of spectral displacement at which the building reaches the threshold of the damage state, ds.

Fragility curves for Philippine building types considered in the GMMA-RAP are provided by UPD-ICE (UPD-ICE, 2013). The curves are developed to encompass the variability associated with different building height and vintage categories. In addition to the fragility curves, vulnerability curves were also developed (UPD-ICE, 2013). Vulnerability curves describe the loss ratio (i.e. ratio of repair cost to building replacement value) as a function of the ground shaking. These curves are useful for obtaining a financial loss estimate for our earthquake scenarios. The full mapping of building types and the associated fragility/vulnerability models is provided in Appendix I.

The exposure database provides an estimate of the predominant era of construction for in a given land use polygon (e.g., Pre-1972, 1972-1992, Post-1992, and No Development). Depending on the era of construction period assigned to the polygon, different fragility and vulnerability functions are used that are appropriate to that era category.

Following the criteria outlined above, the probability that a given structure type (with height and vintage considered) being in a given damage state for a given ground-shaking intensity is estimated. The total floor area of the combined building types being in a given damage state (i.e. slight, moderate, extensive and complete) is then summed for each land-use polygon. The proportional floor area in any damage state can then be calculated by simply dividing by the total floor area of all buildings in each polygon. Whilst this representation can be informative, it can also be misleading when mapping the estimated damage, particularly for emergency response. For example, a rural polygon, which may have a relatively small total floor area comprised within a large spatial area might have the same proportional damage as a dense urban polygon. However, the number of people

affected will be considerably different, and in an emergency situation, emergency services should be directed to the regions of the highest consequence. Consequently, the proportional damage that is calculated herein should be normalized by the total land area of the polygon to determine the emergency response or disaster mitigation priorities. In this report, we refer to losses normalized by the polygon footprint as “damaged floor area equivalent”. A worked example on how losses were estimated in this study is provided in Appendix J.

The approach for prioritising emergency response and mitigation programs indicated above is appropriate for residential areas. However, it will artificially reduce the apparent consequences to critical facilities that may be located in large land use polygons (e.g. airports, hospitals, schools, water and power generation utilities, etc.). For this reason, it is important to evaluate the damage to these facilities on a case-by-case basis.

Each polygon in the exposure database has a number of attributes to enable loss aggregation to a larger spatial extent. Loss estimates in this study can be aggregated to barangay or Local Government Unit (LGU), for example.

4.2.2 Casualty modelling

A key concern in disaster management in any earthquake impact assessment is provision of an estimate of the human impact in terms of the number of casualties (fatalities and injuries). Since we implement a framework for computing building damage that calculate the probability of a building being in a given damage state, we are able to undertake more sophisticated analyses to estimate the number of casualties resulting from scenario earthquakes using the HAZUS framework (NIBS-FEMA, 2011).

The primary cause of fatalities in earthquakes is due to the collapse of buildings. HAZUS prescribes a complex logic to estimate casualties from earthquakes, which considers factors such as building occupancy with time of day, building collapse rates for a given building type in a complete damage state, and the probability of being in a given casualty severity state, given the damage state of the building. HAZUS defines four casualty severity levels ranging from minor injuries, non-life threatening injuries requiring medical treatment, casualties that require immediate medical treatment to avoid death, to immediate death.

In the present framework, we estimate the number of casualties for each casualty level resulting from the earthquake. Each building type has specific casualty rates for a given level of building damage (slight, moderate, extensive and complete). Additionally, buildings in the complete damage state are further subdivided into collapse and non-collapse. Casualty rates for the four severity levels, as defined by HAZUS, are modified for the Philippine building classifications used in this study. Casualty rates are provided in Appendix J. Since there are no time-dependent population density models for the GMMA, for the casualty modelling purposes, we assume that the entire population is indoors in residential dwellings.

4.3 Scenario 1: Mw 7.2 on the West Valley Fault

Table 4.1. Building damage per LGU (expressed as the sum of Floor Area in m² for each damage state) for a Mw 7.2 scenario.

Municipality	Area (m²)	Slight Damage (m²)	Moderate Damage (m²)	Extensive Damage (m²)	Complete Damage (m²)	Complete Collapse (m²)
Angono	22071349.33	234789.00	377051.00	313024.00	426421.00	57443.00
Antipolo	156685484.57	1504551.00	2293390.00	1919395.00	2814156.00	358508.00
Cainta	14408181.87	610464.00	1226907.00	1450371.00	2290627.00	317201.00
Caloocan	53201841.33	3479806.00	5232422.00	4087406.00	5072855.00	625656.00
Manila	42882802.65	4010957.00	8103927.00	9825526.00	11969904.00	1385187.00
Las Piñas	32020293.07	1898996.00	3036596.00	2420619.00	2990543.00	405359.00
Makati	21731876.50	2239323.00	4291520.00	4261247.00	6223243.00	638784.00
Malabon	15963229.44	1012122.00	1670251.00	1477221.00	1960091.00	227640.00
Mandaluyong	11067798.07	1199782.00	2063208.00	1912450.00	2249883.00	253941.00
Marikina	22646525.80	1214505.00	2396756.00	2707179.00	4003510.00	548329.00
Muntinlupa	41676056.26	1736660.00	3020253.00	2877665.00	3845083.00	476436.00
Navotas	11518068.53	394736.00	707097.00	709673.00	1016382.00	117412.00
Parañaque	47289914.56	2897909.00	4893277.00	4307947.00	5149340.00	681479.00
Pasay	18645495.82	1096852.00	2129076.00	2479783.00	3062884.00	368315.00
Pasig	31464094.80	2213476.00	4156819.00	4708861.00	6922002.00	856014.00
Pateros	1764232.94	83141.00	167761.00	222650.00	472378.00	58103.00
Quezon	165330828.80	11049945.00	17663877.00	14187637.00	15414694.00	1997221.00
Rodriguez	111327167.06	527945.00	951000.00	950853.00	1417909.00	200048.00
San Juan	5879833.98	699746.00	1156132.00	951902.00	920029.00	114219.00
San Mateo	55819846.00	478758.00	910088.00	989324.00	1535712.00	217693.00
Taguig	45183557.79	2014723.00	3373491.00	3300500.00	4594379.00	532398.00
Taytay	28326798.61	883461.00	1466373.00	1356222.00	2104007.00	259143.00
Valenzuela	45751215.96	3321678.00	4786840.00	3073094.00	2633301.00	356300.00
SUM		44,804,325	76,074,112	70,490,549	89,089,333	11,052,829

Table 4.2. Building damage per LGU (expressed as rate per km² for each damage state) for a Mw 7.2 scenario.

Municipality	Slight Damage (per km²)	Moderate Damage (per km²)	Extensive Damage (per km²)	Complete Damage (per km²)	Complete Collapse (per km²)
Angono	29.13	46.88	39.65	55.97	7.57
Antipolo	39.65	63.48	53.55	71.96	9.22
Cainta	34.19	69.54	84.33	127.89	17.02

Municipality	Slight Damage (per km²)	Moderate Damage (per km²)	Extensive Damage (per km²)	Complete Damage (per km²)	Complete Collapse (per km²)
Caloocan	1965.12	3429.84	3286.26	3903.12	491.24
Las Piñas	9353.81	18575.63	23075.20	30139.86	3655.72
Makati	121.59	197.05	166.12	221.85	28.89
Malabon	296.16	568.10	604.68	862.28	99.96
Mandaluyong	137.88	231.76	219.27	331.21	36.79
Manila	310.29	530.59	493.01	573.31	71.18
Marikina	84.94	167.60	192.93	287.42	39.14
Muntinlupa	37.14	65.25	64.39	91.56	11.05
Navotas	90.87	160.17	160.97	239.18	26.69
Parañaque	98.60	168.80	154.88	191.49	24.84
Pasay	1788.46	3553.00	4478.41	6854.11	841.55
Pasig	216.26	397.30	453.79	736.79	89.13
Pateros	46.61	95.88	129.03	264.20	33.73
Quezon	1426.42	2313.44	1918.60	2049.09	277.89
Rodriguez	15.91	31.60	36.03	58.46	8.36
San Juan	256.43	429.46	364.25	384.56	45.04
San Mateo	27.39	54.32	61.79	98.69	14.20
Taguig	146.77	256.77	259.67	381.23	46.42
Taytay	17.06	28.95	27.31	41.95	5.13
Valenzuela	209.92	321.37	230.37	218.96	29.88
SUM	16,751	31,757	36,554	48,185	5,911

Table 4.3. Economic loss per LGU for a Mw 7.2 scenario.

Municipality	Loss (millions of pesos)
Angono	8797.00
Antipolo	52527.00
Cainta	45306.00
Caloocan	119027.00
Las Piñas	400031.00
Makati	70436.00
Malabon	234339.00
Mandaluyong	41751.00
Manila	76352.00
Marikina	87926.00
Muntinlupa	101281.00

Municipality	Loss (millions of pesos)
Navotas	20429.00
Parañaque	131392.00
Pasay	100406.00
Pasig	190686.00
Pateros	7263.00
Quezon	449214.00
Rodriguez	28559.00
San Juan	31760.00
San Mateo	29263.00
Taguig	118643.00
Taytay	39483.00
Valenzuela	87908.00
SUM	2,472,779

Table 4.4. Economic loss per LGU (expressed as rate per km²) for a Mw 7.2 scenario.

Municipality	Loss (millions of pesos per km²)
Angono	11443.90
Antipolo	15026.87
Cainta	28458.87
Caloocan	1174491.09
Las Piñas	8141569.65
Makati	49820.16
Malabon	267014.95
Mandaluyong	62002.21
Manila	170283.22
Marikina	65143.79
Muntinlupa	22627.17
Navotas	45714.86
Parañaque	49236.45
Pasay	1578074.34
Pasig	190826.50
Pateros	43075.54
Quezon	591784.76
Rodriguez	12410.13
San Juan	132508.64
San Mateo	19256.07

Municipality	Loss (millions of pesos per km²)
Taguig	79327.67
Taytay	7880.22
Valenzuela	68131.81
SUM	12,826,109

Table 4.5. Casualties per LGU for a Mw 7.2 scenario.

Municipality	Slight Injuries	Serious Injuries	Life-threatening Injuries	Fatalities
Angono	2303	659	64	179
Antipolo	25665	7427	910	2030
Cainta	13040	4044	536	1239
Caloocan	41243	11567	1295	3114
Las Piñas	62895	18845	2775	5449
Makati	19231	5582	616	1491
Malabon	15458	4670	609	1427
Mandaluyong	10325	3046	403	874
Manila	10271	3001	392	817
Marikina	18129	5511	657	1617
Muntinlupa	16259	4677	514	1206
Navotas	9344	2733	354	740
Parañaque	18616	5396	496	1385
Pasay	12977	3641	565	1117
Pasig	25649	7908	1135	2387
Pateros	2747	834	117	239
Quezon	73549	20871	2232	5524
Rodriguez	6911	1882	229	553
San Juan	3667	1046	105	306
San Mateo	9760	2878	369	828
Taguig	29529	8700	1018	2366
Taytay	12648	3646	411	997
Valenzuela	15656	4398	468	1169
SUM	455,872	132,962	16,270	37,054

Table 4.6. Casualties per LGU (expressed as rate per km²) for a Mw 7.2 scenario.

Municipality	Slight Injuries (per km²)	Serious Injuries (per km²)	Life-threatening Injuries (per km²)	Fatalities (per km²)
Angono	2688.56	780.04	87.11	215.10
Antipolo	8153.96	2382.87	305.79	662.53
Cainta	4702.94	1468.81	165.73	440.63
Caloocan	297251.14	88303.99	12644.96	26830.97
Las Piñas	2283791.02	690714.69	105456.69	205446.39
Makati	14850.86	4367.86	526.19	1161.00
Malabon	38129.26	11652.19	1585.68	3617.75
Mandaluyong	17460.07	5170.63	692.91	1438.95
Manila	35130.56	10507.52	1462.13	3096.78
Marikina	12660.37	3865.69	476.36	1154.65
Muntinlupa	4118.54	1187.04	136.96	301.83
Navotas	22433.26	6549.53	864.04	1810.73
Parañaque	6778.37	1980.05	202.94	515.06
Pasay	395332.39	104264.89	17965.51	32835.88
Pasig	37020.27	11460.46	1645.82	3428.12
Pateros	15391.05	4690.89	679.24	1368.03
Quezon	88620.92	25748.54	2997.37	7327.68
Rodriguez	2770.61	802.57	109.42	237.35
San Juan	16564.76	4813.98	491.42	1359.23
San Mateo	10093.77	3107.50	473.81	969.72
Taguig	32709.19	9708.47	1225.50	2681.28
Taytay	2589.29	749.42	85.53	206.65
Valenzuela	11597.55	3361.36	395.46	920.70
SUM	3,360,839	997,639	150,677	298,027

4.4 Scenario 2: Mw 6.5 on the West Valley Fault

Table 4.7. Building damage per LGU (expressed as Floor Area in m² for each damage state) for a Mw 6.5 scenario.

Municipality	Area (m²)	Slight Damage (m²)	Moderate Damage (m²)	Extensive Damage (m²)	Complete Damage (m²)	Complete Collapse (m²)
Angono	22071349.33	271353.00	373889.00	255195.00	317584.00	42420.00
Antipolo	156685484.57	1652637.00	2201994.00	1578586.00	2178067.00	275371.00
Cainta	14408181.87	724301.00	1340655.00	1371475.00	1883732.00	260987.00
Caloocan	53201841.33	3853199.00	4835351.00	3061767.00	3581438.00	432400.00

Municipality	Area (m²)	Slight Damage (m²)	Moderate Damage (m²)	Extensive Damage (m²)	Complete Damage (m²)	Complete Collapse (m²)
Las Piñas	32020293.07	2330099.00	2611438.00	1383304.00	1588286.00	211146.00
Makati	21731876.50	2403197.00	4279915.00	3737945.00	5105240.00	518920.00
Malabon	15963229.44	1149934.00	1603254.00	1125472.00	1384318.00	156396.00
Mandaluyong	11067798.07	1257346.00	2005898.00	1644127.00	1836853.00	205651.00
Manila	42882802.65	4550921.00	8333247.00	8297589.00	8903956.00	1023092.00
Marikina	22646525.80	1393716.00	2559335.00	2558779.00	3389267.00	463026.00
Muntinlupa	41676056.26	2225591.00	2568469.00	1479455.00	1687140.00	197819.00
Navotas	11518068.53	478276.00	730627.00	573558.00	713175.00	80224.00
Parañaque	47289914.56	3470505.00	4675064.00	3094234.00	3331421.00	433264.00
Pasay	18645495.82	1237666.00	2192608.00	2154446.00	2339074.00	280492.00
Pasig	31464094.80	2443651.00	4363918.00	4439840.00	5821393.00	717873.00
Pateros	1764232.94	95347.00	183913.00	220949.00	418197.00	51196.00
Quezon	165330828.80	11843158.00	16811157.00	11523553.00	12153898.00	1563506.00
Rodriguez	111327167.06	664438.00	995916.00	778375.00	970692.00	137418.00
San Juan	5879833.98	732786.00	1094751.00	774511.00	726194.00	89821.00
San Mateo	55819846.00	556324.00	970974.00	922857.00	1274334.00	180911.00
Taguig	45183557.79	2222938.00	3381051.00	2859322.00	3681368.00	419665.00
Taytay	28326798.61	1001138.00	1478649.00	1177188.00	1682381.00	204341.00
Valenzuela	45751215.96	3659665.00	4226508.00	2069224.00	1678128.00	223088.00
SUM		50,218,186	73,818,581	57,081,751	66,646,136	8,169,027

Table 4.8. Building damage per LGU (expressed as rate per km² for each damage state) for a Mw 6.5 scenario.

Municipality	Slight Damage (per km²)	Moderate Damage (per km²)	Extensive Damage (per km²)	Complete Damage (per km²)	Complete Collapse (per km²)
Angono	33.72	46.72	32.65	41.95	5.63
Antipolo	45.21	61.37	41.78	52.34	6.62
Cainta	40.47	76.02	79.52	104.18	13.84
Caloocan	2237.08	3388.92	2614.48	2806.98	349.16
Las Piñas	149.43	175.95	103.45	127.55	16.18
Makati	323.96	578.00	540.48	708.04	81.80
Malabon	159.71	228.76	172.38	237.13	25.63
Mandaluyong	330.15	518.69	422.83	464.33	57.49
Manila	10650.74	19250.82	19716.14	22832.41	2769.01
Marikina	97.06	178.97	182.98	244.08	33.18
Muntinlupa	48.10	58.47	36.15	43.33	4.96

Municipality	Slight Damage (per km²)	Moderate Damage (per km²)	Extensive Damage (per km²)	Complete Damage (per km²)	Complete Collapse (per km²)
Navotas	108.81	163.92	129.36	169.01	18.35
Parañaque	116.77	164.48	116.94	130.13	16.63
Pasay	2078.73	3803.31	4090.83	5450.34	669.34
Pasig	237.12	416.39	430.85	629.19	75.95
Pateros	53.67	105.44	128.24	233.35	29.70
Quezon	1525.02	2206.20	1563.12	1614.71	219.01
Rodriguez	20.98	35.91	32.30	41.99	6.02
San Juan	265.61	401.87	292.63	305.04	35.50
San Mateo	32.08	58.84	58.76	82.75	11.93
Taguig	165.65	258.87	224.10	301.88	36.48
Taytay	19.40	29.37	23.82	33.66	4.05
Valenzuela	239.12	296.63	162.27	139.70	18.83
SUM	18,979	32,504	31,196	36,794	4,505

Table 4.9. Economic loss per LGU for a Mw 6.5 scenario.

Municipality	Loss (millions of pesos)
Angono	6867.00
Antipolo	41417.00
Cainta	39554.00
Caloocan	86882.00
Las Piñas	38950.00
Makati	199832.00
Malabon	30167.00
Mandaluyong	64154.00
Manila	318391.00
Marikina	78001.00
Muntinlupa	48250.00
Navotas	15292.00
Parañaque	91262.00
Pasay	81218.00
Pasig	168269.00
Pateros	6664.00
Quezon	362651.00
Rodriguez	21337.00
San Juan	25802.00

Municipality	Loss (millions of pesos)
San Mateo	25544.00
Taguig	98051.00
Taytay	32339.00
Valenzuela	59433.00
SUM	1,940,327

Table 4.10. Economic loss per LGU (expressed as rate per km²) for a Mw 6.5 scenario.

Municipality	Loss (millions of pesos per km²)
Angono	8969.56
Antipolo	11189.35
Cainta	24727.54
Caloocan	898766.28
Las Piñas	29453.69
Makati	228635.63
Malabon	45545.28
Mandaluyong	142119.80
Manila	6512849.34
Marikina	57965.92
Muntinlupa	11469.67
Navotas	34066.16
Parañaque	35588.16
Pasay	1325699.50
Pasig	169295.78
Pateros	39501.50
Quezon	477900.29
Rodriguez	9871.76
San Juan	106510.15
San Mateo	17031.77
Taguig	65153.58
Taytay	6482.21
Valenzuela	47154.96
SUM	10,305,948

Table 4.11. Casualties per LGU for a Mw 6.5 scenario.

Municipality	Slight Injuries	Serious Injuries	Life-threatening Injuries	Fatalities
Angono	1789.00	494.00	40.00	122.00
Antipolo	20361.00	5785.00	702.00	1517.00
Cainta	11224.00	3436.00	416.00	1012.00
Caloocan	29999.00	8070.00	824.00	2045.00
Las Piñas	11256.00	2908.00	317.00	681.00
Makati	13085.00	3886.00	481.00	1130.00
Malabon	7731.00	2223.00	252.00	596.00
Mandaluyong	8760.00	2504.00	310.00	670.00
Manila	50437.00	14731.00	2152.00	4234.00
Marikina	15995.00	4776.00	522.00	1371.00
Muntinlupa	8996.00	2359.00	249.00	519.00
Navotas	7095.00	2050.00	235.00	536.00
Parañaque	12924.00	3357.00	291.00	742.00
Pasay	10533.00	2924.00	449.00	893.00
Pasig	22596.00	6868.00	954.00	2047.00
Pateros	2499.00	749.00	105.00	213.00
Quezon	60681.00	16743.00	1654.00	4209.00
Rodriguez	4857.00	1263.00	127.00	365.00
San Juan	2984.00	836.00	63.00	216.00
San Mateo	8346.00	2392.00	285.00	666.00
Taguig	24829.00	7162.00	781.00	1865.00
Taytay	10594.00	2960.00	308.00	769.00
Valenzuela	11390.00	3025.00	290.00	730.00
SUM	358,961	101,501	11,807	27,148

Table 4.12. Casualties per LGU (expressed as rate per km²) for a Mw 6.5 scenario.

Municipality	Slight Injuries (per km²)	Serious Injuries (per km²)	Life-threatening Injuries (per km²)	Fatalities (per km²)
Angono	2123.77	607.23	55.01	156.32
Antipolo	6233.34	1761.93	224.16	473.90
Cainta	4045.01	1223.38	128.58	356.69
Caloocan	226281.83	66073.55	9336.88	19266.42
Las Piñas	9485.27	2557.75	310.58	632.56
Makati	32414.10	9773.04	1288.13	2884.04
Malabon	13105.45	3781.98	437.68	990.41
Mandaluyong	29623.84	8562.26	1192.93	2532.04

Municipality	Slight Injuries (per km²)	Serious Injuries (per km²)	Life-threatening Injuries (per km²)	Fatalities (per km²)
Manila	1832612.39	540210.03	82547.79	160632.18
Marikina	11184.65	3362.13	385.20	979.82
Muntinlupa	2430.24	652.02	72.18	147.86
Navotas	16913.40	4905.38	582.84	1308.39
Parañaque	4947.78	1333.01	126.41	319.71
Pasay	319835.88	84205.61	14899.83	27037.15
Pasig	32979.16	10030.80	1429.41	2994.63
Pateros	14010.17	4217.30	595.98	1232.66
Quezon	72410.52	20498.23	2162.97	5591.67
Rodriguez	2056.72	580.38	72.02	173.47
San Juan	13627.85	3922.39	353.05	961.99
San Mateo	8753.40	2640.23	389.30	802.11
Taguig	26507.08	7692.28	904.92	2072.67
Taytay	2190.33	619.65	64.83	161.78
Valenzuela	8351.70	2285.98	242.42	574.41
SUM	2,692,124	781,497	117,803	232,283

5 Discussion

5.1 Discussion of earthquake risk results

The five damage states (slight, moderate, extensive, complete with no collapse of collapse as well as economic loss) were derived from the fragility curves and these were computed for a Magnitude 7.2 and for a Magnitude 6.5 earthquake scenario along the West Valley Fault. The earthquake vulnerability curves were used to compute for the four types of casualties (slight injuries, non-life threatening, life threatening and fatalities) and economic loss. Results are presented in terms of actual count and normalized according to barangay land area. The total results are 20 maps each for the Magnitude 7.2 scenario and another 20 maps for the Magnitude 6.5 scenario. For the Magnitude 7.2 scenario, Figures A.1 to A.10 will be the earthquake risk maps showing actual count while Figures B.1 to B.10 show risk maps with normalized values. In this case, normalization for physical damage in 10,000 square meter of floor area per one square kilometer barangay area. The normalization was suggested to account damage, economic loss and casualties with respect to the land area. The original results were presented in terms of land use but this was later revised when results were aggregated per barangay. Figures C.1 to C.10 show the actual count and Figures D.1 to D.10 for normalized values the Magnitude 6.5 scenario. The results are also tabulated per barangay. These are shown in Tables 4.1 to 4.6 for the Magnitude 7.2 scenario for both barangay-level and city-level results, respectively. For Magnitude 6.5, the results are presented in Tables 4.7 to 4.12, again for barangay-level and city-level, respectively.

Meanwhile, foregoing discussions will only be presented for Magnitude 7.2 scenario as the values generally show same peaks although the values are lower for the Magnitude 6.5 scenario. Also, only highlights will be discussed as possible reasons for high values differ and should be reviewed for each individual barangays. Possible reasons are large barangay area, presence of multi-storey structures that gives high number of floor area and pre-code era of construction. All those with peaks give a predominant C1 type of construction.

5.2 Physical Damage

For a Magnitude 7.2 event scenario, the high number of collapse in terms of floor area is found for Barangay Mayamot in Antipolo City, Barangay Rosario in Pasig City and Barangay BF Homes in Paranaque. For the three barangays, the high value may be due to their big barangay land area because when the values are normalized according to barangay land area size, the high values dissipated. Other high values are also found for Barangay Cupang also in Antipolo City, Barangays San Andres and San Isidro in Cainta, Barangay San Jose in Rodriguez, Barangays Manggahan in Pasig City. The above mentioned barangays came up under the “complete damage with no collapse” category. In addition, other barangays which came up with high values in the “complete damage with no collapse” category are Barangay Santa Ana in Taytay and in Metro Manila, in Barangays Bel-Air and San Lorenzo in Makati City, Barangays Alabang and Cupang in Muntinlupa, Barangay Bagumbayan in Quezon City and Barangay Fort Bonifacio in Taguig City.

The predominant Era of Construction classifications are Pre-1972 for the Makati barangays and Barangay Cupang in Muntinlupa City. Meanwhile the rest of the barangays have 1972-1992 Era of Construction except for the Taguig City barangay of Fort Bonifacio which has a predominant Post-1992 Era of Construction category. The high values may again be attributable to big land areas, predominant era of construction and presence of many high rise structures resulting in total large floor areas. Again, when the values were normalized according to barangay land areas, the values dissipate. Interestingly, one barangay which is Barangay 544 in the City of Manila, showed no damage and no casualties. A review would show that the barangay as per barangay boundary only hosts a vacant lot.

5.3 Casualties

For a similar earthquake magnitude (Magnitude 7.2) scenario, the highest numbers of fatalities are found from among the same barangays where the “collapse” and “complete damage with no collapse” categories are found. These are Barangays Cupang and Mayamot in Antipolo City, Barangays San Andres and San Isidro in Cainta and Barangay Rosario in Pasig City. One barangay, Batasan Hills, in Quezon City consistently came out from fatalities to injuries categories despite it not being prominent in damage list. A possible explanation could be its high population count. Barangays Cupang and Mayamot in Antipolo City came out consistently from injuries to fatalities list, possibly due to its barangay land area size. Again, when normalized according the high values for these big barangays dissipated. Meanwhile, what came out are peaks for small-sized barangays notably pronounced in the high-density area of old like in the City of Manila.

5.4 Economic Loss

The barangays which registered the high economic loss were for Barangays San Lorenzo and Bel-Air both in Makati City, Barangay San Antonio in Pasig City, Barangay Bagumbayan in Quezon City and Barangay Fort Bonifacio in Taguig City. The abovementioned two Makati barangays only figured prominently under the “complete damage with no collapse” category. Both had predominant pre-1972 era of construction. When normalized, the two barangays still retained their prominence in normalized economic loss category. The Pasig City barangay of San Antonio, only came up prominently in the slightly damage category. Despite this, it came up high as among the top five in the economic loss. It is possible that some buildings in this barangay suffered also severe damage other than just “slight damage”. When normalized, the barangay again came up prominent. The two other barangays, Barangay Bagumbayan in Quezon City and Barangay Fort Bonifacio in Taguig City, initially came up in the “complete damage with no collapse” category. Just like the other barangays, the two barangays show up even in normalized map version.

The abovementioned barangays which sustained the highest economic losses were not from the barangays which registered the highest number of collapsed category. A major factor could be the possible high replacement costs for these highly urbanized barangays rather than the count of total floor area damaged.

5.5 General Observations

The interpretation of these earthquake risk results should be done with caution especially when presenting to local government units and other stakeholders. It should be emphasized that the results are indicative only and came from an exposure database derived from a statistical approach and from vulnerability curves derived from a population of buildings types. Results can be improved if the exposure database can be further enhanced with the help of LGUs through more field validation or through provision of actual local data. For example, building types per barangay and population per building if can be provided by LGUs can improve results of physical damage and casualties. Economic loss can also be improved if LGU can provide local replacement costs. The advantage of this work is that the methodology was shared to PHIVOLCS by GA and who now can use it to teach other stakeholders or apply to other areas in the Philippines.

6 Acknowledgements

Eric Thompson of Tufts University is thanked for providing initial guidance on developing a geotechnical database schema. Most of the maps in this report were produced using Generic Mapping Tools (Wessel and Smith, 1991).

7 References

Abeki N., T. Enomoto, T. Kobayashi, R. S. Punongbayan, B. C. Bautista, A. G. Lanuza, and I. C. Narag, 1994. On the dynamic characteristics in the area around Dagupan City by Microtremor Observation. In Proceedings of IRTC Civil Engineering Conference.

Aki, K., and P. G. Richards, 2002. Quantitative Seismology, 700 pp. University Science Books, Sausalito, CA, United States (USA).

Akin, M. K., S. L. Kramer, and T. Topal, 2004. Empirical correlations of shear wave velocity (Vs) and Penetration Resistance (SPT-N) for different soils in an earthquake-prone area (Erbaa-Turkey). Engineering Geology, 119, 1–17.

Akkar, S., and J.J. Bommer, 2010. Empirical Equations for the Prediction of PGA , PGV, and Spectral Accelerations in Europe, the Mediterranean Region, and the Middle East. Seismological Research Letters Vol. 81, No. 2, pp. 195-206 March/April 2010.

Allen, T. I., and D. J. Wald, 2009. Evaluation of ground-motion modeling techniques for use in Global ShakeMap: a critique of instrumental ground-motion prediction equations, peak ground motion to macroseismic intensity conversions, and macroseismic intensity predictions in different tectonic settings. U.S. Geological Survey Open-File Report 2009-1047 114.

Allen, T. I., and D. J. Wald, 2009. On the use of high-resolution topographic data as a proxy for seismic site conditions (VS30). Bull. Seism. Soc. Am. 99, 935–943.

Allen, T. I., D. J. Wald, and C. B. Worden, 2012. Intensity attenuation for active crustal regions. J. Seismol. 16, 409–433.

Ambraseys, N. N., J. Douglas, S.K. Sarma, and P.M. Smit, 2005. Equations for the Estimation of Strong Ground Motions from Shallow Crustal Earthquakes Using Data from Europe and the Middle East: Horizontal Peak Ground Acceleration and Spectral Acceleration. Bulletin of Earthquake Engineering, (2005), pp. 1–53.

Anderson, J. A., and H. O. Wood, 1925. Description and theory of the torsion seismometer. Bull. Seism. Soc. Am. 15, 1-72.

Asia Development Bank, 2009. Poverty in the Philippines: causes, constraints, and opportunities. Mandaluyong City, Philippines, Asian Development Bank, pp 124.

Aurelio, M. A., 2000. Shear partitioning in the Philippines: constraints from Philippine fault and global positioning system data. The Island Arc, 9, 584–597.

Barrier, E., P. Hunchon, and M. A. Aurelio, 1991. Philippine fault: a key to Philippine kinematics. Geology, 19, 32–35.

Bautista, B. C., et al., 1994. Site response evaluation of Eastern Metro Manila using microtremor observations. In Proceedings of the 9th Japan Earthquake Engineering Symposium.

Bautista, M. L. P., 1996. Estimation of the magnitude and epicenters of Philippine historical earthquakes. Master's thesis, Kyoto University, Kyoto, Japan.

Bautista, M. L. P., 2000. Destructive earthquakes that affected Metro Manila, Philippines from 1589 to 1999. In Proceedings of the International Workshop on the Integration of Data for Seismic Disaster Mitigation in Metro Manila, pp. 87–120.

Bautista, M. L. P., and K. Oike, 2000. Estimation of the magnitudes and epicenters of Philippine historical earthquakes. Tectonophys. 317, 137–169

Beyreuther, M., R. Barsch, L. Krischer, T. Megies, Y. Behr, and J. Wassermann, 2010. ObsPy: A Python Toolbox for Seismology. Seismological Research Letters, 81 (3), 530–533.

Bhaduri, B., E. Bright, P. Coleman, and J. Dobson, 2002. LandScan – locating people is what matters. Geoinformatics 5, 34-37.

BMGS, 1982. Geology and Mineral Resources of the Philippines, Vol. 1. Bureau of Mines and Geosciences, Ministry of Natural Resources.

Boore, D. M.,2004. Estimating Vs30 (or NEHRP Site Classes) from shallow velocity models (depths < 30 m). Bulletin of the Seismological Society of America, 94, 591–597.

Boore, D.M., and G.M. Atkinson, 2008. Ground-Motion Prediction Equations for the Average Horizontal Component of PGA, PGV, and 5%-Damped PSA at Spectral Periods between 0.01 s and 10.0 s. Earthquake Spectra, Vol. 24, No. 1, pp. 99–138, February 2008.

Building Seismic Safety Council (BSSC), 2004. NEHRP Recommended provisions for seismic regulations for new buildings and other structures, 2003 edition (FEMA 450). Building Seismic Safety Council, National Institute of Building Sciences, Washington, D.C.

Chiou, S.J., and R.R. Youngs, 2008. An NGA Model for the Average Horizontal Component of Peak Ground Motion and Response Spectra. Earthquake Spectra, Vol. 24, No. 1, pp. 173–215, February 2008.

Crowley, H., D. Monelli, M. Pagani, V. Silva, and G. Weatherill, 2011. OpenQuake User's Manual. Pavia, GEM Foundation 122.

Daligdig, J. A., 1996. Recent faulting and paleoseismicity along the Philippine Fault Zone, North Central Luzon, Philippines. Ph.D. thesis, Hiroshima University, Hiroshima, Japan.

Daligdig, J. A., R. S. Punongbayan, G. M. Besana, and N. Tun˜gol, 1997. The Marikina Valley Fault System: Active Faulting in Eastern Metro Manila. PHIVOLCS Professional Paper

Farr, T. G., and M. Kobrick, 2000. Shuttle Radar Topography Mission produces a wealth of data. EOS Trans. 81, 583-585.

Fukushima, Y., and T. Tanaka, 1990. A New Attenuation Relation for Peak Horizontal Acceleration of Strong Earthquake Ground Motion in Japan. Bulletin of the Seismological Society of America, Vol. 80, No. 4, pp. 757-782, August 1990.

Gervasio, F. C., 1968. The geology, structures, and landscape development of Manila and suburbs. The Philippine Geologist, 22, 178–192.

Grutas, R., and H. Yamanaka, 2012. Mapping the seismic site conditions in Metro Manila, Philippines based on microtremor measurements, topographic data and geomorphology. 9th International Conference on Urban Earthquake Engineering & 4th Asia Conference on Earthquake Engineering, Tokyo Institute of Technology, Tokyo, Japan.

Horspool, N., and H. Ghasemi, 2012. OpenQuake Workshop Tutorials for PHIVOLCS Workshop in Manila, Philippines 24-28 September 2012: Release Version of OpenQuake: 0.8. Canberra, Geoscience Australia 39.

Iwatate, T., and S. S. Dy, 2000. Seismic response evaluation of surface ground of Western Manila, Philippines. In Proceedings of Sixth International Conference on Seismic Zonation.

Kanno, T., A.Narita, N. Morikawa, H. Fujiwara, and Y. Fukushima, 2006. A New Attenuation Relation for Strong Ground Motion in Japan Based on Recorded Data. Bulletin of the Seismological Society of America, Vol. 96, No. 3, pp. 879–897, June 2006.

Martinez, M. M. L., and S. N. Williams, 1999. Basaltic andesite to andesite scoria pyroclastic flow deposits from Taal Caldera, Philippines. Journal of the Geological Society of the Philippines, 54 (1–2), 1–18.

Matsuda, I., T. Enomoto, E. L. Banganan, and I. C. Narag, 1998. Regional division of Metro Manila on the basis of geological and geomorphological conditions. Bull. Inst. Sci. Tech. Kanto Gakuin University, 25, 101–112.

Matsuda, I., T. Enomoto, and I. C. Narag, 2000. Regional division of Marikina Valley and Coastal Lowland, Metro Manila on the basis of soil condition. In Proceedings of the International Workshop on the Integration of Data for Seismic Disaster Mitigation in Metro Manila, pp. 43–62.

Matsuoka, M., K. Wakamatsu, K. Fujimoto, and S. Midorikawa, 2005. Nationwide site amplification zoning using GIS-based Japan engineering geomorphologic classification map. International Conference on Structural Safety and Reliability, 9, Rome, Italy, June 19-23, 2005, Proceedings: Rotterdam, Netherlands, Millpress 239-246.

MMEIRS, 2004. Earthquake impact reduction study for Metropolitan Manila, Republic of the Philippines. Tech. rep., Philippine Institute of Volcanology and Seismology.

Murray, A. S., and J. M. Olley, 2002. Precision and accuracy in the Optically Stimulated Luminescence dating of sedimentary quartz: A status review. Geochronometria, 21, 1–16.

Narag, I. C., et al., 2000. Microtremor observation of Metropolitan Manila. In Proceedings of the International Workshop on the Integration of Data for Seismic Disaster Mitigation in Metro Manila, 164.

National Institute of Building Sciences and Federal Emergency Management Agency, 2011. Multi-hazard loss estimation methodology, earthquake model, Hazus®–MH 2.0 technical manual. Washington, D.C., Federal Emergency Management Agency 736.

Nelson, A. R., S. F. Personius, R. E. Rimando, R. S. Punongbayan, N. Tuñgol, H. Mirabueno, and A. Rasdas, 2000. Multiple large earthquakes in the past 1500 years on a fault in metropolitan Manila, the Philippines. Bull. Seism. Soc. Am. 90, 73–85.

Pagani, M., D. Monelli, H. Crowley, L. Danciu, E. H. Field, S. Wiemer and D. Giardini, 2010. GEM1 Hazard: Description of input models, calculation engine and main results. GEM Technical Report 2010-3. GEM Foundation, Pavia, Italy.

Pacheco, B.M. et al., 2013. Development of vulnerability curves of key building types in the Greater Metro Manila Area, Philippines. Institute of Civil Engineering, University of the Philippines Diliman, Quezon City.

Papiona, K. L., and M. I. Abigania, 2013. 1:50,000 Scale Preliminary Ground rupture hazard map of the province of Bulacan. GMMA-READY Project.

Papiona, K. L., and Y. Kinugasa, 2008. Trenching surveys along the Masbate segment of the Philippine Fault Zone. Journal of the Geological Society of the Philippines, 64 (2), 19–36.

Papiona, K. L., J. S. Perez, M. T. Cahulogan, M. I. Abigania, and M. L. P. Melosantos, 2013. West Valley Fault Map on 1:5,000 scale. GMMA-READY Project.

Perez, J. S., H. Tsutsumi, M. T. Cahulogan, D. Ishimura and D. P. Cabanlit, 2010. Paleoseismic evidence along the Surigao Segment of the Philippine Fault Zone, North-eastern Mindanao, Philippines. In Proceedings of Hokudan Symposium on Active Faulting, pp. 84–85.

PHIVOLCS, 1999. Annual Report of the Philippine Institute of Volcanology and Seismology. Tech. rep., Department of Science and Technology.

PHIVOLCS, 2008a. PHIVOLCS Active Fault Map. Tech. Rep. PHIVOLCS Bldg., C.P. Garcia Ave., UP Diliman, Quezon City, Philippines, Philippine Institute of Volcanology and Seismology.

PHIVOLCS, 2008b. PHIVOLCS Active Fault Map (updated). Tech. rep., Philippine Institute of Volcanology and Seismology, PHIVOLCS Bldg., C.P. Garcia Ave., UP Diliman, Quezon City, Philippines.

Richter, C. F., 1935. An instrumental earthquake magnitude scale. Bull. Seism. Soc. Am. 25, 1-32.

Richter, C. F., 1958. Elementary seismology. San Francisco, California, W. H. Freeman and Co.

Rimando, R. E., and P. L. K. Knuepfer, 2006. Neotectonics of the Marikina Valley fault system (MVFS) and tectonic framework of structures in northern and central Luzon, Philippines. Tectonophys. 415, 17–38.

Sadigh, K., C.Y. Chang, J.A. Egan, F. Makdisi, R.R. Youngs, 1997. Attenuation Relationships for Shallow Crustal Earthquakes Based on California Strong Motion Data. Seismological Research Letters Vol 68, No. 1, pp. 180–189, January/February 1997.

Scherbaum, F., 1996. Of poles and zeros: fundamentals of digital seismology. Dordrecht, Kluwer Academic Press.

SEASEE, 1985. Philippines. In Southeast Asian Association of Seismology and Earthquake Engineering, edited by E. P. Arnold, Series on Seismology IV, p. 843, SEASEE.

Tsutsumi, H., J. A. Daligdig, N. Tun˜gol, H. Kondo, T. Nakata, M. Okuno, and N. Sugito, 2006. Timing of Surface-Rupturing Earthquakes on the Philippine Fault Zone in Central Luzon Island,

Philippines. In EOS Trans. AGU Fall Meeting Suppl. Abstract, vol. 87, pp. 52, T33A–0510, American Geophysical Union.

Vanmarcke, E. H., and S.-S. P. Lai, 1980. Attenuation of intensity with epicentral distance in the Philippines. Bull. Seism. Soc. Am. 70, 1287-1291.

Wald, D. J., and T. I. Allen, 2007. Topographic slope as a proxy for seismic site conditions and amplification. Bull. Seism. Soc. Am. 97, 1379-1395.

Wells, D. L., and K. J. Coppersmith, 1994. New empirical relationships among magnitude, rupture length, rupture width, rupture area, and surface displacement. Bull. Seism. Soc. Am. 84, 974-1002.

Wessel, P., and W. H. F. Smith, 1991. Free software helps map and display data. Eos Trans. 72, 441.

Wills, C. J., M. Petersen, W. A. Bryant, M. Reichle, G. J. Saucedo, S. Tan, G. Taylor, and J. Treiman, 2000. A site-conditions map for California based on geology and shear-wave velocity. Bull. Seism. Soc. Am. 90, S187–S208.

Worden, C. B., M. C. Gerstenberger, D. A. Rhoades, and D. J. Wald, 2012. Probabilistic relationships between ground-motion parameters and Modified Mercalli Intensity in California. Bull. Seism. Soc. Am. 102, 204-221.

Zhao J.X., et. al.,2006. Attenuation Relations of Strong Ground Motion in Japan Using Site Classification Based on Predominant Period. Bulletin of the Seismological Society of America, Vol. 96, No. 3, pp. 898–913, June 2006.

Appendix A – Risk Maps for a M7.2 Earthquake (Absolute values)

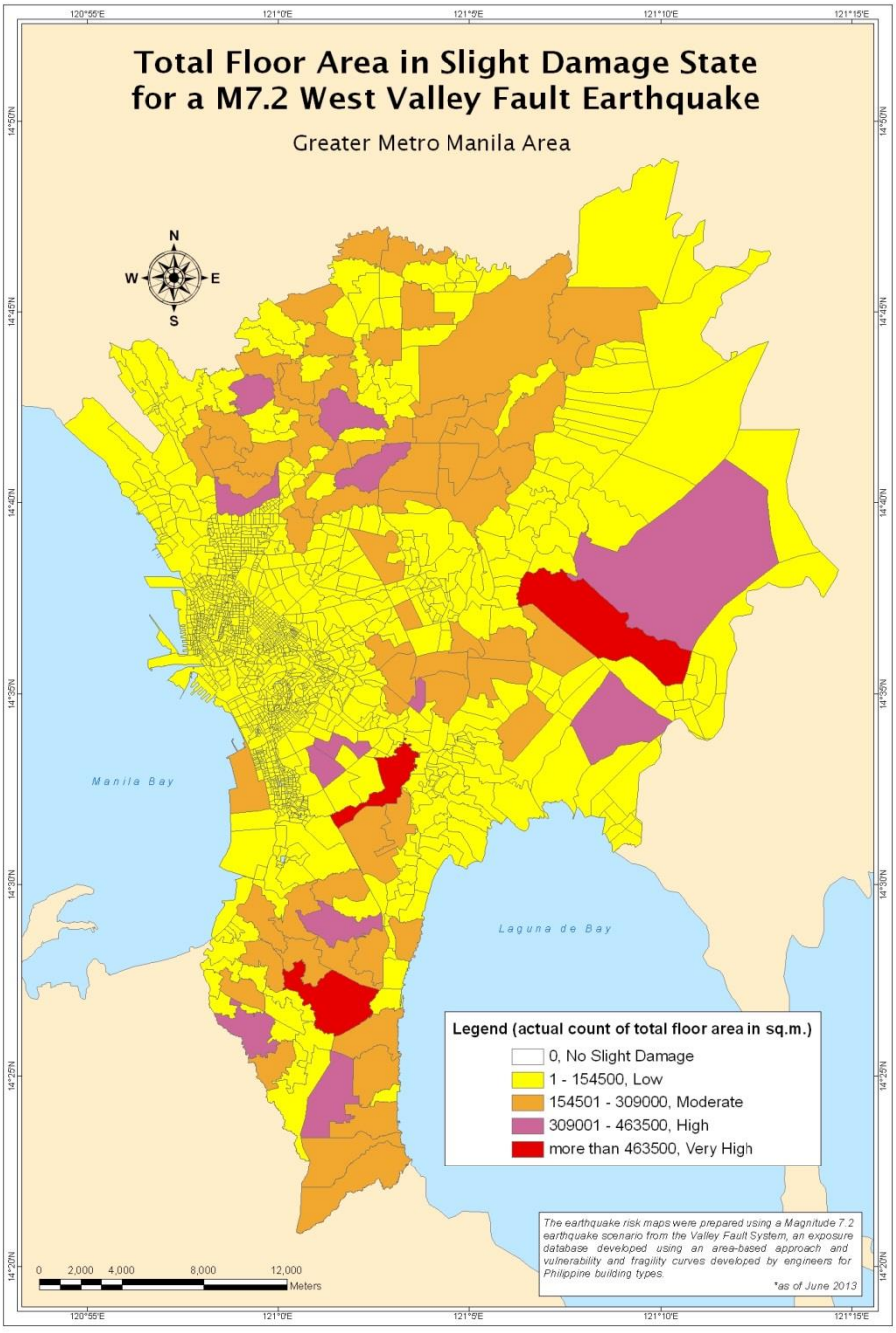

Figure A.1. Total Floor Area in Slight Damage State for a M7.2 earthquake.

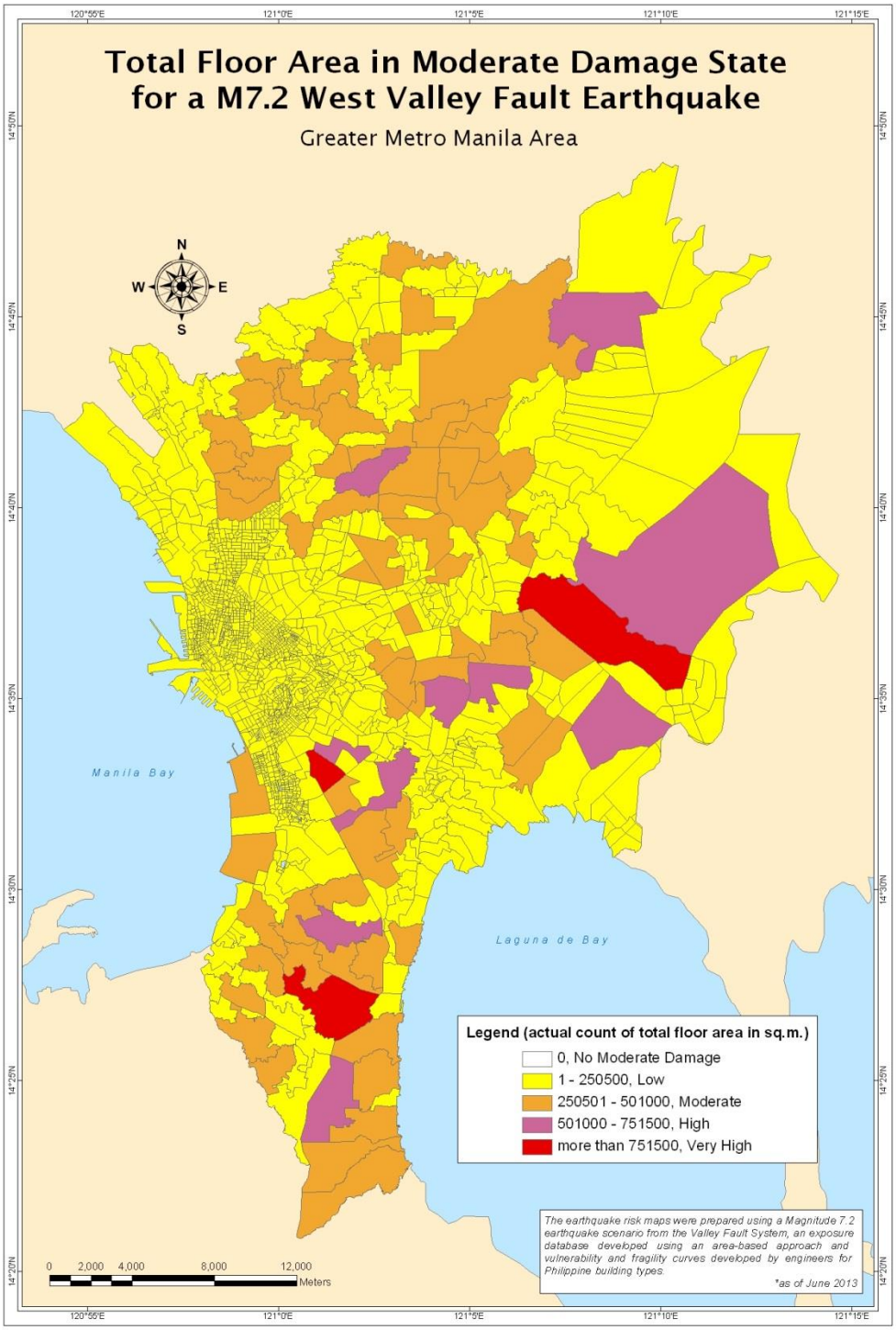

Figure A.2. Total Floor Area in Moderate Damage State for a M7.2 earthquake.

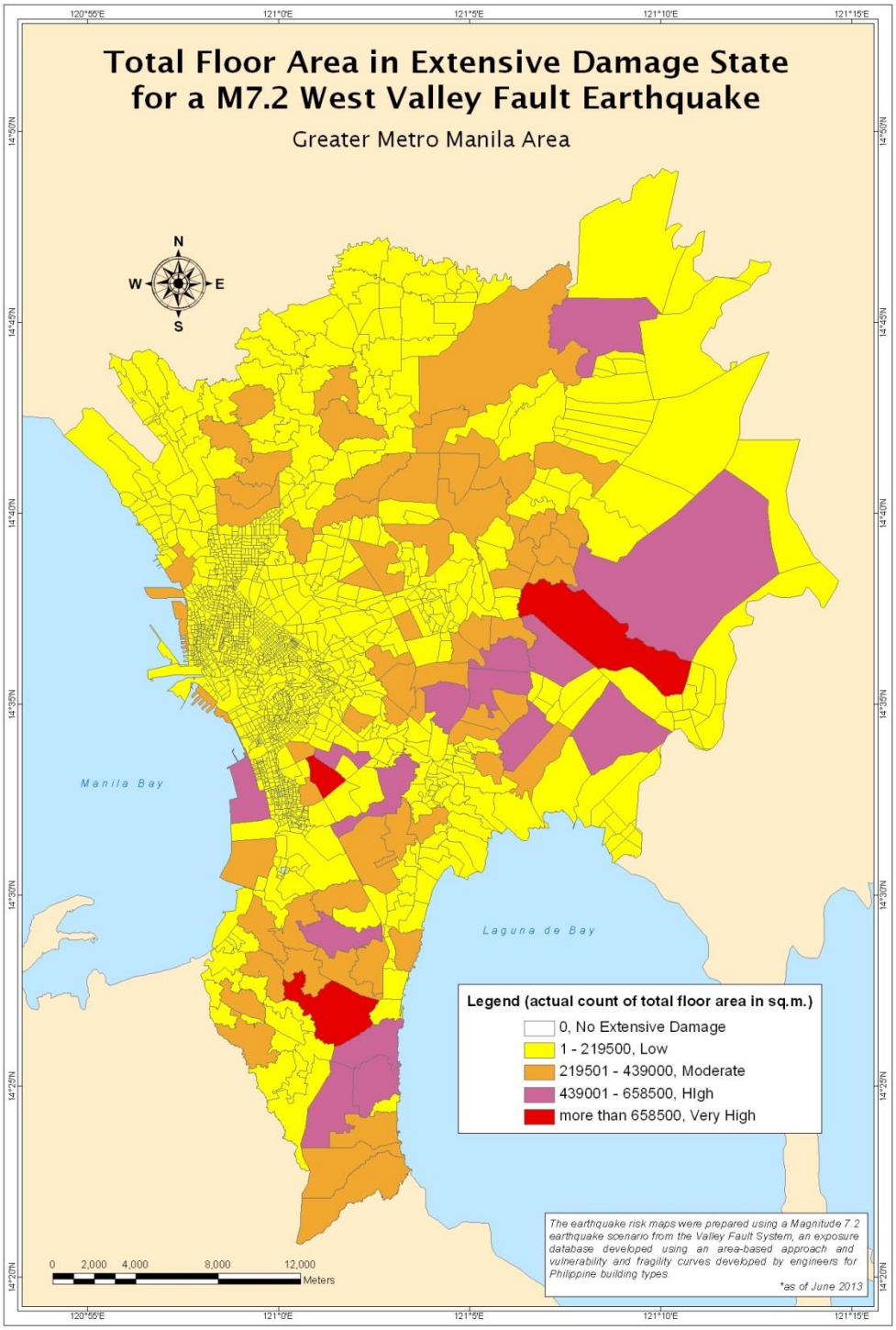

Figure A.3. Total Floor Area in Extensive Damage State for a M7.2 earthquake.

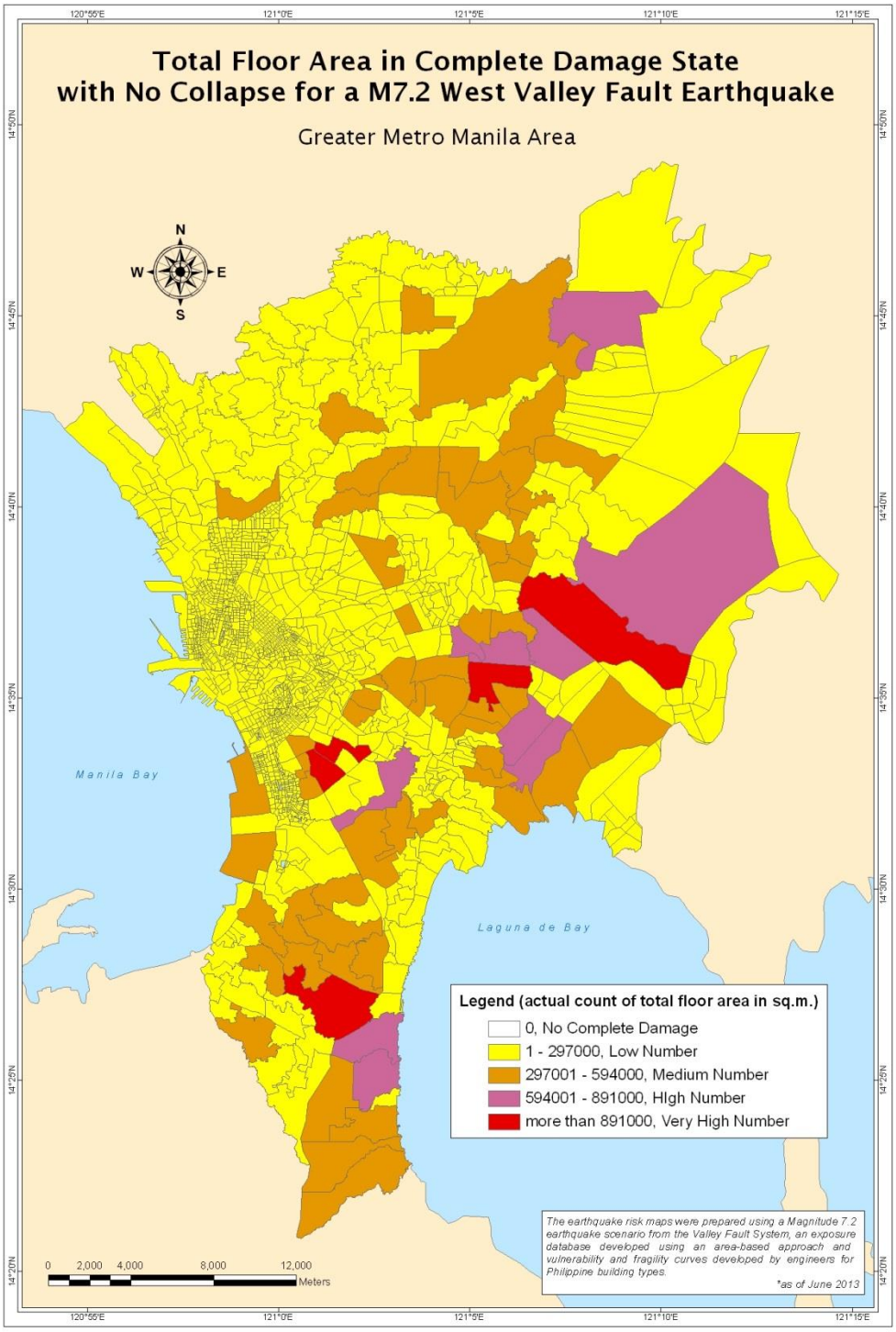

Figure A.4. Total Floor Area in Complete Damage State with No Collapse for a M7.2 earthquake.

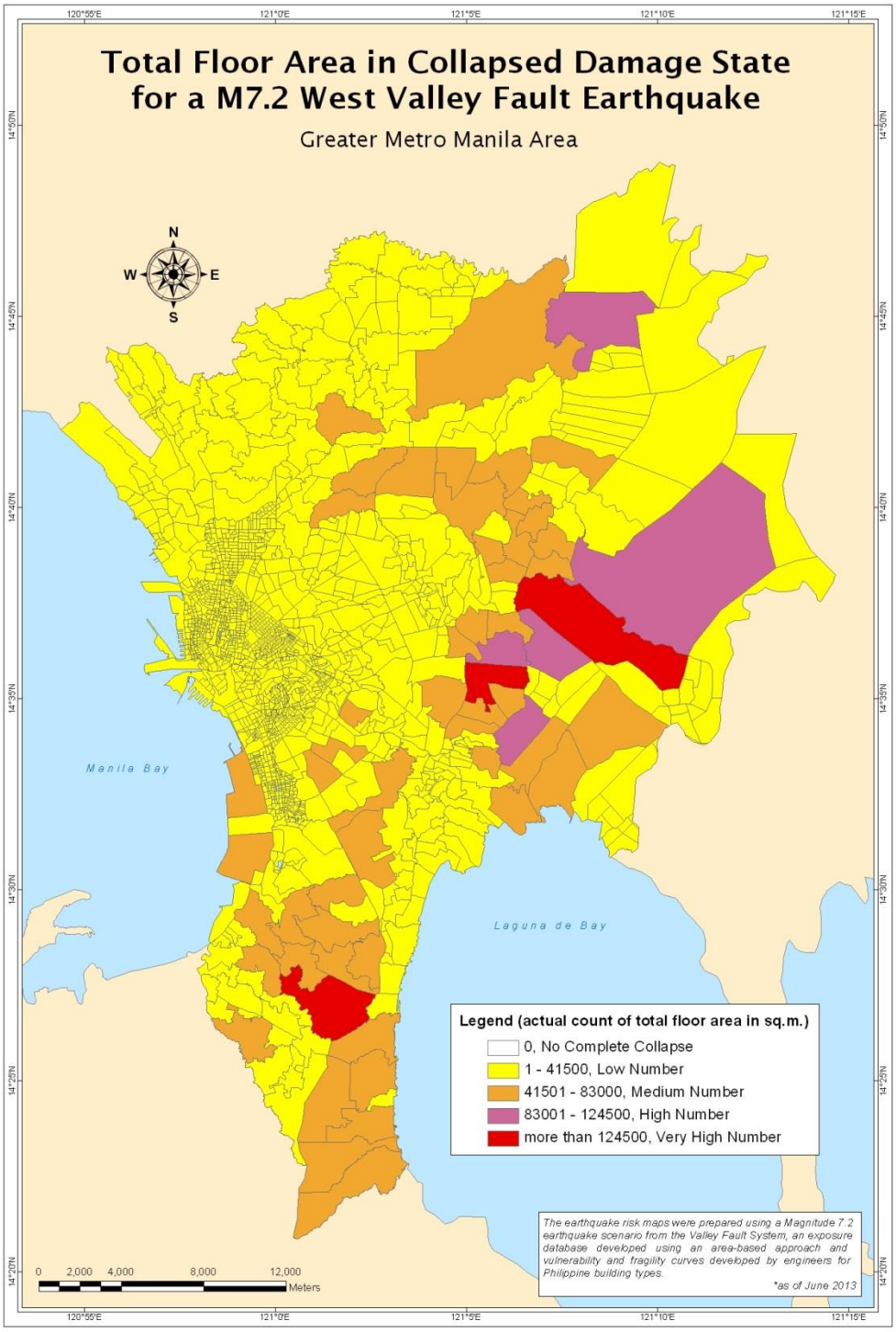

Figure A.5. Total Floor Area in Collapsed Damage State for a M7.2 earthquake.

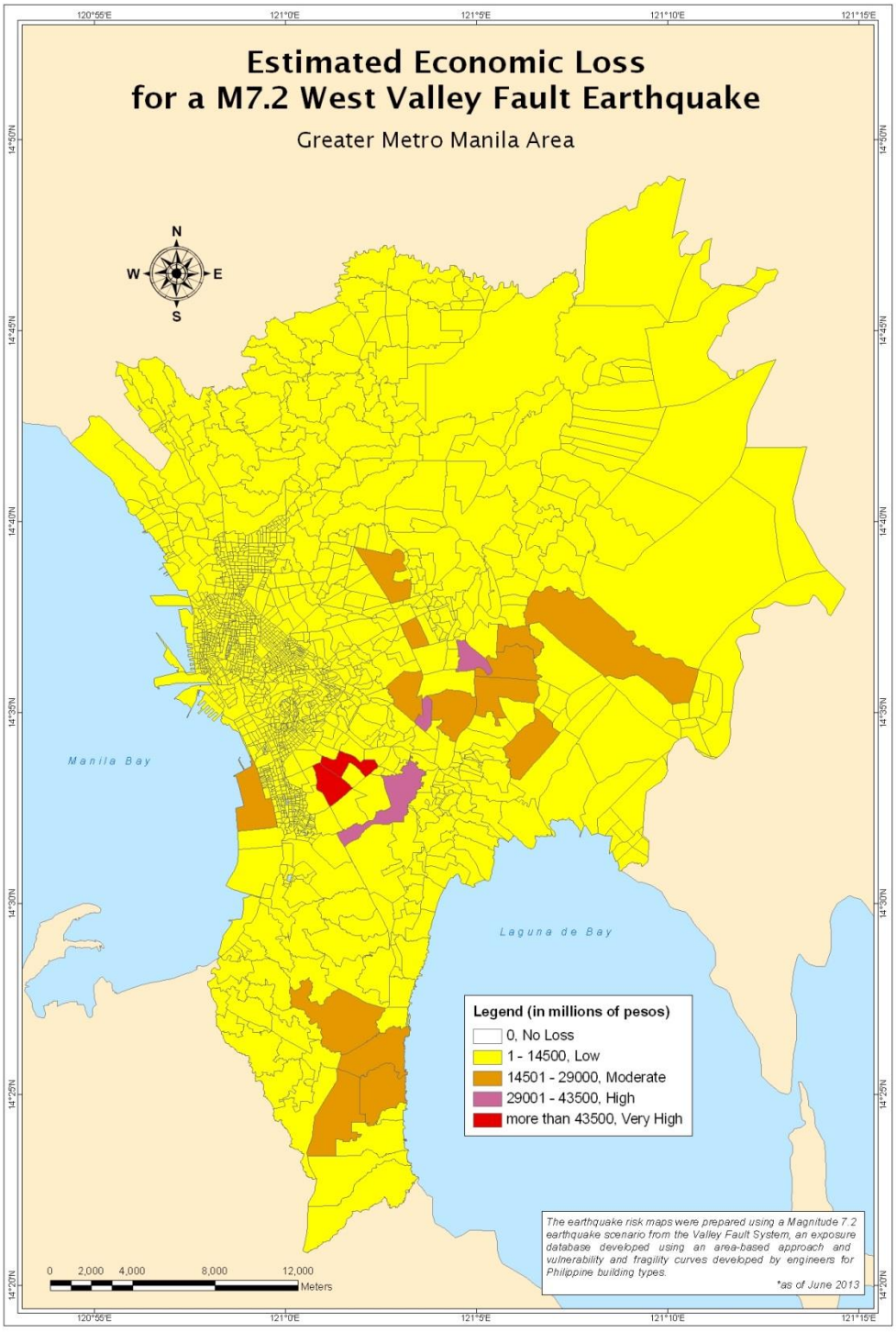

Figure A.6. Estimated Economic Loss for a M7.2 earthquake.

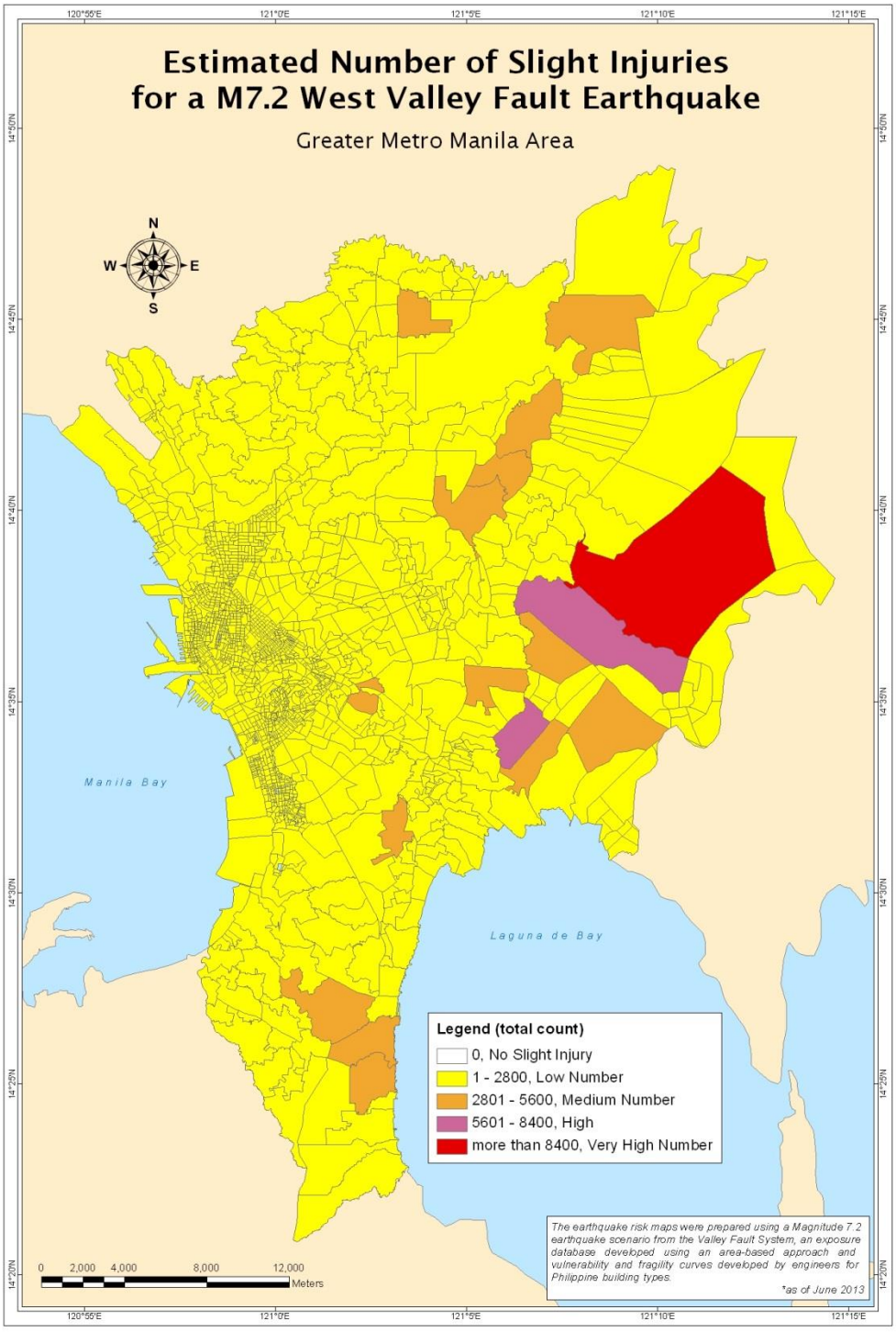

Figure A.7. Estimated Number of Slight Injuries for a M7.2 earthquake.

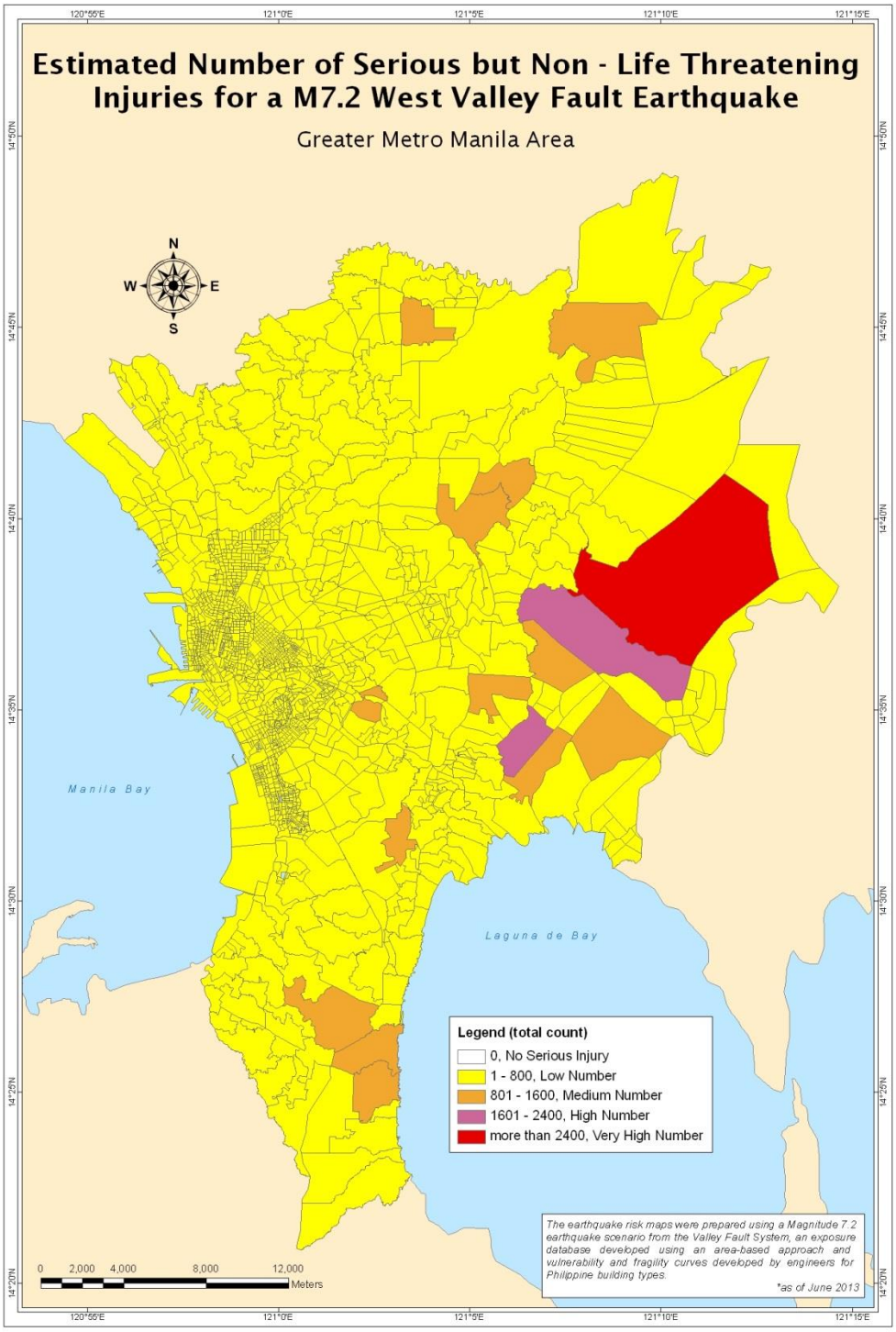

Figure A.8. Estimated Number of Serious but Non-Life Threatening Injuries for a M7.2 earthquake.

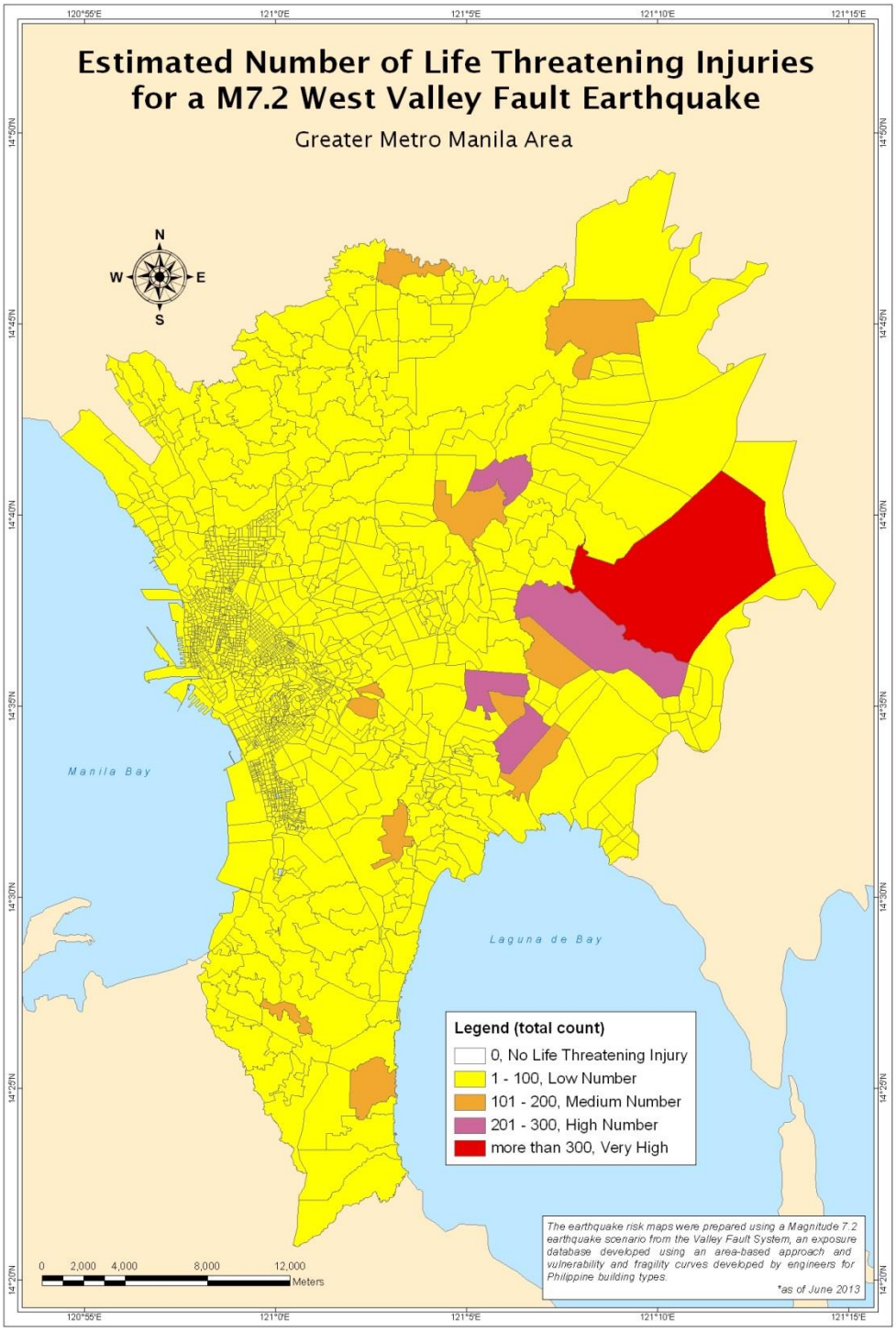

Figure A.9. Estimated Number of Life Threatening Injuries for a M7.2 earthquake.

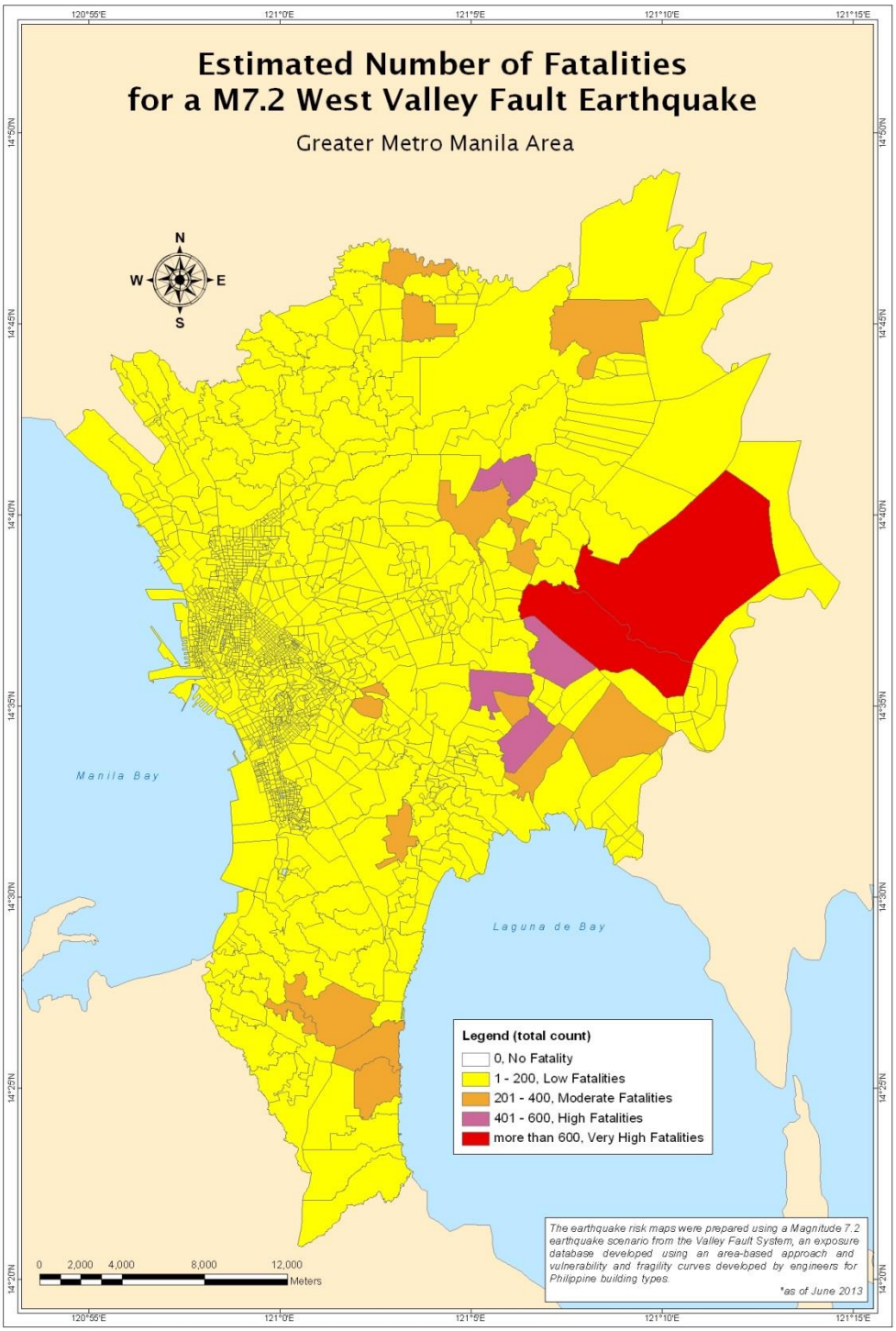

Figure A.10. Estimated Number of Fatalities for a M7.2 earthquake.

Appendix B – Risk Maps for a M7.2 Earthquake (Normalized per Barangay)

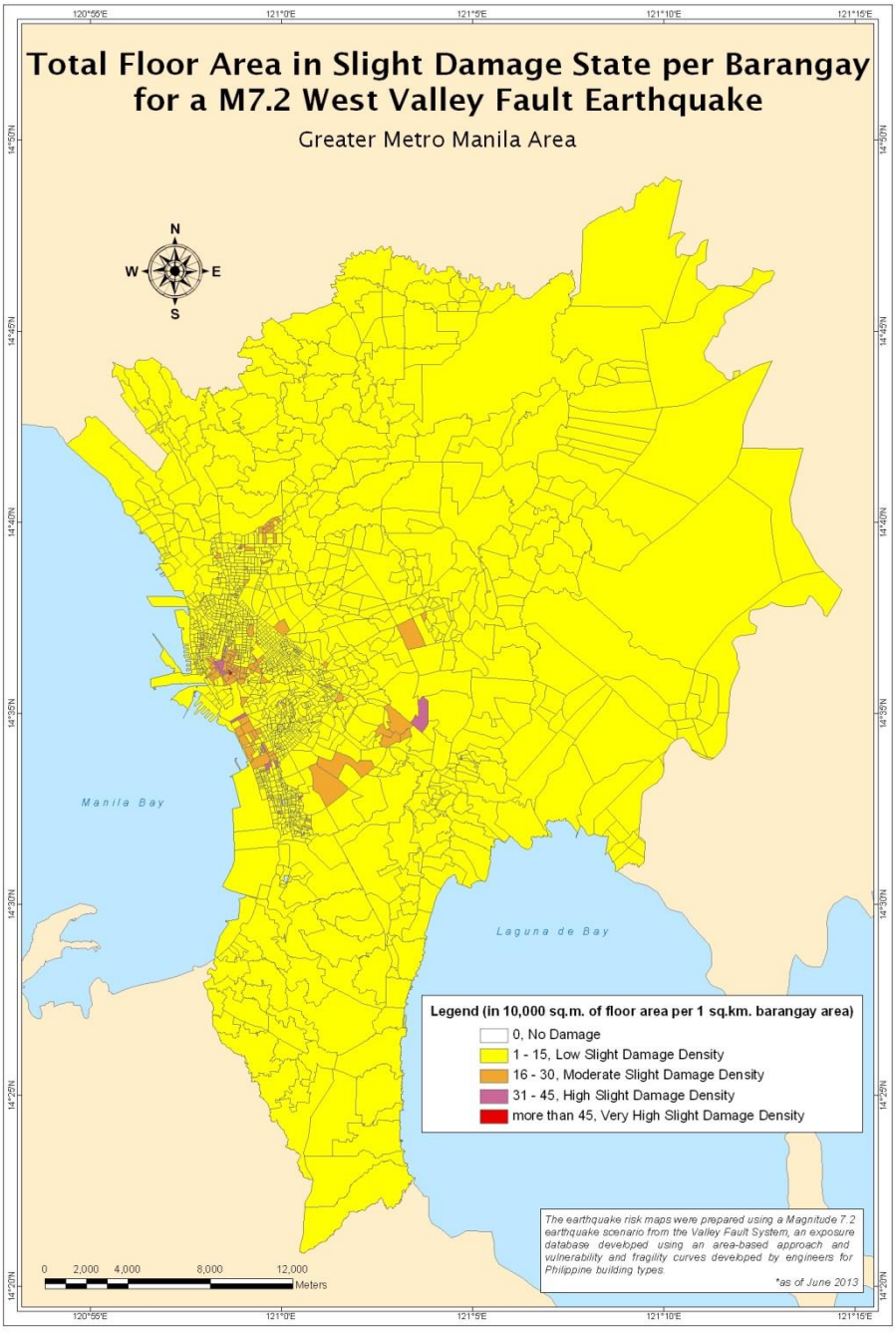

Figure B.1. Total Floor Area (Normalized per Barangay) in Slight Damage State for a M7.2 earthquake

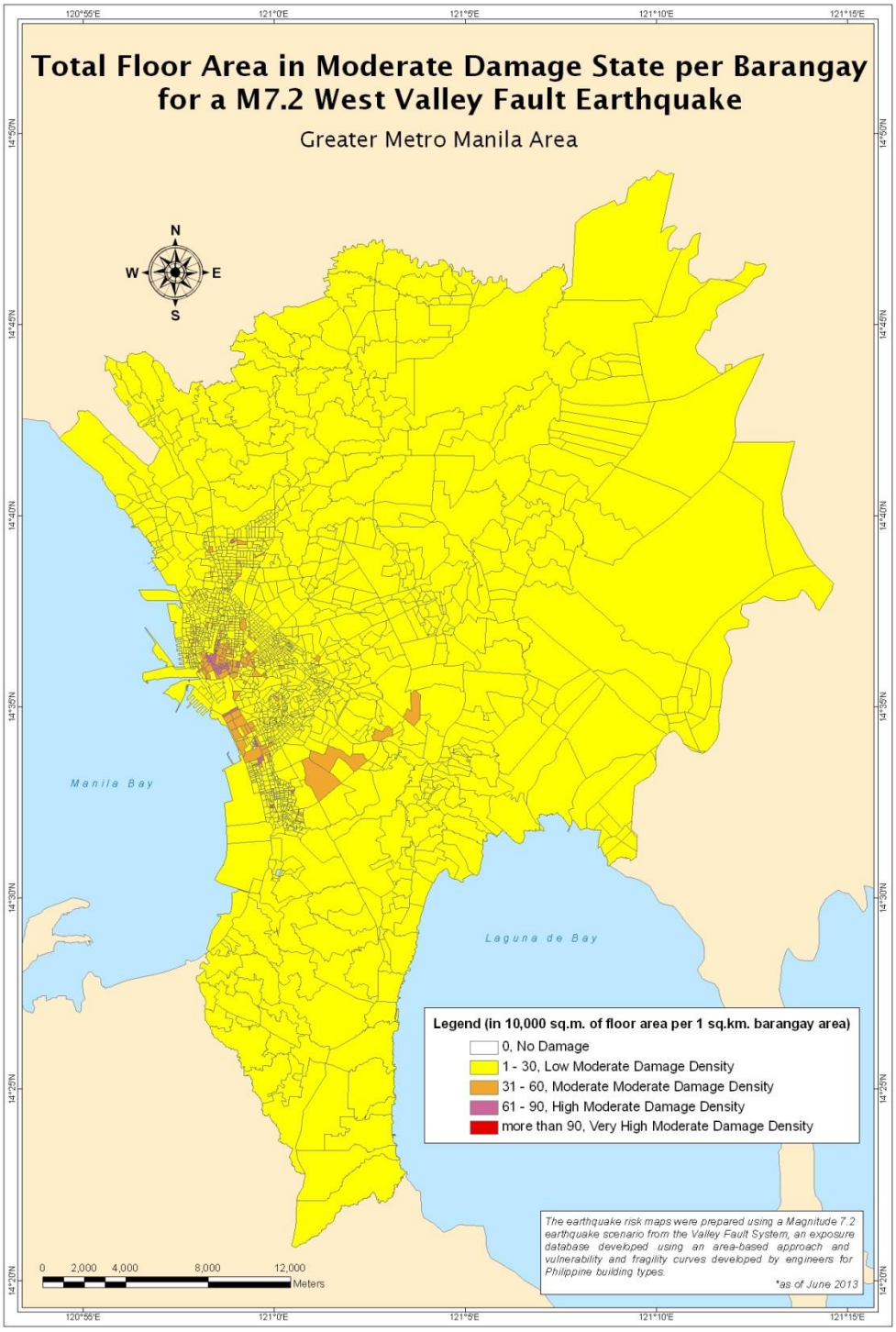

Figure B.2. Total Floor Area (Normalized per Barangay) in Moderate Damage State for a M7.2 earthquake.

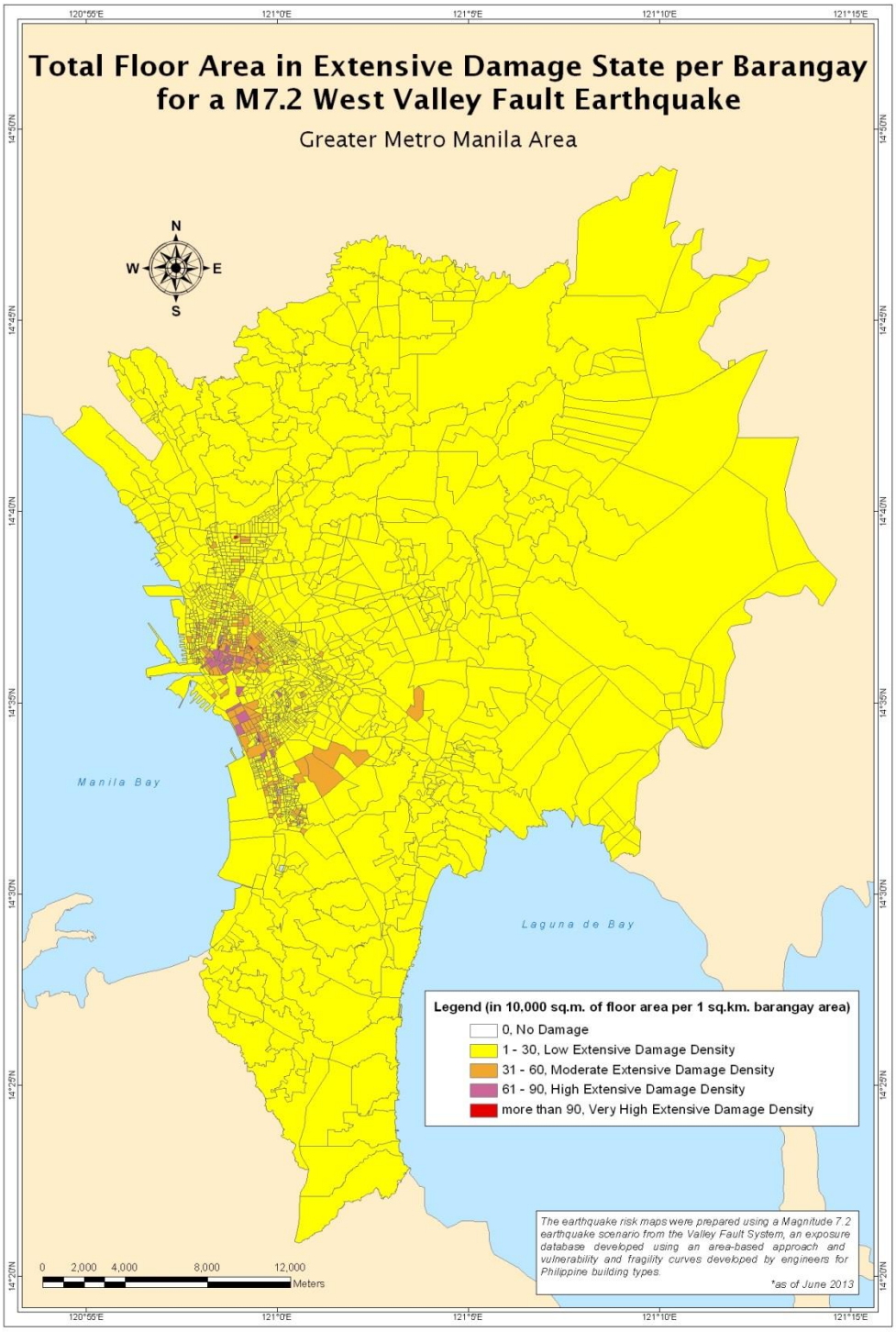

Figure B.3. Total Floor Area (Normalized per Barangay) in Extensive Damage State for a M7.2 earthquake.

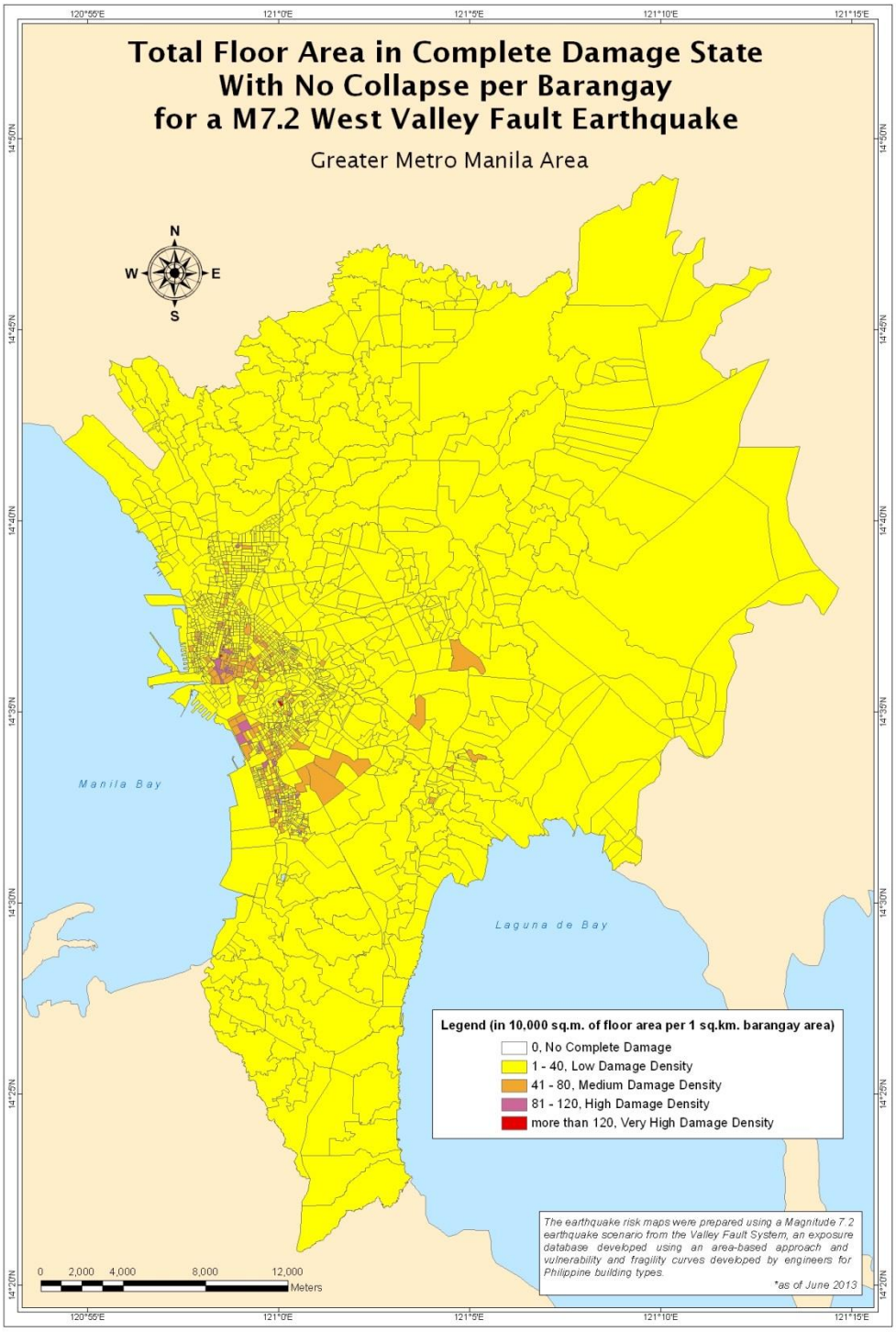

Figure B.4. Total Floor Area (Normalized per Barangay) in Complete Damage State with No Collapse for a M7.2 earthquake.

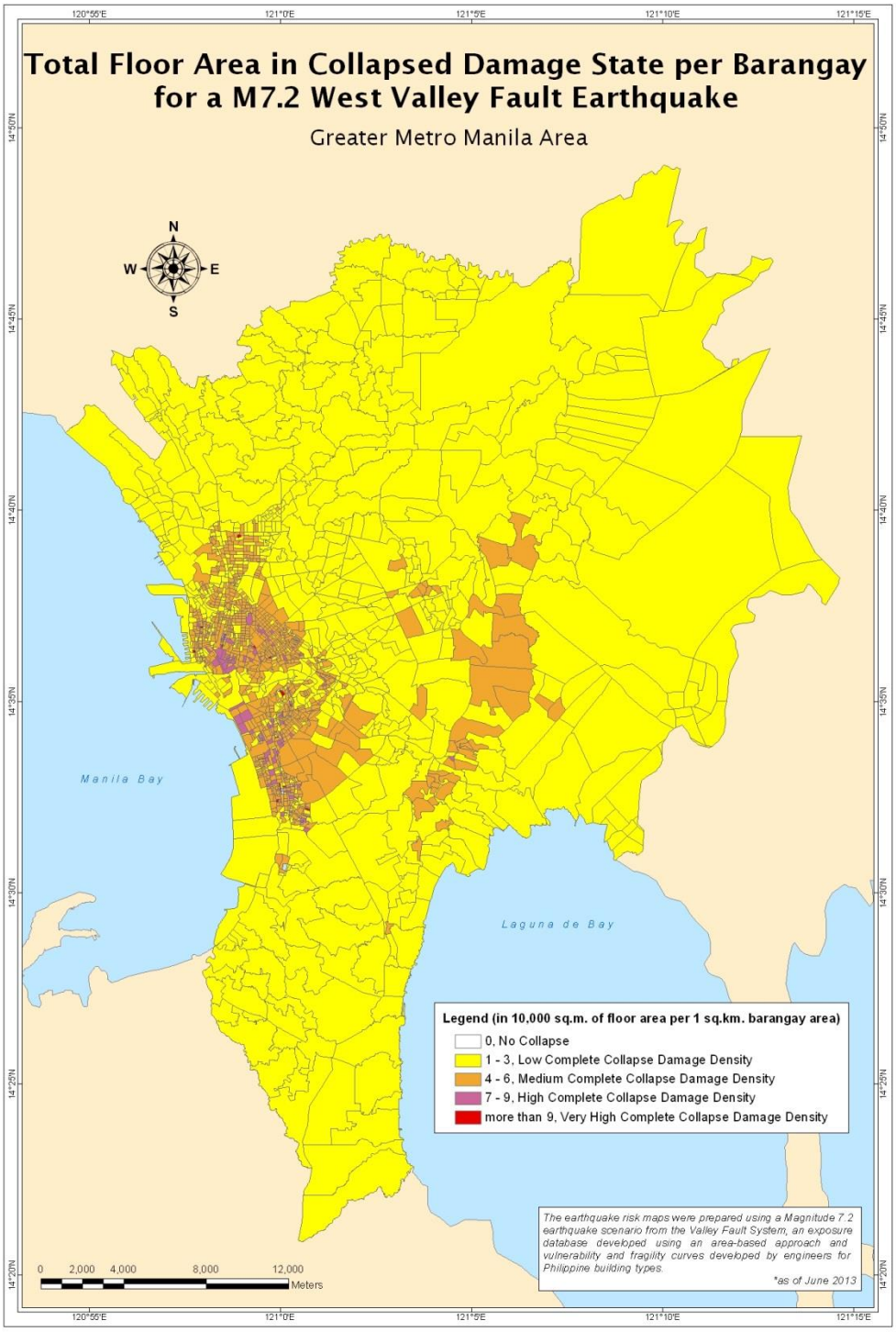

Figure B.5. Total Floor Area (Normalized per Barangay) in Collapsed Damage State for a M7.2 earthquake.

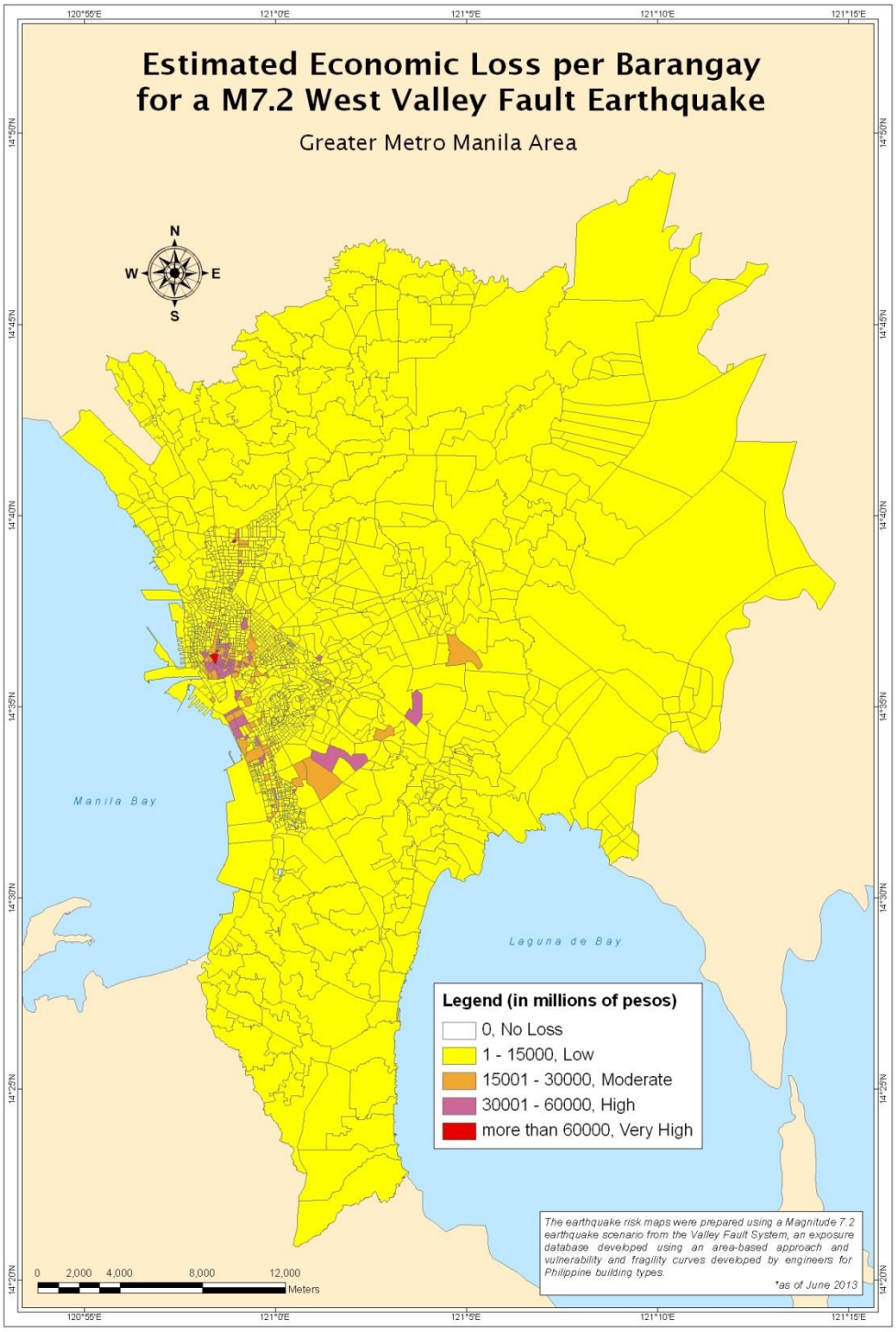

Figure B.6. Estimated Economic Loss (Normalized per Barangay) for a M7.2 earthquake.

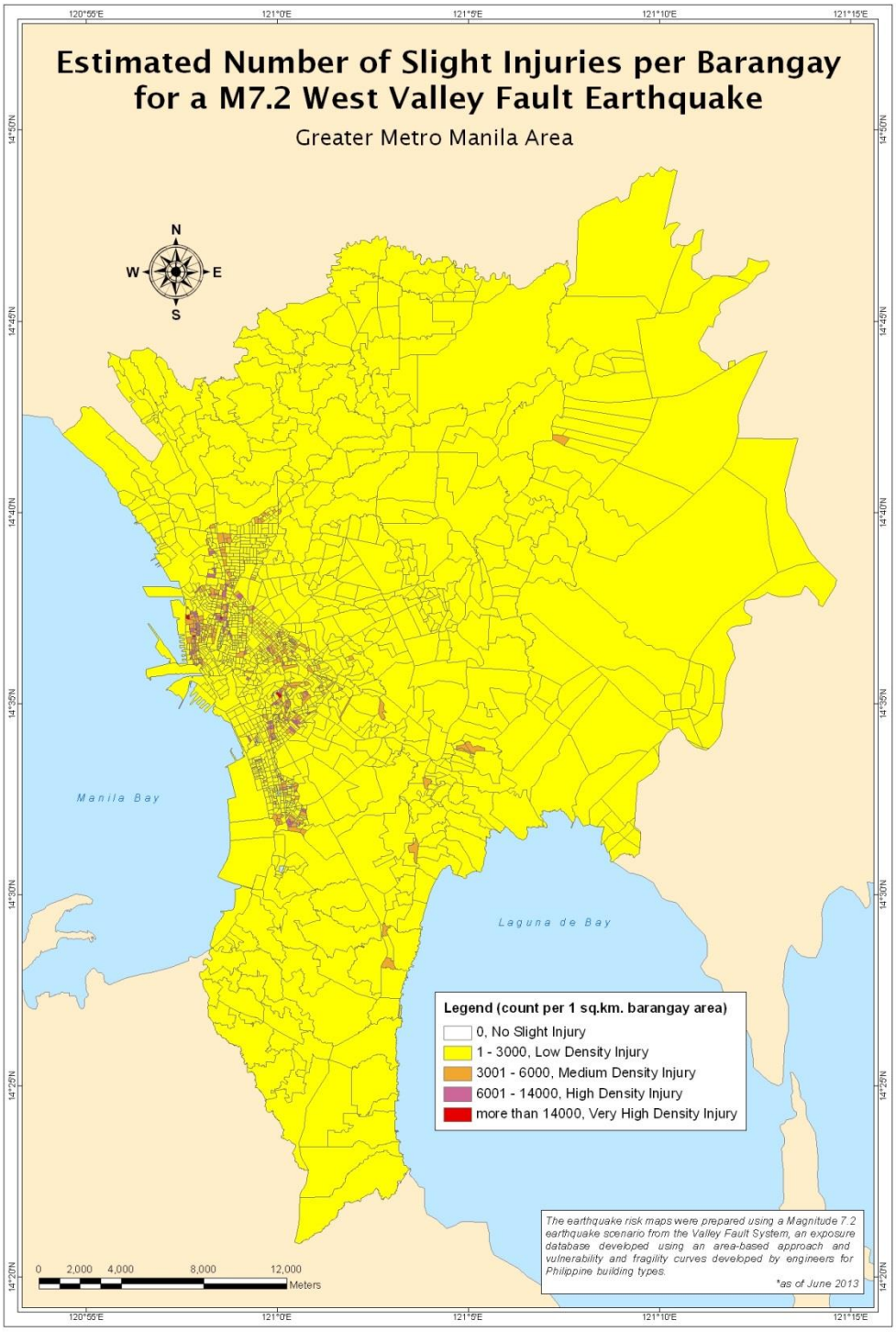

Figure B.7. Estimated Number of Slight Injuries (Normalized per Barangay) for a M7.2 earthquake.

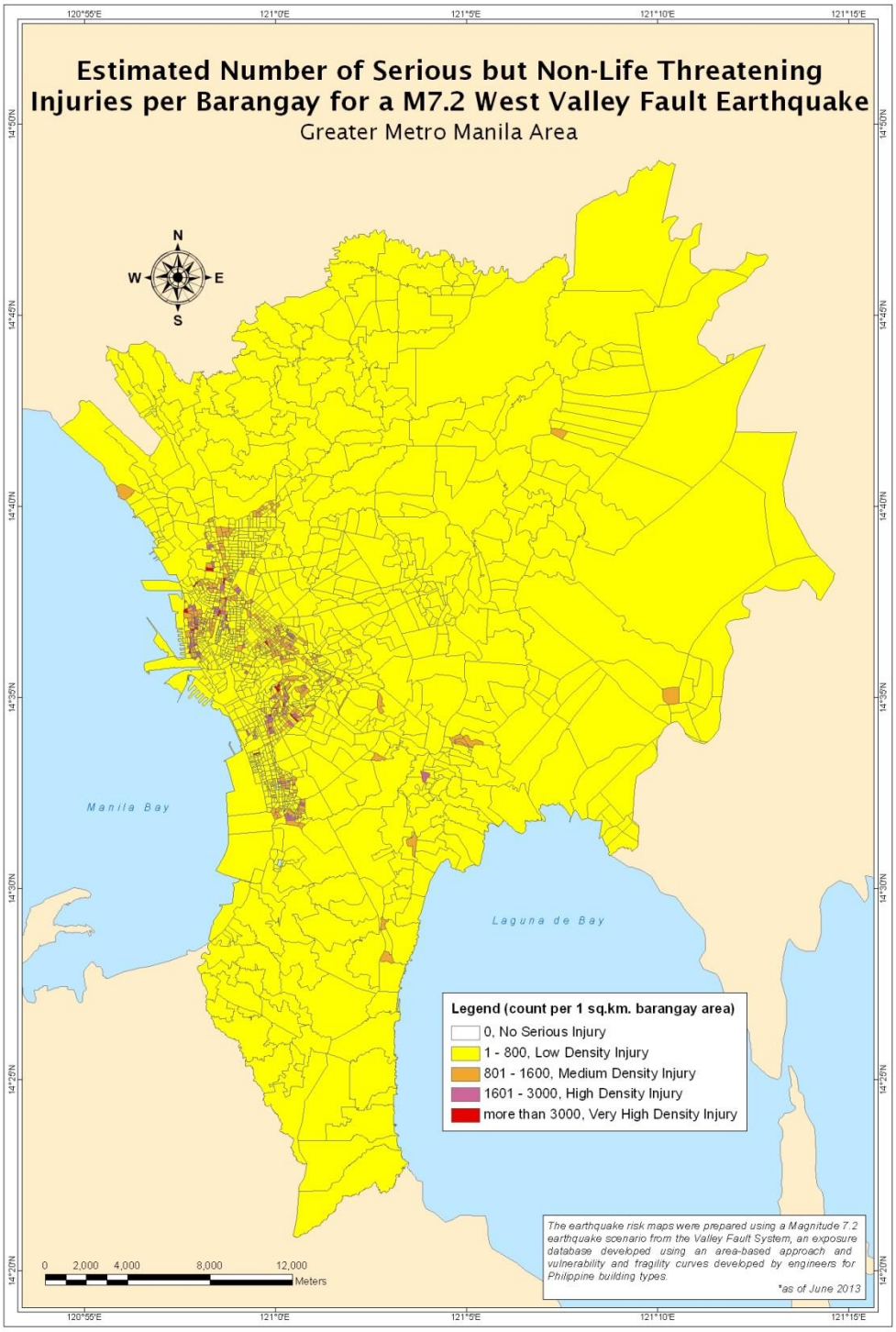

Figure B.8. Estimated Number of Serious but Non-Life Threatening Injuries (Normalized per Barangay) for a M7.2 earthquake.

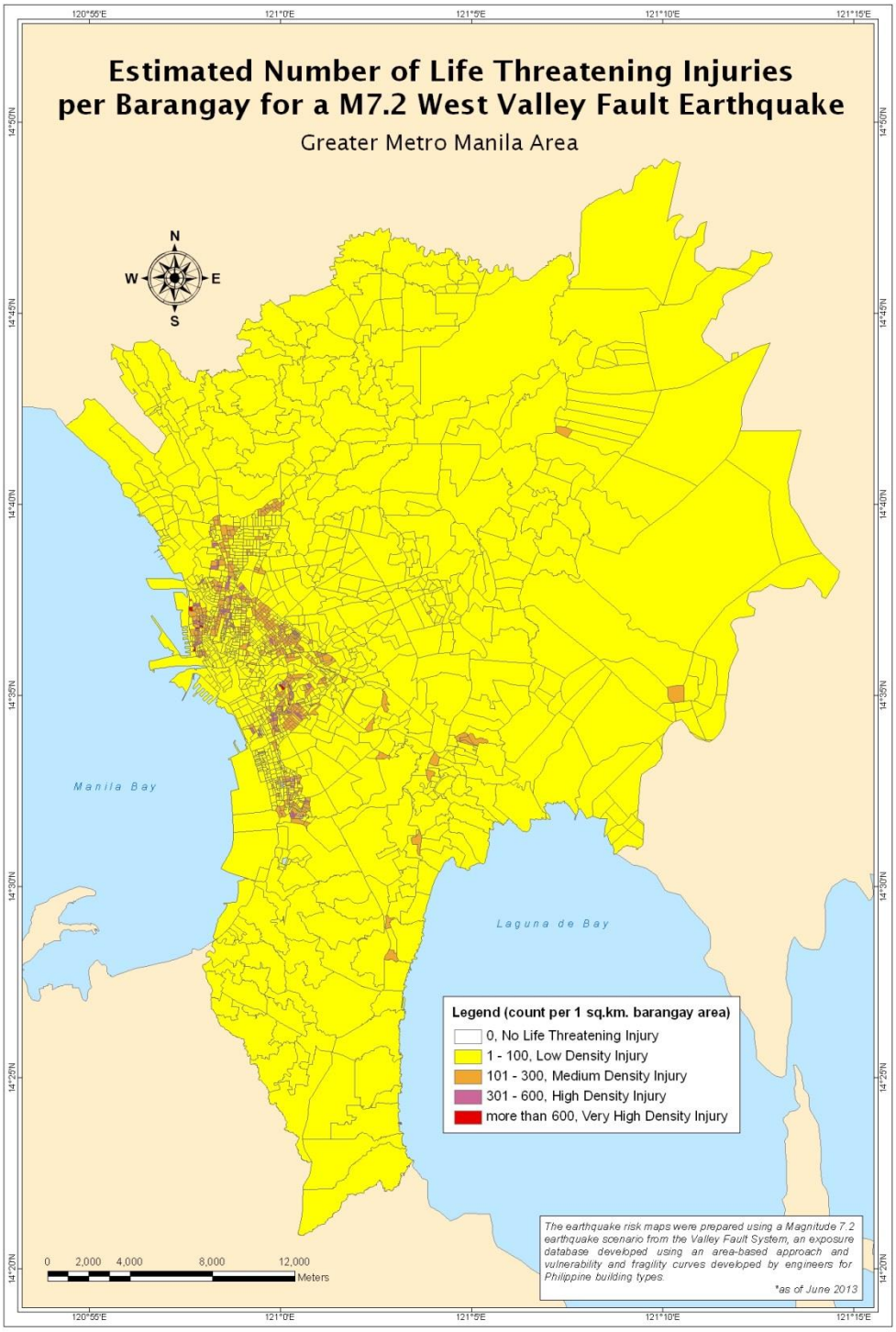

Figure B.9. Estimated Number of Life Threatening Injuries (Normalized per Barangay) for a M7.2 earthquake.

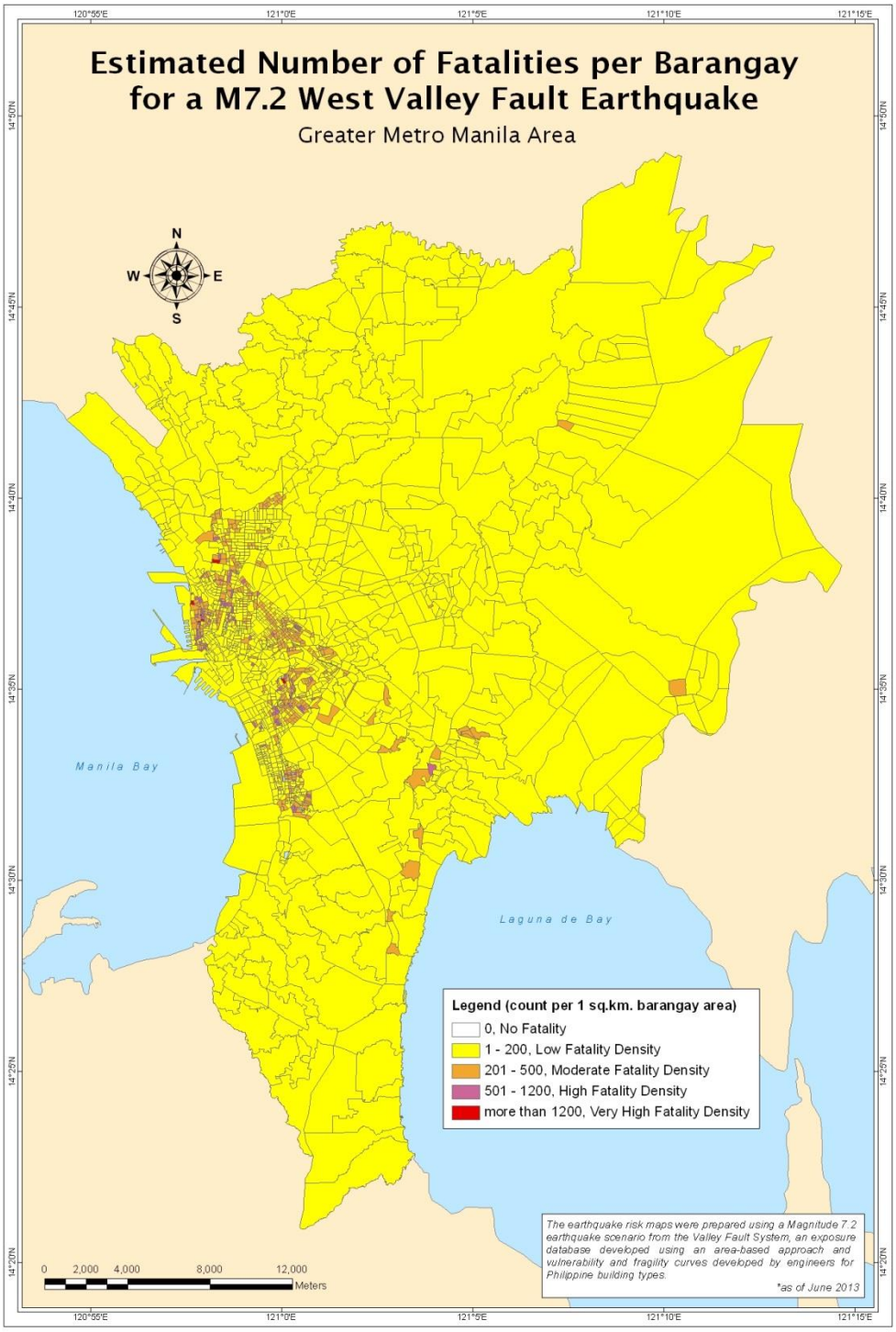

Figure B.10. Estimated Number of Fatalities (Normalized per Barangay) for a M7.2 earthquake.

Appendix C – Risk Maps for a M6.5 Earthquake (Absolute values)

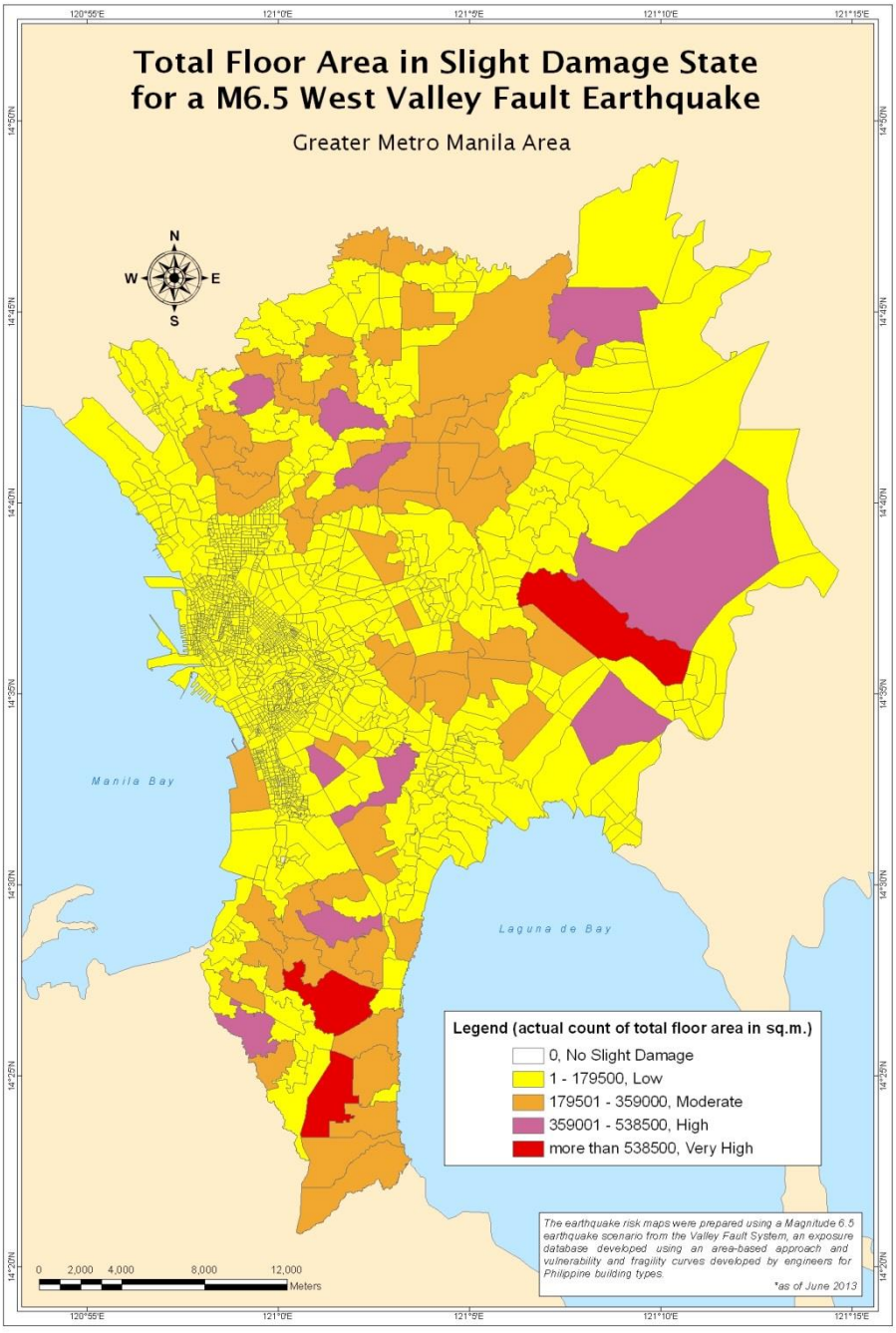

Figure C.1. Total Floor Area in Slight Damage State for a M6.5 earthquake.

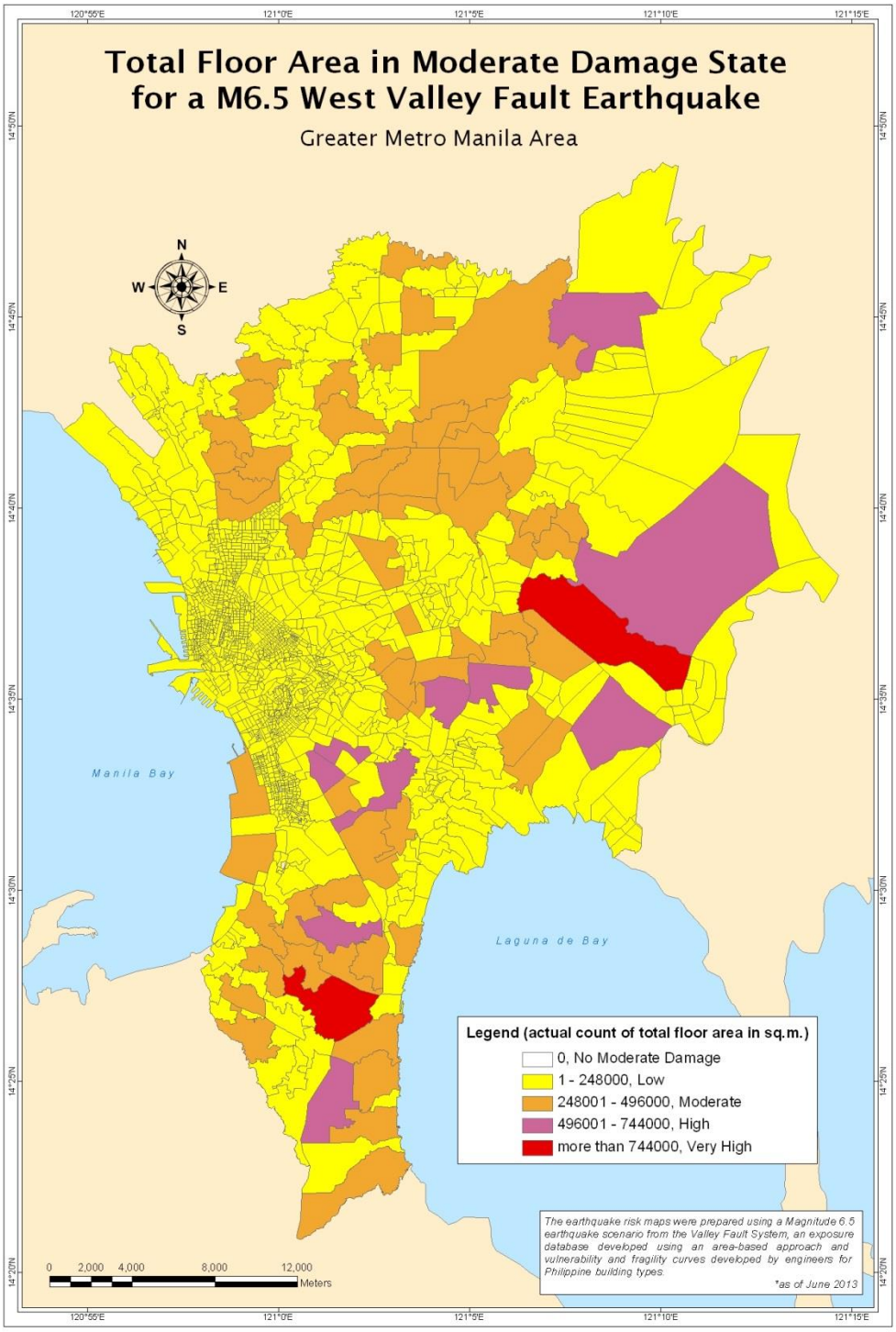

Figure C.2. Total Floor Area in Moderate Damage State for a M6.5 earthquake.

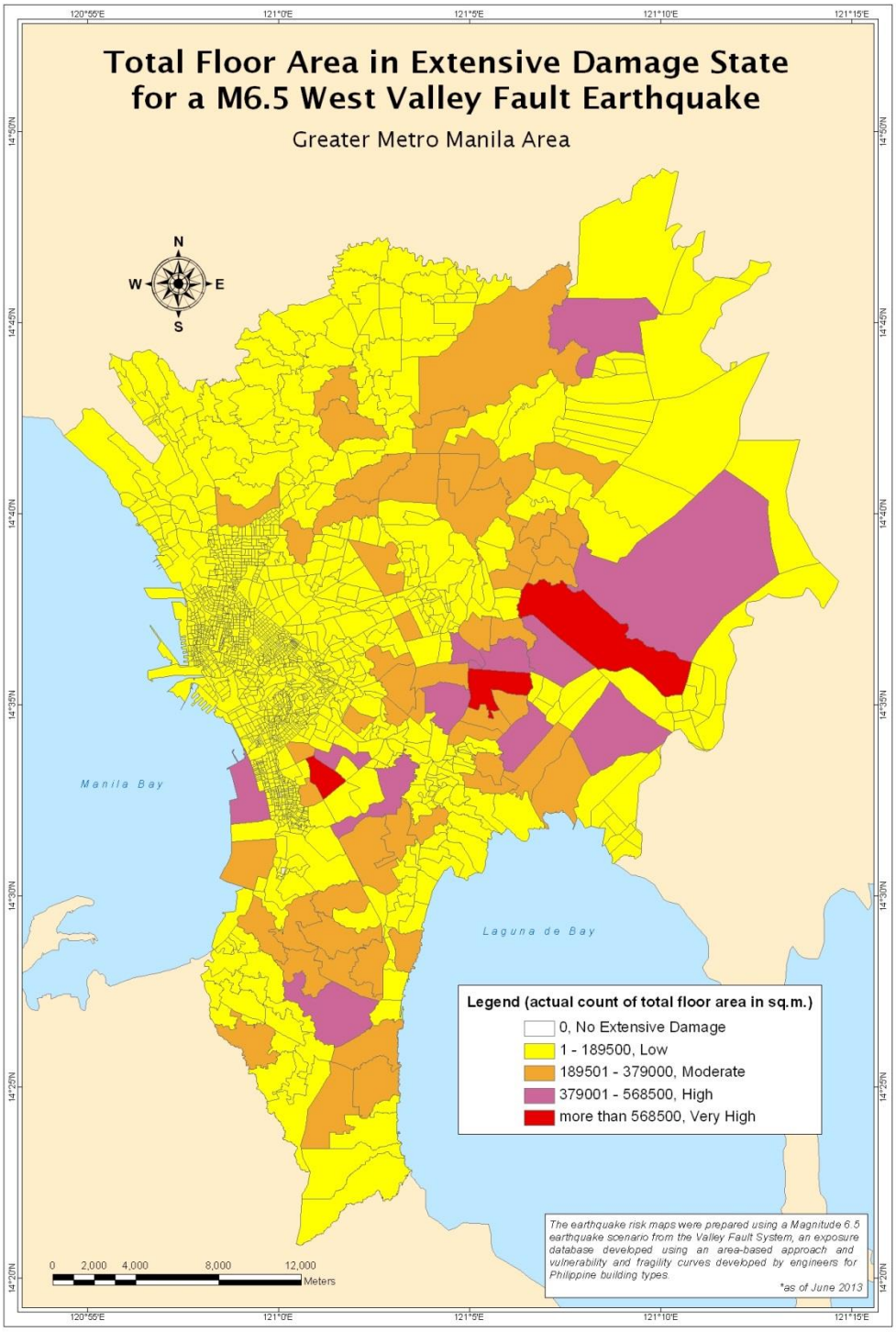

Figure C.3. Total Floor Area in Extensive Damage State for a M6.5 earthquake.

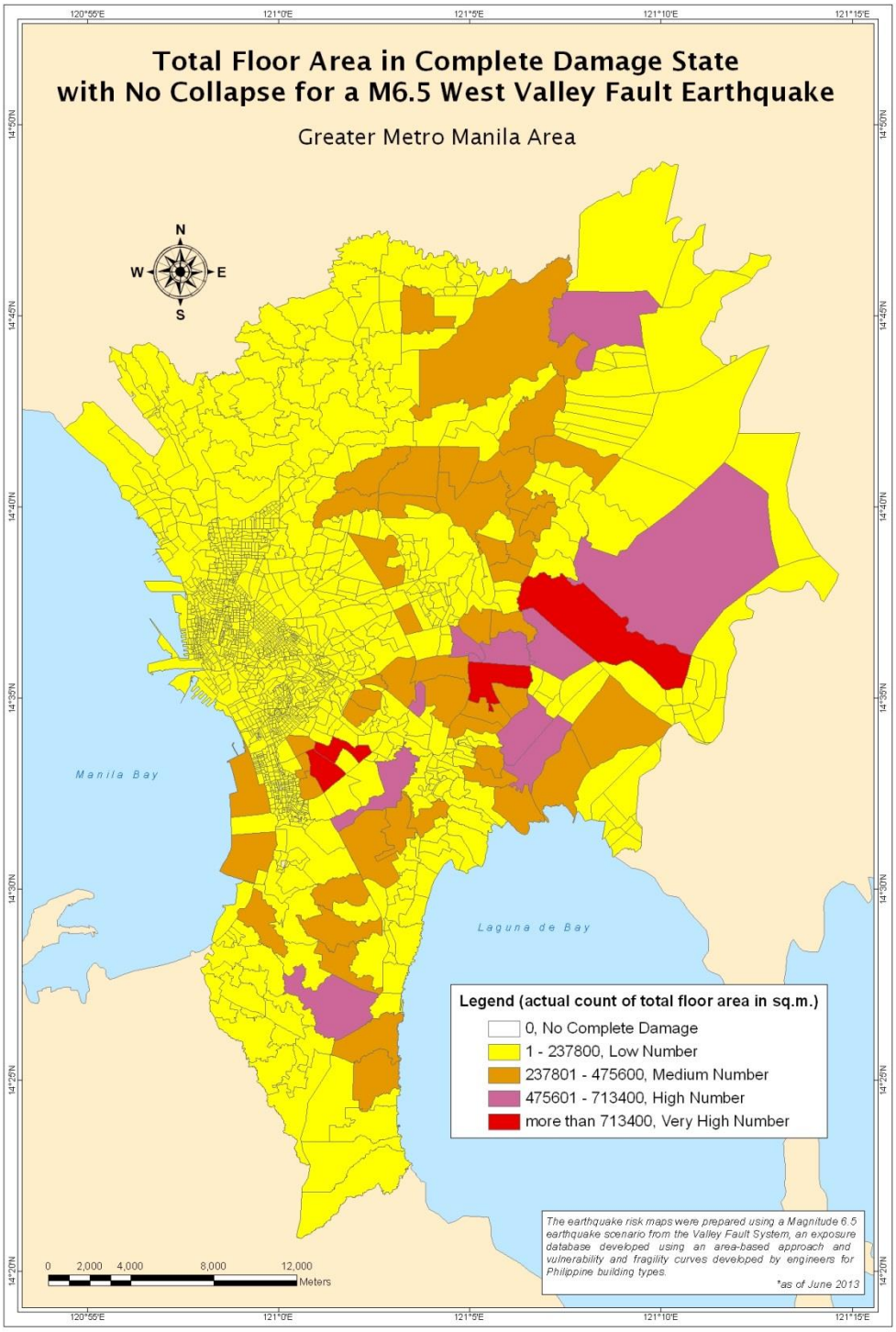

Figure C.4. Total Floor Area in Complete Damage State with No Collapse for a M6.5 earthquake.

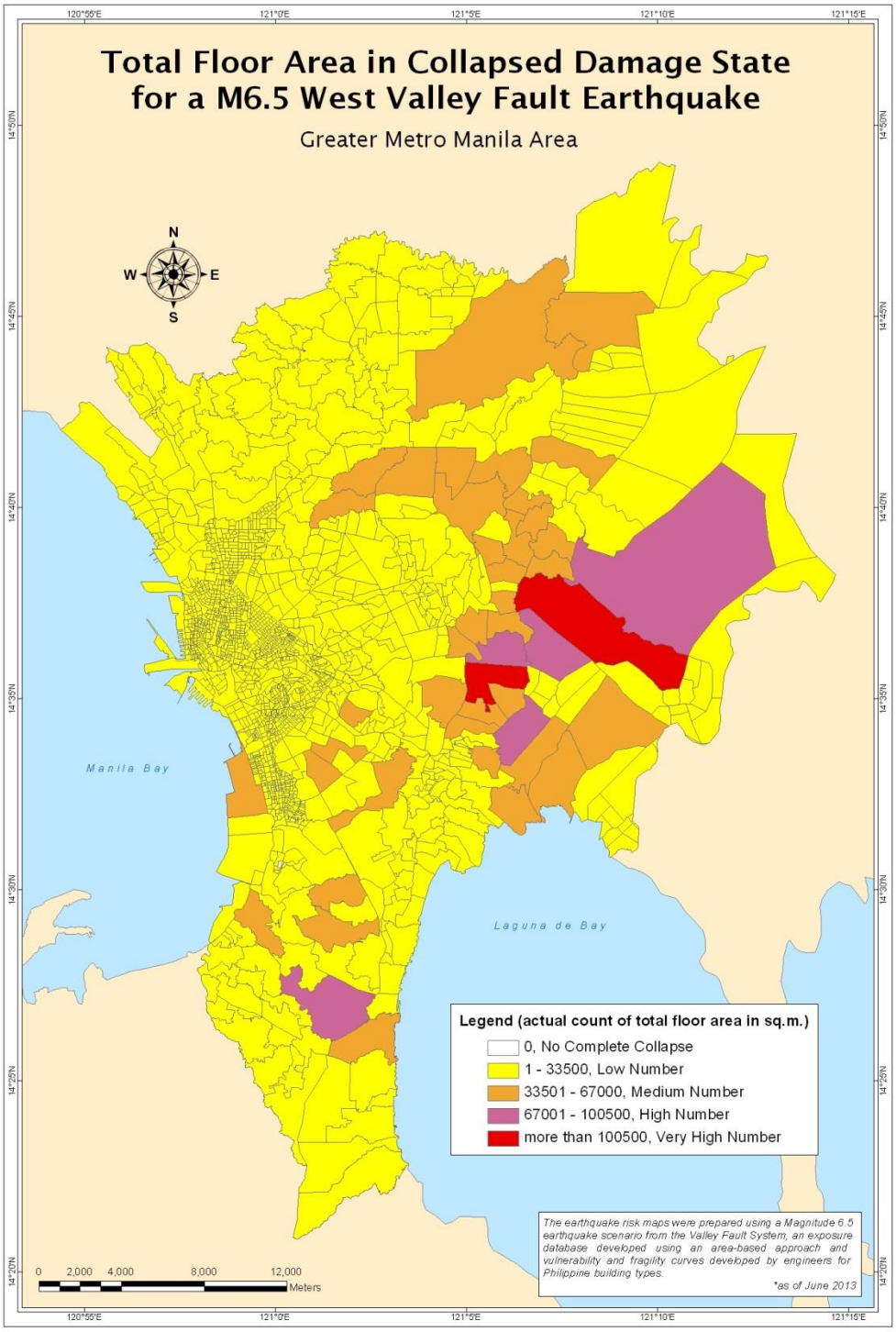

Figure C.5. Total Floor Area in Collapsed Damage State for a M6.5 earthquake.

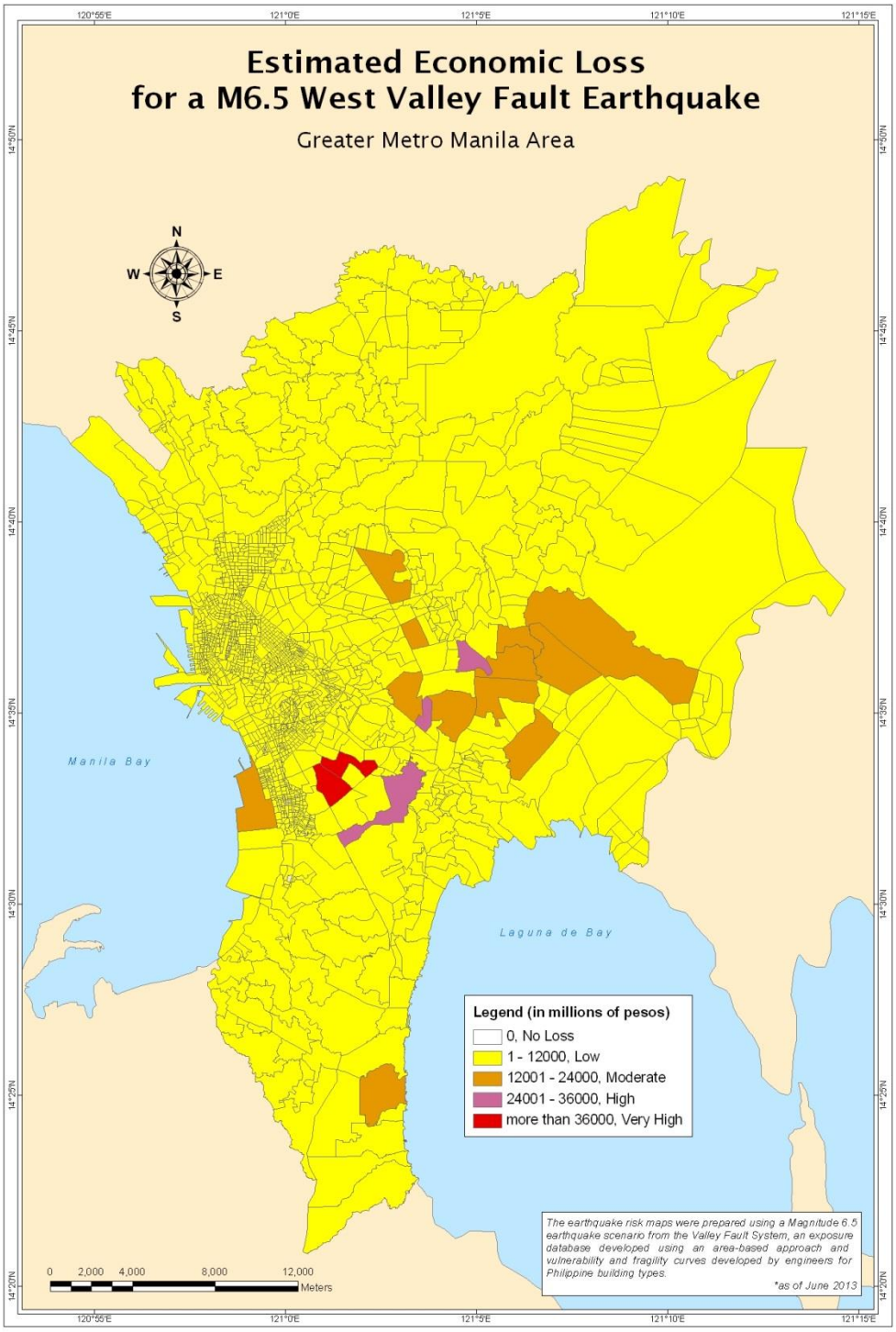

Figure C.6. Estimated Economic Loss for a M6.5 earthquake.

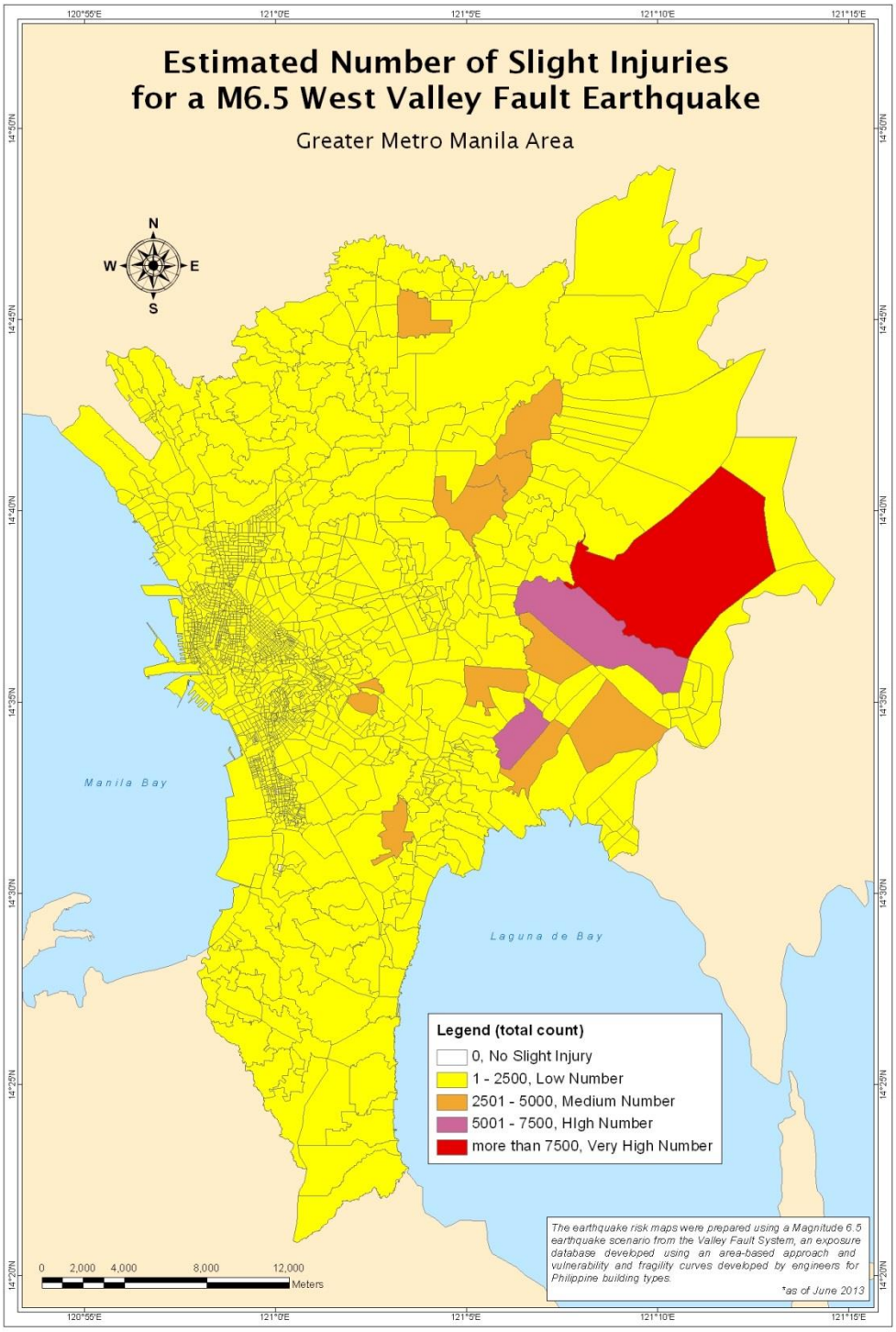

Figure C 7. Estimated Number of Slight Injuries for a M6.5 earthquake.

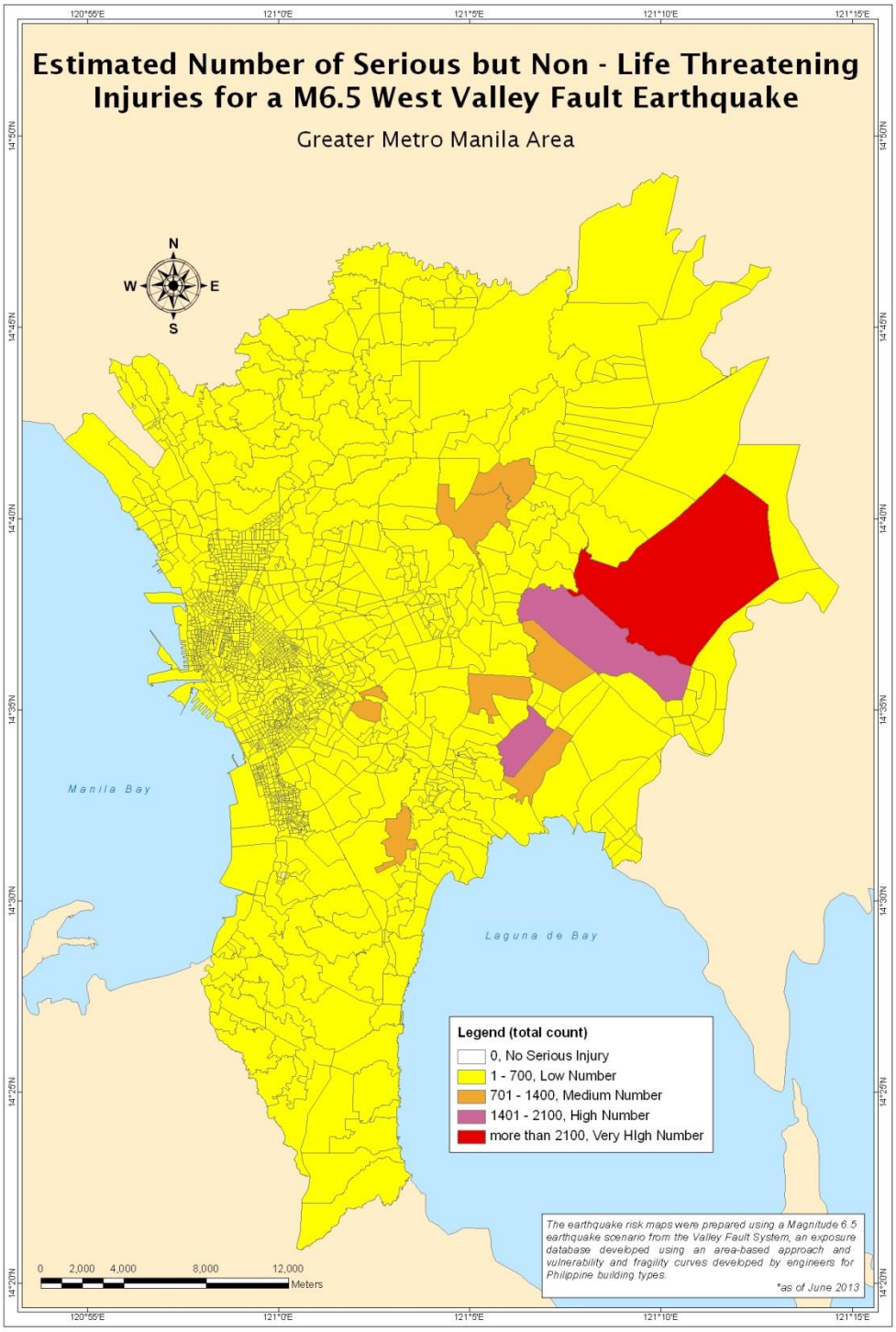

Figure C.8. Estimated Number of Serious but Non-Life Threatening Injuries for a M6.5 earthquake.

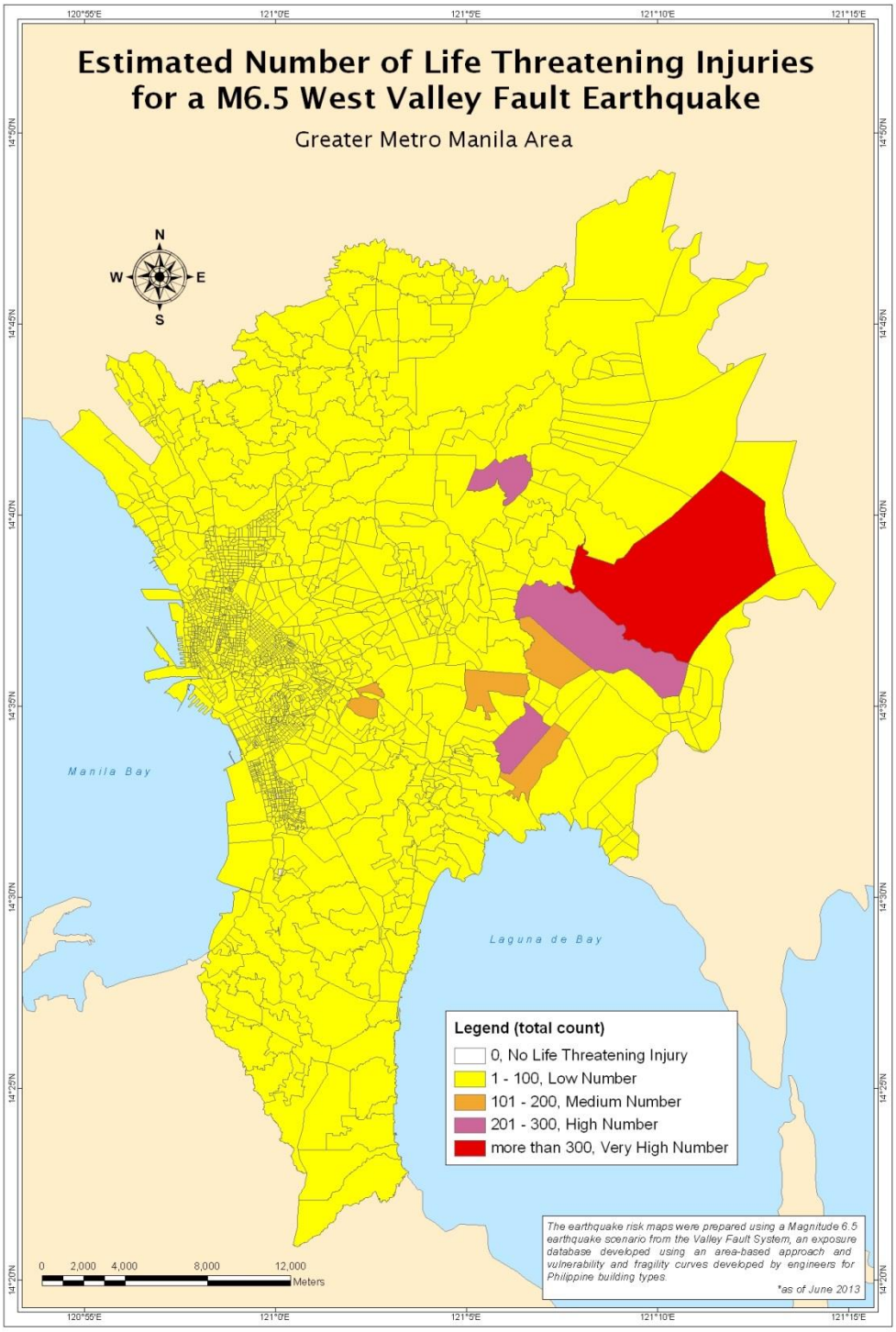

Figure C.9. Estimated Number of Life Threatening Injuries for a M6.5 earthquake.

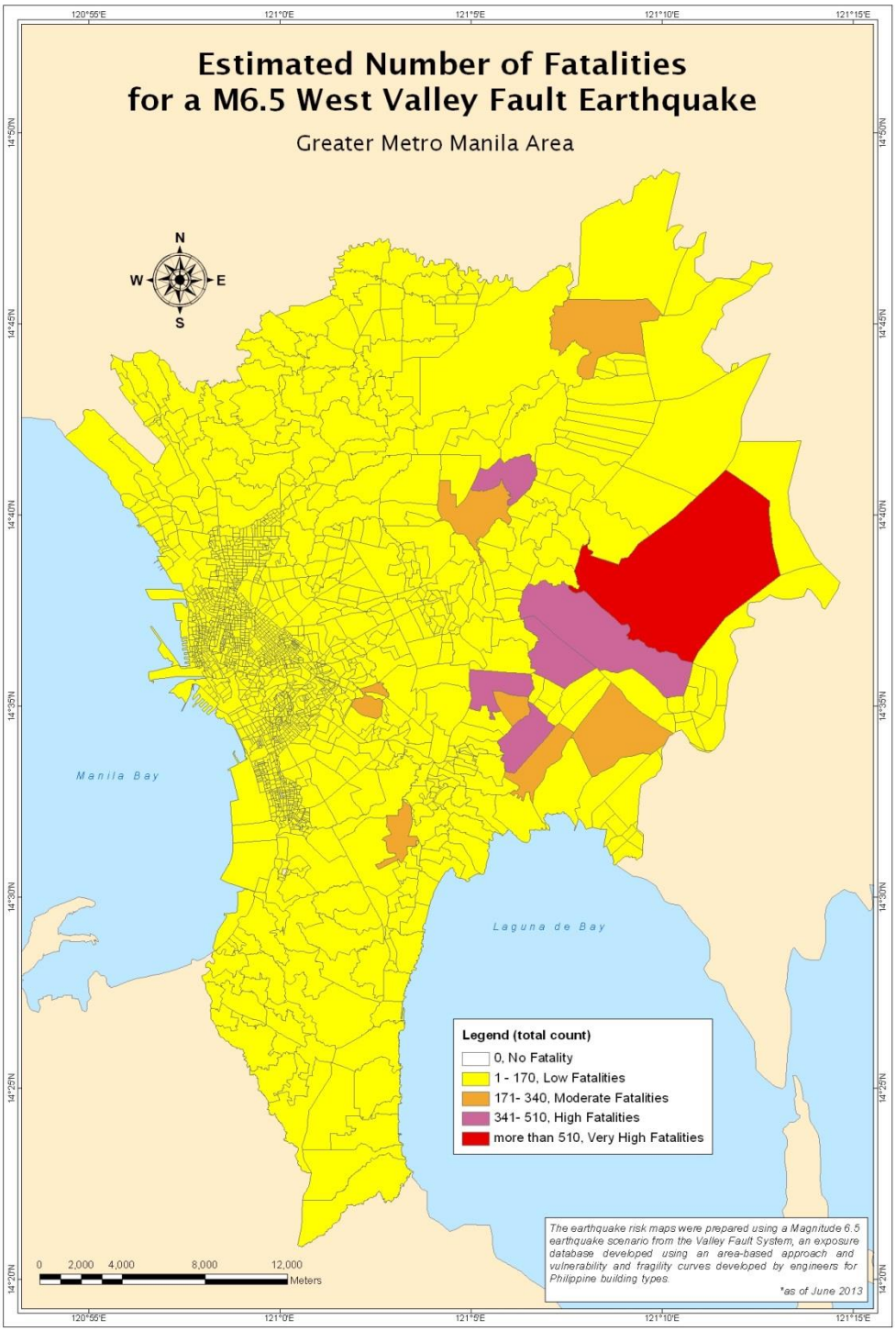

Figure C.10. Estimated Number of Fatalities for a M6.5 earthquake.

Appendix D - Risk Maps for a M6.5 Earthquake (Normalized per Barangay)

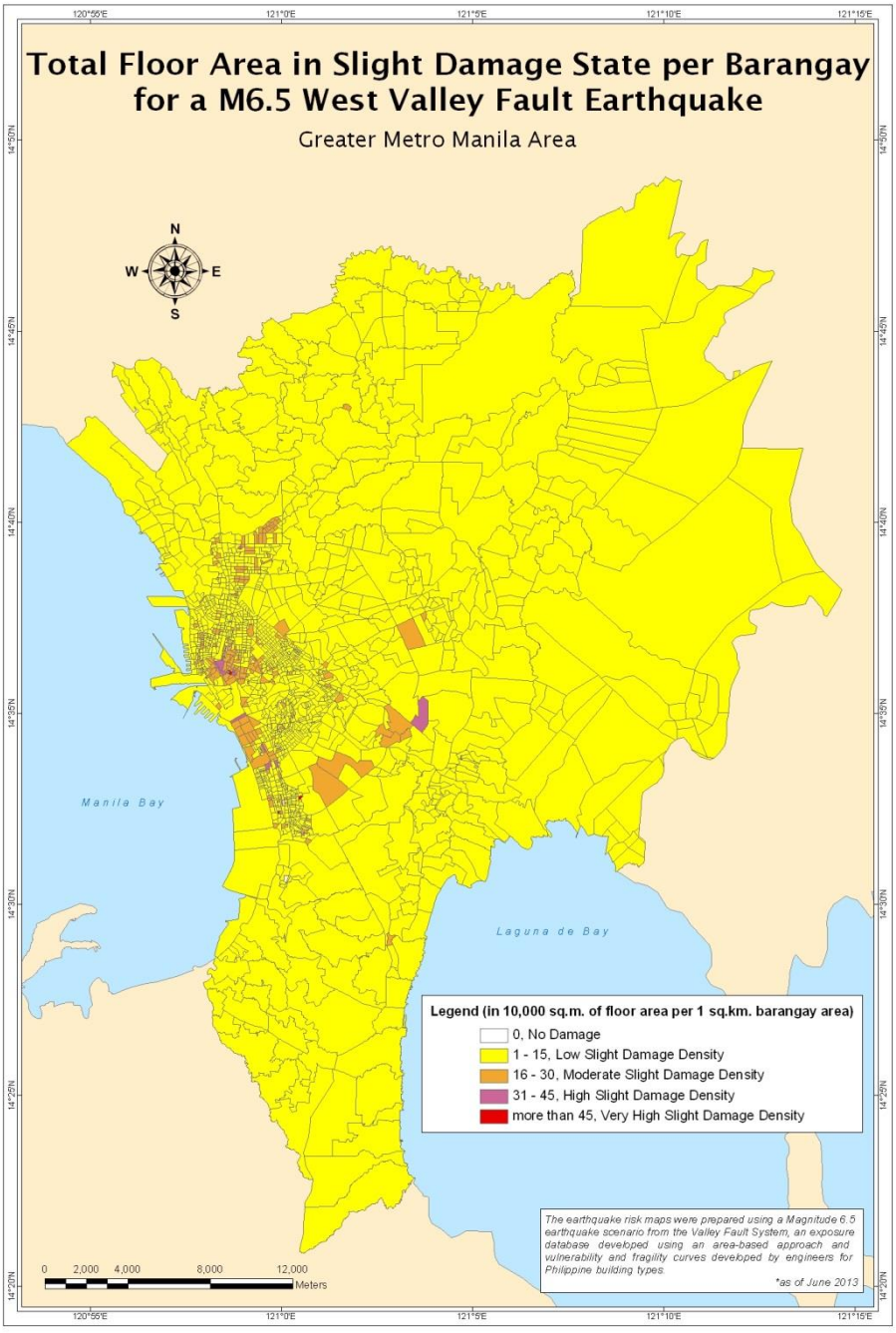

Figure D.1. Total Floor Area (Normalized per Barangay) in Slight Damage State for a M6.5 earthquake.

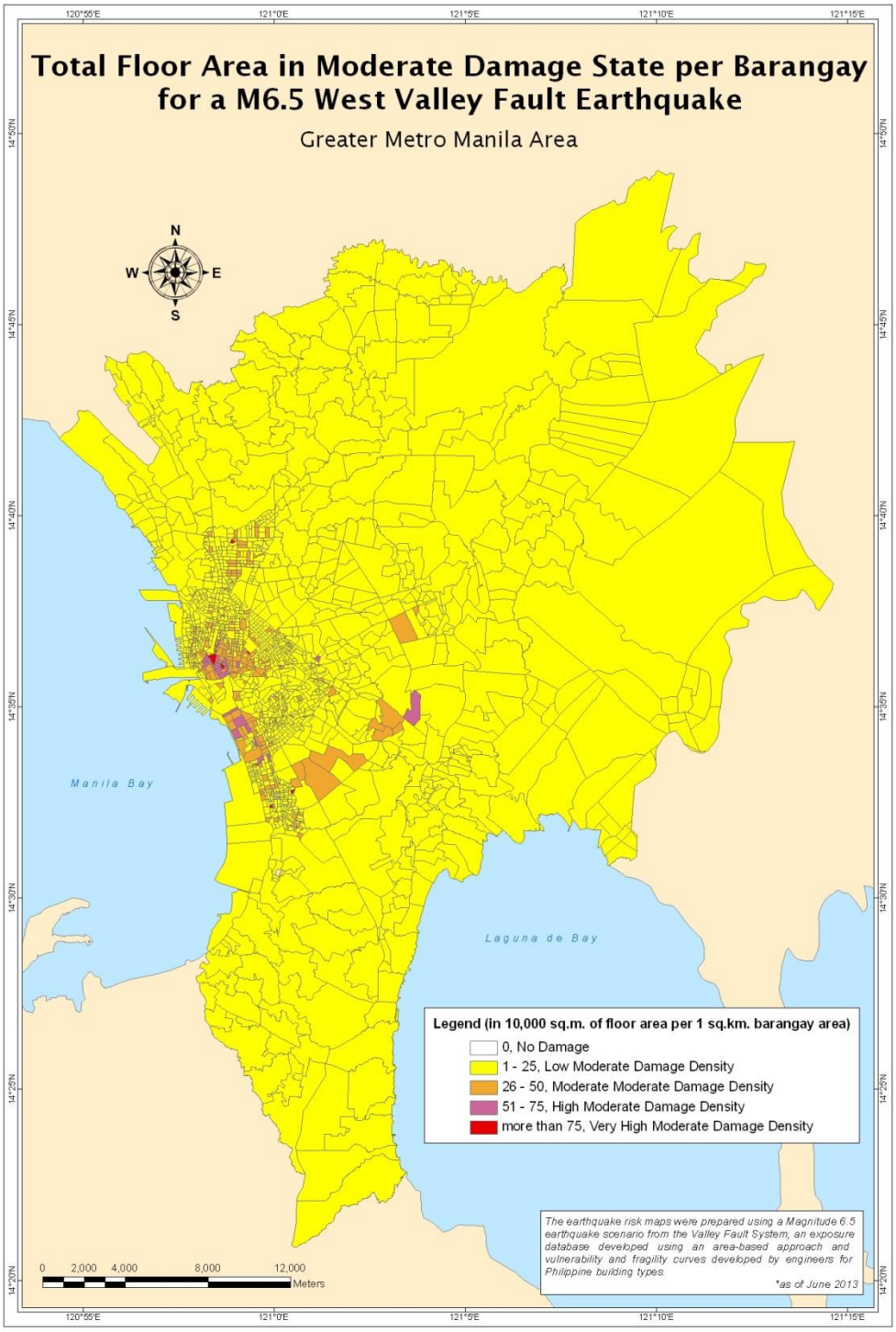

Figure D.2. Total Floor Area (Normalized per Barangay) in Moderate Damage State for a M6.5 earthquake.

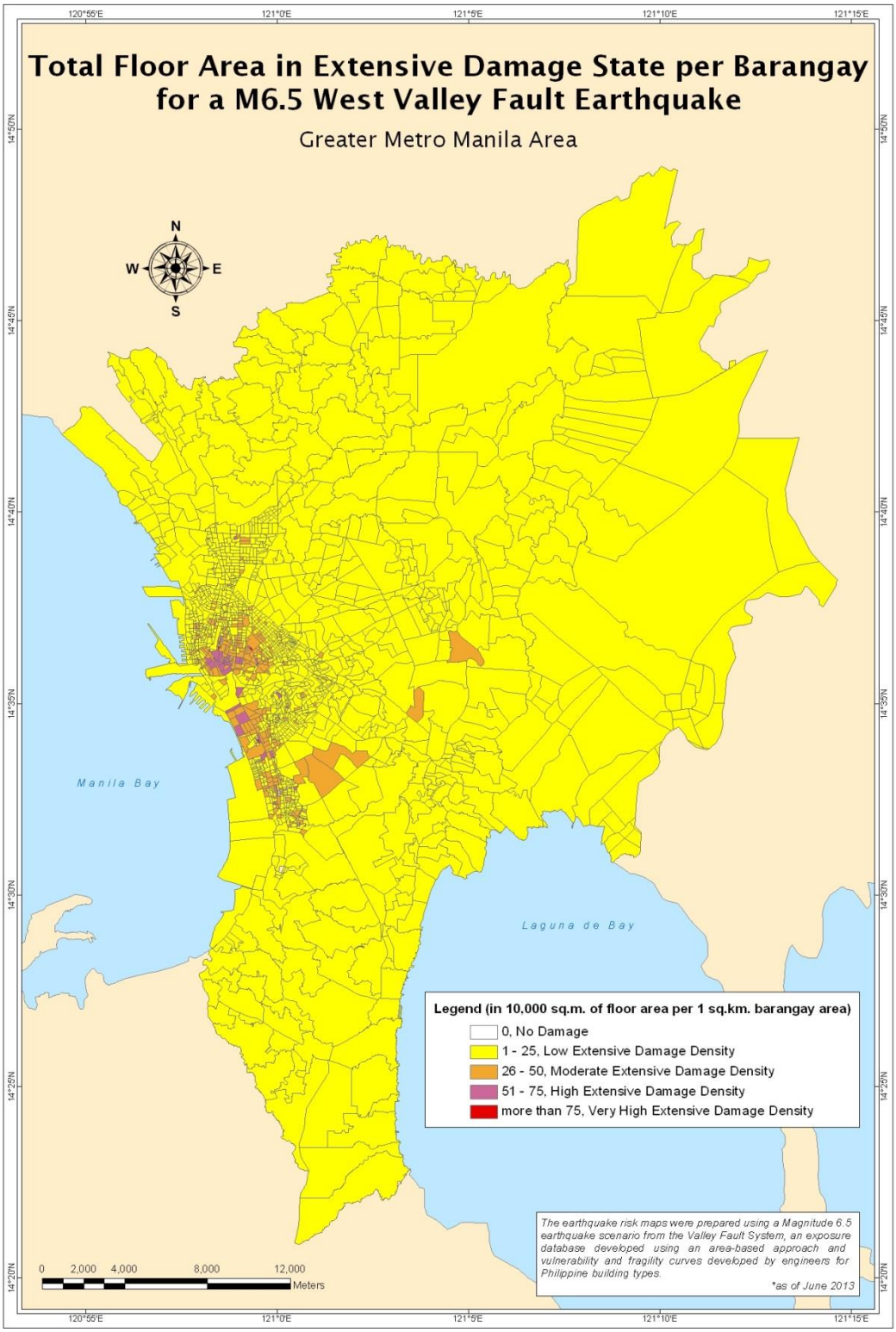

Figure D.3. Total Floor Area (Normalized per Barangay) in Extensive Damage State for a M6.5 earthquake.

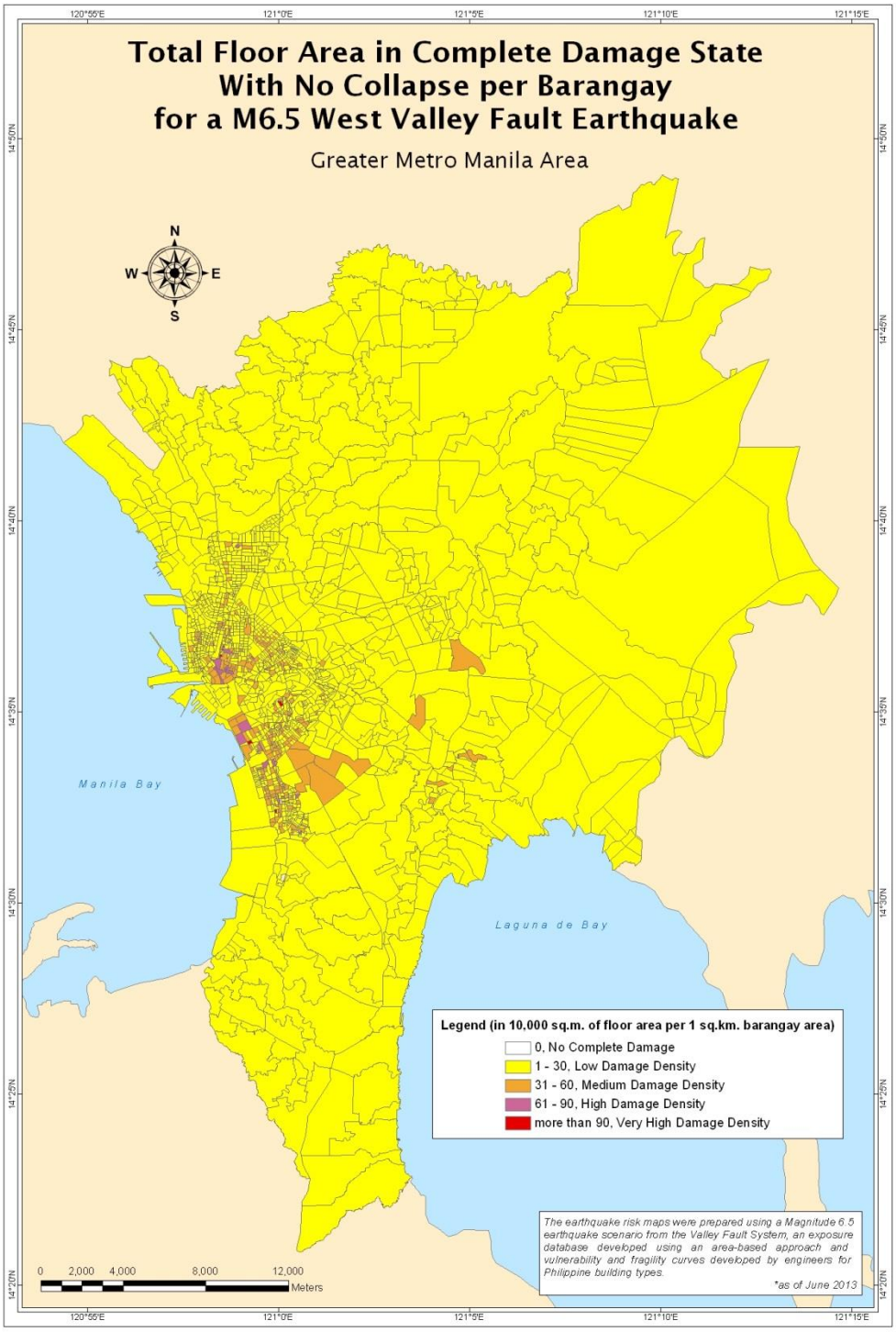

Figure D.4. Total Floor Area (Normalized per Barangay) in Complete Damage State with No Collapse for a M6.5 earthquake.

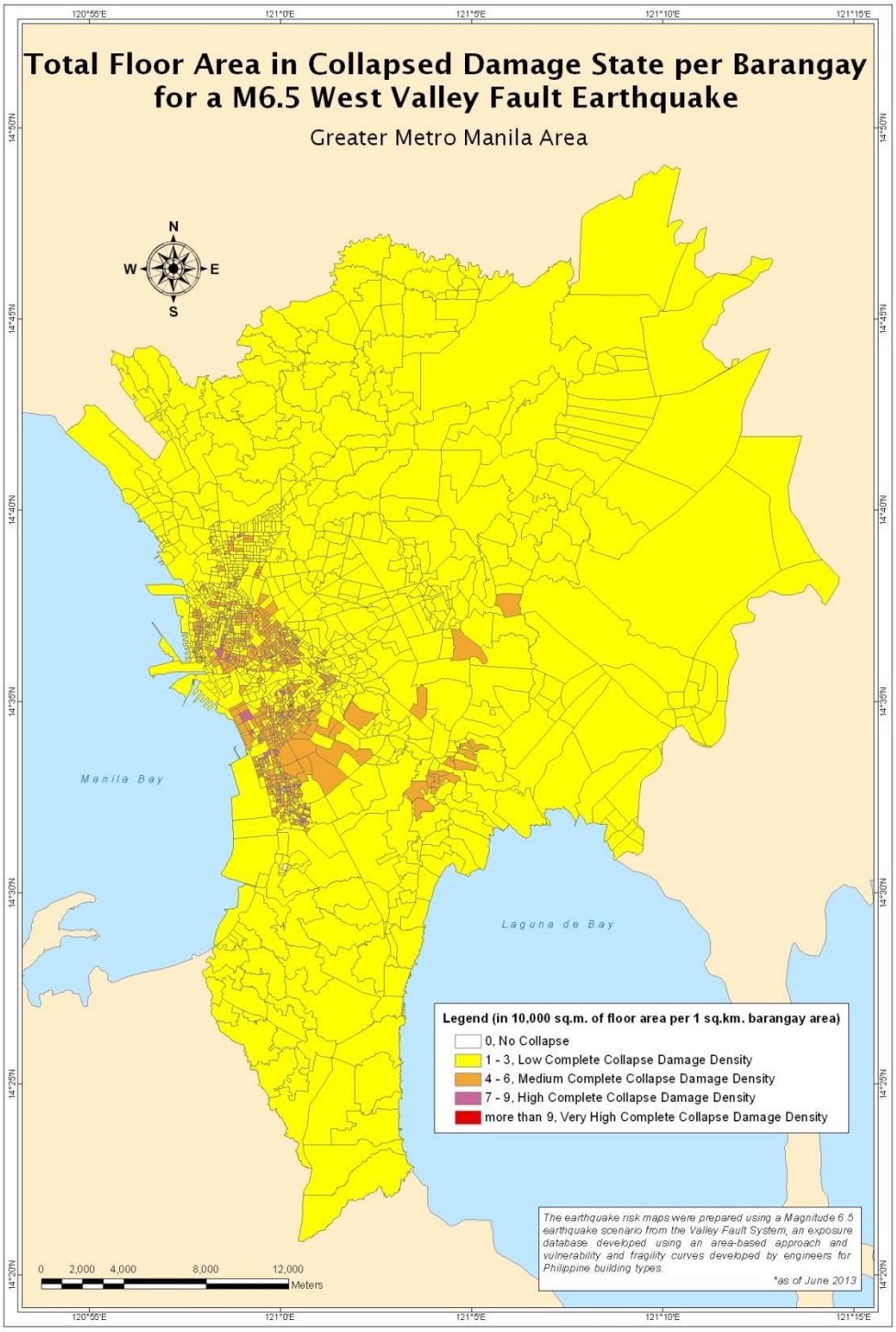

Figure D.5. Total Floor Area (Normalized per Barangay) in Collapsed Damage State for a M6.5 earthquake.

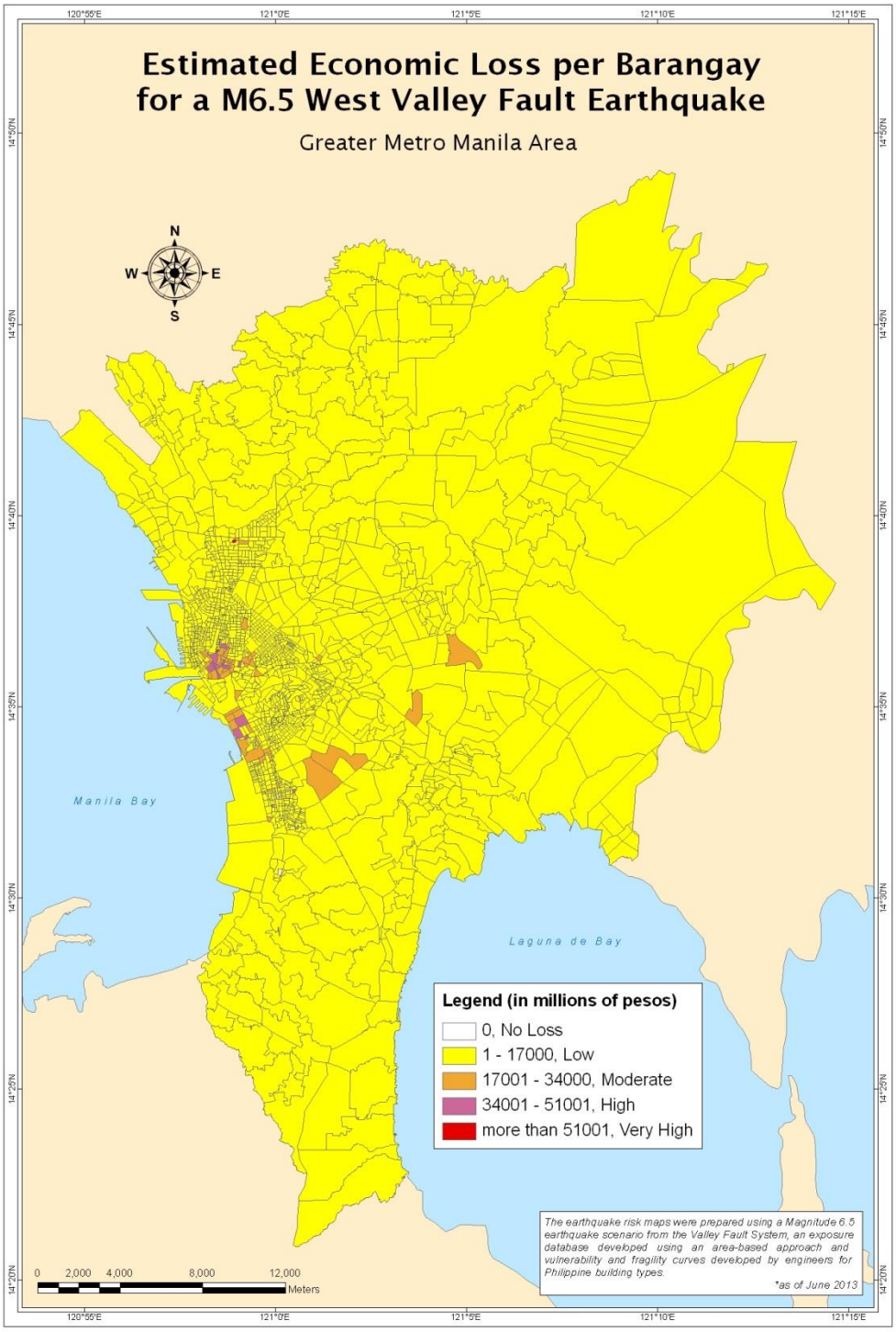

Figure D.6. Estimated Economic Loss (Normalized per Barangay) for a M6.5 earthquake.

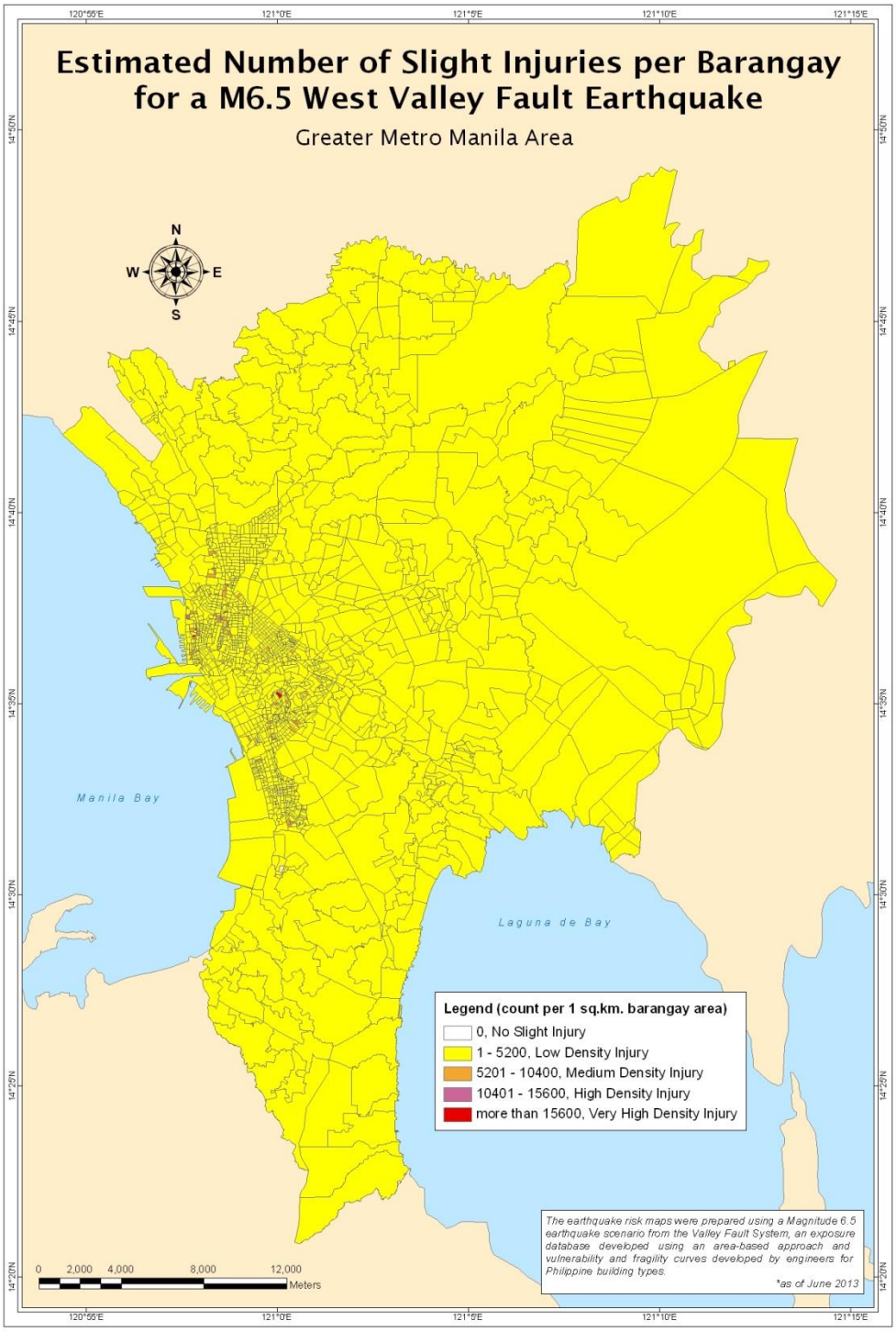

Figure D.7. Estimated Number of Slight Injuries (Normalized per Barangay) for a M6.5 earthquake.

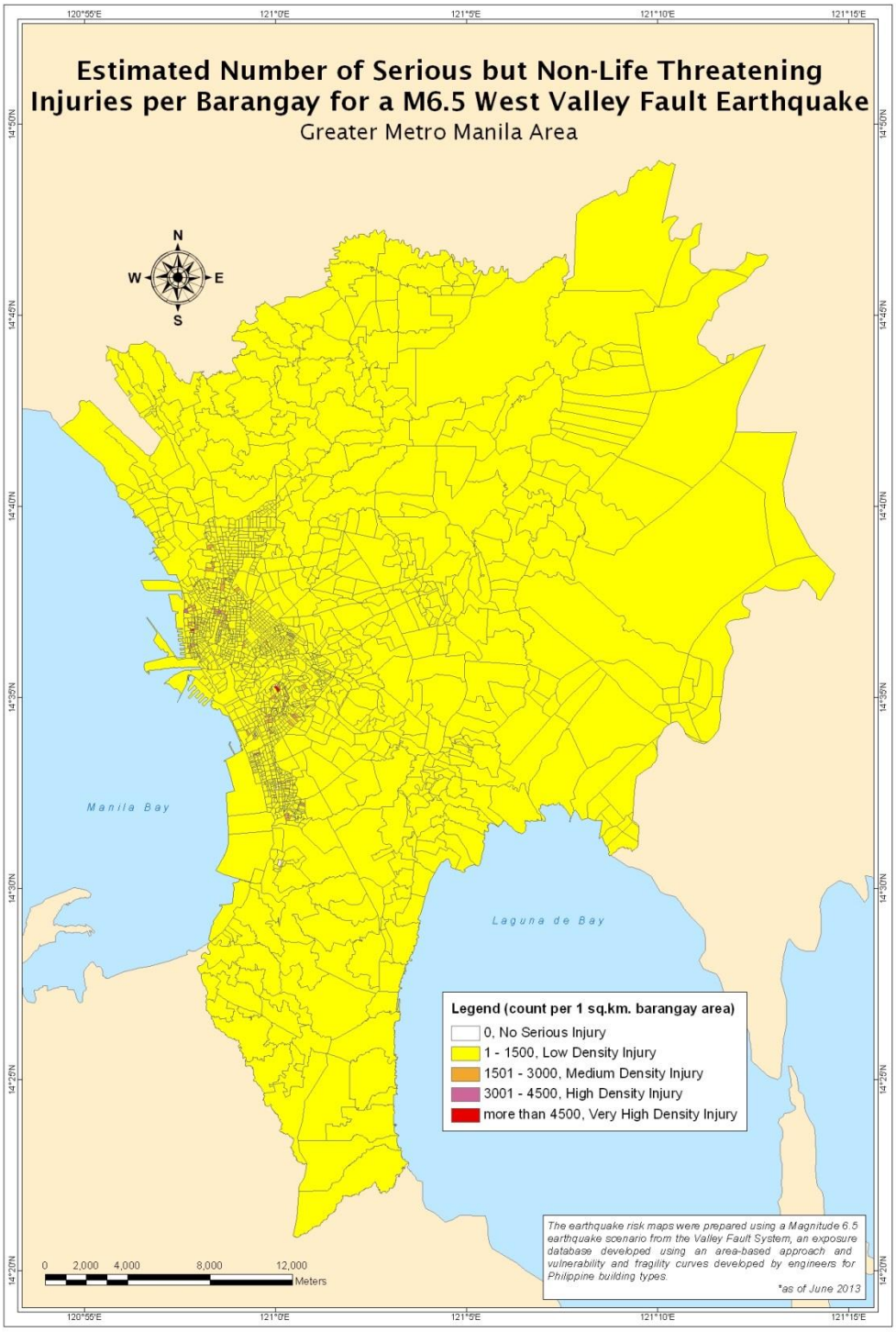

Figure D.8. Estimated Number of Serious but Non-Life Threatening Injuries (Normalized per Barangay) for a M6.5 earthquake.

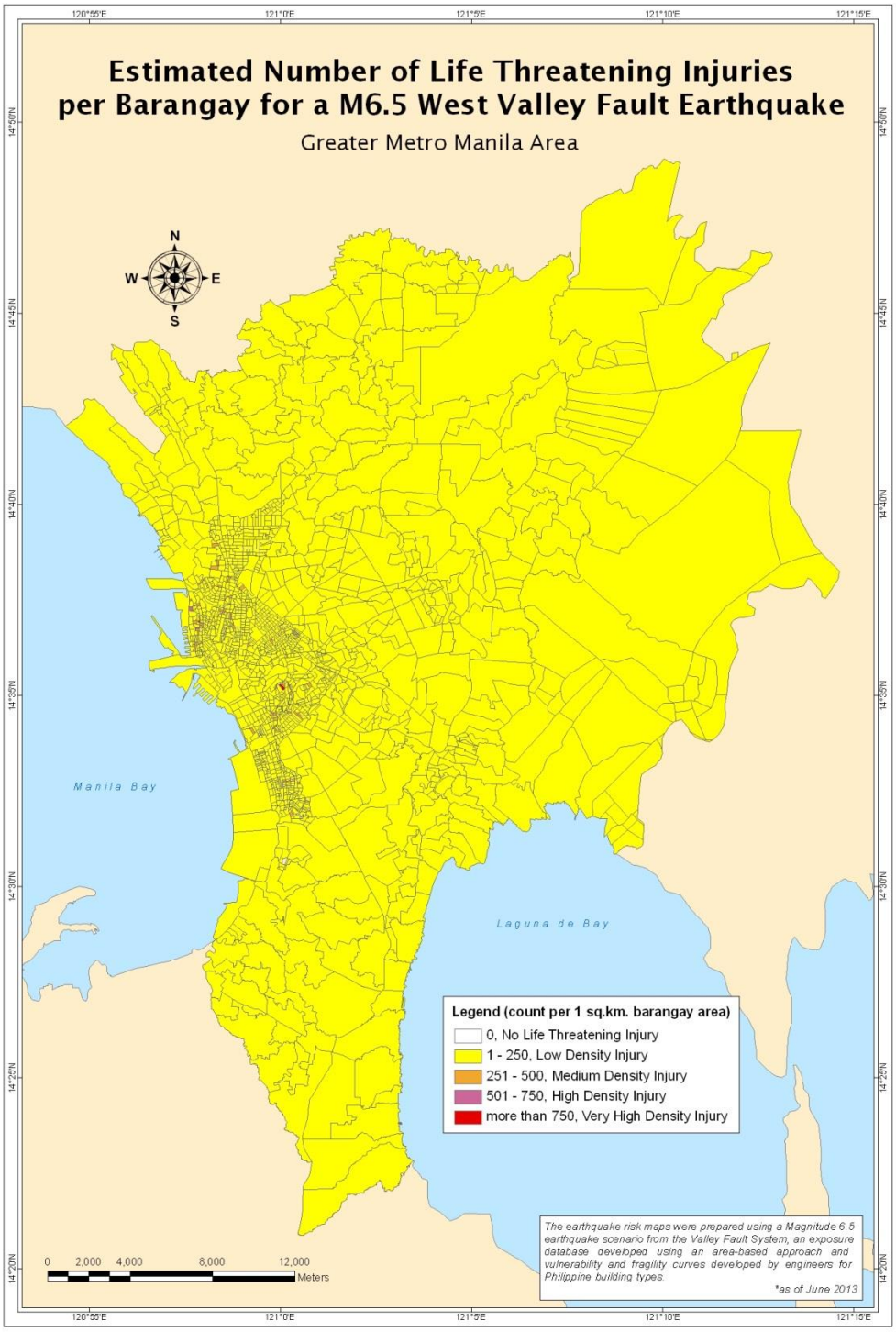

Figure D.9. Estimated Number of Life Threatening Injuries (Normalized per Barangay) for a M6.5 earthquake.

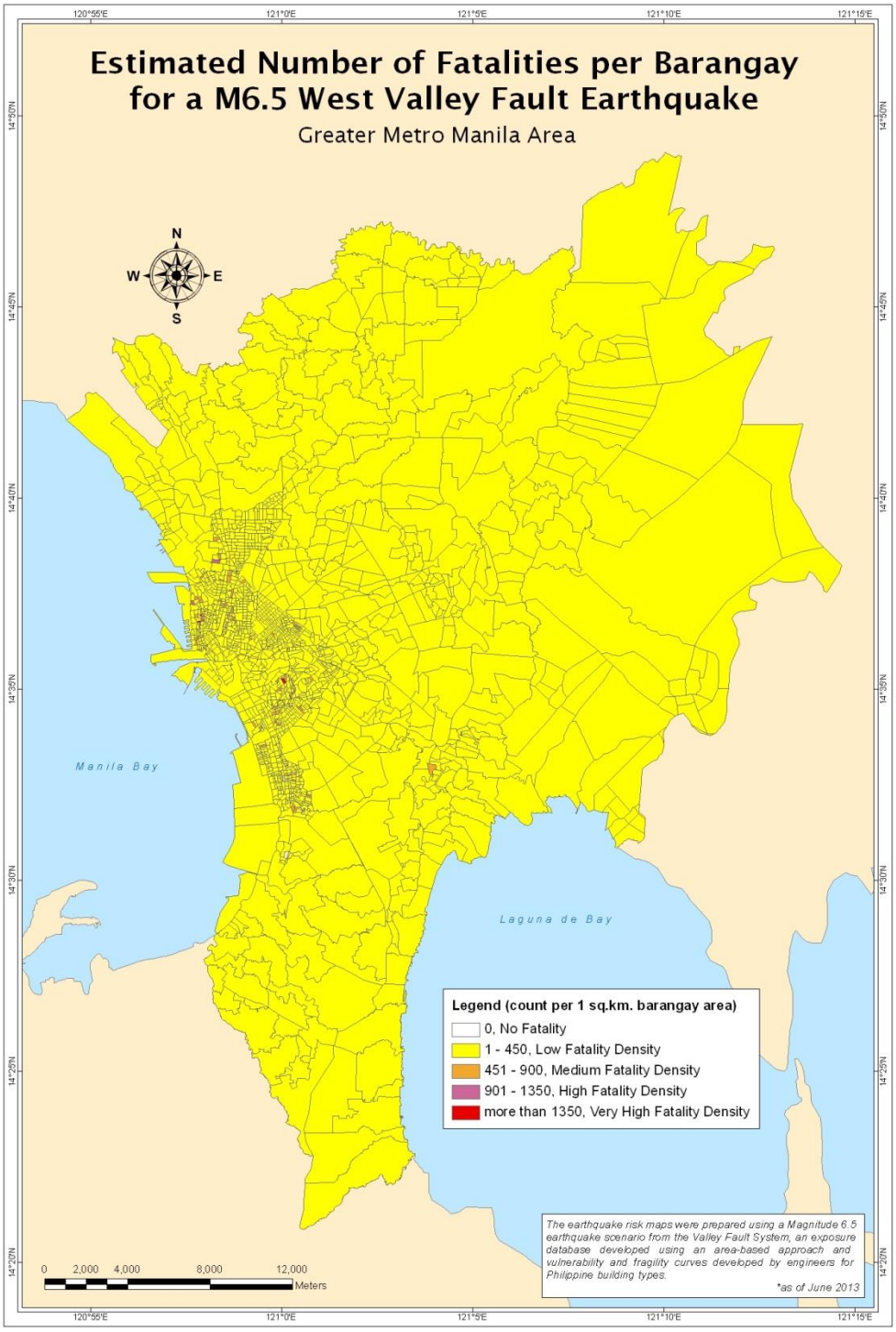

Figure D.10. Estimated Number of Fatalities (Normalized per Barangay) for a M6.5 earthquake.

Appendix E - Geotechnical Database Schema

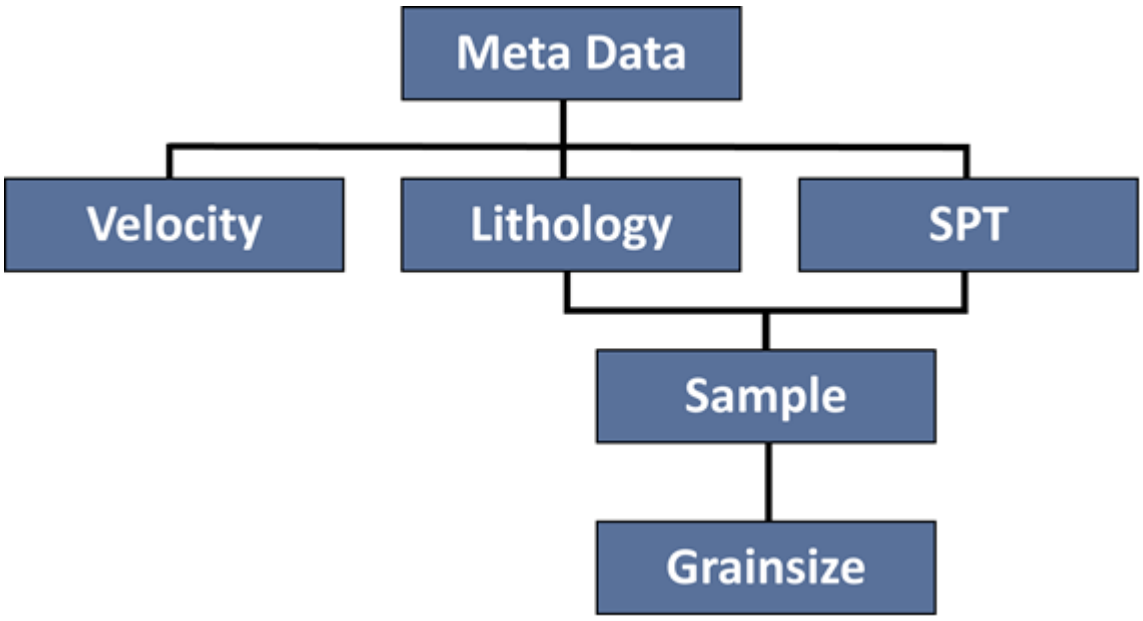

Figure E.1. Schematic diagram of Geotechnical Database Schema

E.1 Meta Data – Tier 1

Attribute	Type	Description
ID	numeric	Unique identifier
Borehole ID	numeric	Uses NSO codes as part of sequence (province, municipal, barangay, id)
Site Name, Project Name and/or Test Name	character	Name of particular project or test (e.g., MMEIRS)
Well Number	character	Project well number
Geotechnical Services Provider	character	Name of service provider
Service Provider ID	character	ID for service provider reference
Street address	character	
Barangay	character	
Municipality/city	character	
Province	character	
Latitude	numeric	
Longitude	numeric	
X reference	numeric	e.g. relative to cadastral points, UTM (no automatic georeferencing)
Y reference	numeric	e.g. relative to cadastral points, UTM (no automatic georeferencing)
Location reference type	character	e.g. cadastral points, UTM

Attribute	Type	Description
Elevation	numeric	Elevation above sea level (m)
Date of survey	date	
Last modified	date	Date record was last modified
Total borehole depth	numeric	
Data custodian	character	name of, or reference to data collection project
Custodian borehole ID	character	Reference ID given by data custodian if applicable
Method	character	Type of data gathered- if Vs measured then Vs table populated, if borehole, then Lithology table populated
Vs30	numeric	Vs30 of site
Station Owner	character	Seismic station information (e.g., PHIVOLCS)
Station ID	character	Seismic station information
Station distance	numeric	Distance from site to seismic station
Surface geology	character	e.g., Quaternary gravels, etc
Surface geology source	character	e.g, field observation, geological map, etc
Geomorphic terrain	character	e.g., flood plain, river terrace, hill slope, reclaimed land, etc
Water Table Depth	numeric	Depth to water table (m)
Files	character	Link and filename of scanned paper records (e.g., pdf, jpg)
Data encoder	character	Name of data encoder

E.2 VS measurements – Tier 2

Attribute	Type	Description
id	numeric	unique identifier
Borehole ID	numeric	Uses NSO codes as part of sequence (province, municipal, barangay, id)
From depth/layer top	numeric	upper depth of sample (m)
To depth/layer bottom	numeric	lower depth of sample (m)
Vs	numeric	measured VS for layer

E.3 Lithology – Tier 2

Attribute	Type	Description
id	numeric	
Borehole ID	numeric	
Layer ID	numeric	
from depth/layer top	numeric	upper depth of sample (m)
to depth/layer bottom	numeric	lower depth of sample (m)
Soil classification (USCS)	character	Unified Soil Classification System (e.g.G(ravel), S(and))
Soil layer thickness	numeric	
consistency	character	e.g., Very soft, soft, medium stiff, very stiff, hard (Cohesive soil) . Loose, medium loose, dense, very dense (Noncohesive soil)

E.4 SPT – Tier 2

Attribute	Type	Description
id	numeric	
Borehole ID	numeric	
Layer ID	numeric	Used if sample from borehole log
SPT ID	numeric	Used if sample from SPT
Depth to top of SPT penetration	numeric	upper depth of sample (m)
Depth to bottom of SPT penetration	numeric	lower depth of sample (m)
SPT-N - raw	numeric	N value (blow count (blows/300mm)) raw data
SPT-N - corrected	numeric	N value (blow count (blows/300mm)) corrected for overburden
SCPT - raw	numeric	(Fs/Qc, Qc=tip resistance, Fs=side resistance)
SCPT - corrected	numeric	(Fs/Qc, Qc=tip resistance, Fs=side resistance)

E.5 Sample – Tier 3

Attribute	Type	Description
id	numeric	
Borehole ID	numeric	
Layer ID	numeric	Used if sample from borehole log
SPT ID	numeric	Used if sample from SPT
Sample ID		
Depth to top of sample	numeric	Depth of sampling
Depth to bottom of sample	numeric	Depth of sampling
moisture content	numeric	% ??? Vol/Vol, g/g?
plasticity index	numeric	PI=Liquid Limit (LL)-Plastic Limit (PL)
density	numeric	Material density (g/cm^3)
maximum compressive stress	numeric	result from unconfined compression test (kg/cm^2)
cohesion	numeric	result from direct shear test (kg/cm^2)
angle internal friction	numeric	result from direct shear test (degrees)

E.6 Grainsize – Tier 4

Attribute	Type	Description
id	numeric	
Borehole ID	numeric	
Layer ID	numeric	Used if sample from borehole log
SPT ID	numeric	Used if sample from SPT
Sample ID		
Grainsize	numeric	ASTM classification
Proportion	numeric	Percentage per grainsize

Appendix F - List of Borehole V_{S30} Estimates

Table F.1. List of Borehole VS30 Estimates.

Longitude	Latitude	V_{S30} (Lithology)	V_{S30} (SPT-N)	V_{S30} (Mean)
120.984010	14.584419	182.6346	211.7178	197.1762
120.984052	14.584692	206.2391	224.2930	215.2661
120.984090	14.585086	244.1689	246.6605	245.4147
120.982733	14.579875	273.3892	274.0856	273.7374
120.982969	14.580018	209.6957	203.8269	206.7613
120.983331	14.580208	174.5080	187.2346	180.8713
120.969680	14.591726	148.8149	166.7632	157.7891
120.969433	14.591534	148.9218	155.3421	152.1320
120.969449	14.591809	146.8720	155.3720	151.1220
120.969202	14.592030	174.4304	161.8081	168.1193
120.969452	14.592105	147.4907	166.1575	156.8241
120.969181	14.591428	142.5847	148.5930	145.5889
120.983764	14.579291	205.4249	220.8642	213.1446
120.983909	14.578980	229.8279	233.5785	231.7032
120.983904	14.578884	224.4892	211.2939	217.8916
120.983976	14.578889	221.3168	218.0876	219.7022
120.983665	14.579478	218.6463	202.0218	210.3341
121.006723	14.576651	287.4361	310.6627	299.0494
121.006836	14.576716	284.8999	292.6961	288.7980
120.975711	14.629667	235.0911	226.3545	230.7228
120.975681	14.629278	254.3852	263.2465	258.8159
120.969681	14.587085	131.0277	124.6097	127.8187
120.983622	14.579592	192.9607	198.8664	195.9136
120.963032	14.634955	294.2355	0.0000	147.1178
120.962678	14.634955	337.8487	286.7442	312.2965
120.958066	14.626929	337.1301	341.1187	339.1244
120.957921	14.626280	382.6619	390.9591	386.8105
120.957132	14.627261	343.0992	355.0313	349.0653
121.096800	14.662200	298.8662	247.9792	273.4227
121.096800	14.662200	281.2860	241.6015	261.4438
121.096800	14.662200	241.5033	242.0742	241.7888

Longitude	Latitude	V_{S30} (Lithology)	V_{s30} (SPT-N)	V_{S30} (Mean)
121.096800	14.662200	276.0597	234.1781	255.1189
121.096800	14.662200	262.7064	0.0000	131.3532
121.086200	14.747200	500.0000	500.0000	500.0000
121.086200	14.747200	460.5263	470.6978	465.6121
121.084900	14.664500	252.2655	199.1751	225.7203
121.123400	14.702900	448.7179	449.7236	449.2208
121.123400	14.702900	535.7143	529.2918	532.5031
121.031822	14.399515	472.0280	476.8265	474.4273
121.031938	14.399372	576.9231	648.8198	612.8715
121.032576	14.399583	630.8411	646.2371	638.5391
121.032689	14.399448	638.5135	639.5438	639.0287
121.032302	14.399409	681.8182	0.0000	340.9091
121.032179	14.399512	700.0000	0.0000	350.0000
121.032378	14.399577	700.0000	0.0000	350.0000
121.032498	14.399455	638.5135	658.1174	648.3155
120.996200	14.499500	154.5946	147.6332	151.1139
120.996200	14.499500	406.1896	0.0000	203.0948
120.996200	14.499500	168.2353	0.0000	84.1177
121.049100	14.452100	116.7347	0.0000	58.3674
121.049100	14.452100	471.9101	0.0000	235.9551
121.049100	14.452100	157.6010	0.0000	78.8005
121.031354	14.459223	623.7624	591.6151	607.6888
120.999426	14.473875	0.0000	394.4948	197.2474
121.030522	14.487424	578.2313	578.2313	578.2313
121.006104	14.512207	362.4535	371.0996	366.7766
121.038559	14.492163	409.7483	406.6955	408.2219
121.010577	14.494734	506.6345	543.6647	525.1496
121.010495	14.494675	529.6343	569.1065	549.3704
121.004066	14.472536	340.9091	407.0834	373.9963
121.042381	14.485938	360.0000	0.0000	180.0000
120.995571	14.530217	360.1695	394.9440	377.5568
120.979658	14.530243	177.9679	183.6796	180.8238
120.979523	14.530232	156.7005	169.1858	162.9432
120.979579	14.530434	165.7670	184.5316	175.1493
120.979493	14.530642	151.9736	139.4558	145.7147
120.979648	14.530679	154.8125	175.0078	164.9102
121.008678	14.538649	216.5541	182.5088	199.5315

Longitude	Latitude	V_{S30} (Lithology)	V_{s30} (SPT-N)	V_{S30} (Mean)
121.008650	14.538207	298.5154	266.9954	282.7554
121.010687	14.538490	293.5967	292.6199	293.1083
121.010460	14.538912	264.1795	229.4054	246.7925
121.011907	14.539008	298.8910	303.0639	300.9775
121.008218	14.538534	305.9435	326.2397	316.0916
121.007954	14.538507	257.5958	268.6834	263.1396
121.006811	14.538347	270.1864	278.7317	274.4591
121.004368	14.538063	254.8154	279.1617	266.9886
121.066491	14.557466	451.4511	429.8200	440.6356
121.066456	14.557577	541.4560	530.9990	536.2275
121.066164	14.557573	586.5922	579.6034	583.0978
121.084421	14.558396	214.3011	188.1951	201.2481
121.083980	14.559158	256.8890	178.6526	217.7708
121.064556	14.542160	156.3074	210.2456	183.2765
121.064622	14.542192	186.2947	231.0867	208.6907
121.047684	14.656724	550.6993	575.3503	563.0248
121.047808	14.656821	609.2843	639.6895	624.4869
121.047897	14.656906	579.5455	634.3983	606.9719
121.068444	14.622196	556.5371	565.5197	561.0284
121.068173	14.622172	361.6533	384.3619	373.0076
121.068200	14.622276	681.8182	681.8182	681.8182
121.045300	14.724300	579.5768	506.0411	542.8090
121.045300	14.724300	579.5768	506.0411	542.8090
121.045300	14.724300	560.9973	491.8194	526.4084
121.045300	14.724300	555.0661	487.2548	521.1605
121.037733	14.651992	690.7895	690.7895	690.7895
121.037981	14.652065	673.0769	673.0769	673.0769
121.038104	14.652162	673.0769	673.0769	673.0769
121.032694	14.726801	494.6319	494.6319	494.6319
121.032694	14.726801	497.3015	497.3015	497.3015
121.094233	14.694582	251.1364	291.2283	271.1824
121.044165	14.635877	649.8603	584.3537	617.1070
121.043802	14.649696	609.2843	612.1967	610.7405
121.044589	14.649015	681.8182	681.8182	681.8182
121.042286	14.648770	690.7895	690.7895	690.7895
121.042988	14.648311	681.8182	681.8182	681.8182
121.042849	14.649309	690.7895	690.7895	690.7895

Longitude	Latitude	V_{S30} (Lithology)	V_{s30} (SPT-N)	V_{S30} (Mean)
121.043641	14.649045	690.7895	690.7895	690.7895
121.043583	14.648590	690.7895	690.7895	690.7895
121.031650	14.653898	594.5222	627.5710	611.0466
121.031919	14.654068	601.3319	626.5376	613.9348
121.032460	14.654420	631.4685	619.0179	625.2432
121.031868	14.653555	610.9364	625.0672	618.0018
121.032452	14.653943	622.3042	654.7761	638.5402
121.032987	14.654289	649.8603	645.5331	647.6967
121.032092	14.653227	558.7437	575.3503	567.0470
121.032361	14.653410	569.6738	588.1532	578.9135
121.032910	14.653778	671.8750	658.9649	665.4200
121.033491	14.654174	685.6492	685.6492	685.6492
121.032300	14.652922	624.4813	566.9324	595.7069
121.032895	14.653304	618.9595	566.9324	592.9460
121.033455	14.653681	685.6492	685.6492	685.6492
121.034038	14.654040	629.2425	611.4932	620.3679
121.032607	14.652562	607.7125	589.8262	598.7694
121.032841	14.652718	625.0000	627.3167	626.1584
121.031502	14.653443	495.6030	499.2543	497.4287
121.032750	14.651517	476.0000	509.2888	492.6444
121.034229	14.649233	570.8955	590.5707	580.7331
121.038977	14.641926	417.0561	479.4606	448.2584
121.042798	14.636081	570.8955	631.8019	601.3487
121.043844	14.634481	579.5455	606.0400	592.7928
121.045369	14.631898	502.9586	523.9597	513.4592
121.046075	14.630389	519.1469	528.2674	523.7072
121.046606	14.629643	634.1030	634.1030	634.1030
121.046890	14.628609	412.1609	406.8448	409.5029
121.047770	14.626680	562.5000	618.9844	590.7422
121.050774	14.619742	480.8728	522.2089	501.5409
121.051825	14.618263	459.3511	489.4096	474.3804
121.052475	14.616026	690.7895	690.7895	690.7895
121.053505	14.614220	616.4384	646.2371	631.3378
121.055038	14.610933	620.6897	635.1789	627.9343
121.055854	14.609163	495.6612	515.6966	505.6789
121.059714	14.599477	634.1030	675.3023	654.7027
121.059652	14.597184	690.7895	690.7895	690.7895

Longitude	Latitude	V_{S30} (Lithology)	V_{S30} (SPT-N)	V_{S30} (Mean)
121.058836	14.594443	690.7895	690.7895	690.7895
121.032963	14.652917	685.6492	668.9832	677.3162
121.032780	14.652963	700.0000	700.0000	700.0000
121.032470	14.653162	700.0000	700.0000	700.0000
121.037300	14.603331	425.4363	402.5519	413.9941
121.037244	14.603233	436.6438	429.7623	433.2031
120.958056	14.630000	368.5039	325.9389	347.2214
120.965833	14.625278	299.3228	304.0828	301.7028
120.963056	14.626667	244.7229	246.2058	245.4644
120.964722	14.626389	232.4243	211.0129	221.7186
120.964722	14.625833	244.7940	227.1282	235.9611
120.964444	14.626111	254.6670	234.6477	244.6574
120.964167	14.626111	236.6167	207.7508	222.1838
120.969167	14.633889	409.1456	406.6710	407.9083
120.968889	14.634722	414.1852	410.2516	412.2184
120.994041	14.576031	207.4079	216.7858	212.0969
120.993975	14.576250	198.7665	203.3379	201.0522
120.991872	14.578190	216.8046	208.9220	212.8633
120.991796	14.578156	199.4665	165.2500	182.3583
120.991908	14.578021	187.7974	169.1255	178.4615
120.991975	14.577777	172.6203	147.3368	159.9786
120.992062	14.577818	189.7068	156.6713	173.1891
120.985064	14.599796	168.6937	168.0971	168.3954
120.985133	14.599975	162.4841	154.9725	158.7283
120.983753	14.601294	156.1764	156.8715	156.5240
120.984916	14.600175	146.3856	140.8121	143.5989
120.984881	14.597705	154.5046	190.0765	172.2906
120.984881	14.597705	182.4068	197.0348	189.7208
120.982921	14.599053	196.3344	176.9269	186.6307
120.982811	14.599034	179.7225	175.1827	177.4526
120.982741	14.598964	179.1463	175.4461	177.2962
120.982805	14.598886	182.9090	147.8300	165.3695
120.983541	14.595342	195.8935	203.8676	199.8806
121.092000	14.647200	491.9908	482.7152	487.3530
121.092000	14.647200	484.2342	430.4849	457.3596
121.092000	14.647200	481.7028	411.1452	446.4240
121.092000	14.647200	489.3778	434.2416	461.8097

Longitude	Latitude	V_{S30} (Lithology)	V_{s30} (SPT-N)	V_{S30} (Mean)
121.121840	14.654090	284.5051	285.3253	284.9152
121.121840	14.654090	313.6135	314.7093	314.1614
121.121840	14.654090	330.1887	386.4561	358.3224
121.121840	14.654090	289.7455	335.9679	312.8567
121.121840	14.654090	296.6102	380.9491	338.7797
121.121840	14.654090	311.6051	327.5128	319.5590
121.086820	14.654960	500.0000	500.0000	500.0000
121.086820	14.654960	460.5263	470.6978	465.6121
121.083056	14.558333	250.9743	186.1150	218.5447
121.085556	14.557222	242.8090	184.9222	213.8656
121.078056	14.554444	273.1409	188.4771	230.8090
121.089722	14.555278	264.2384	175.0584	219.6484
121.091389	14.554444	287.4721	184.8152	236.1437
121.091944	14.555556	308.5405	169.2752	238.9079
121.088889	14.564444	249.9502	162.9558	206.4530
121.092778	14.576944	249.5585	207.6164	228.5875
121.093056	14.572778	233.4368	178.5337	205.9853
121.093333	14.568333	214.0878	193.7471	203.9175
121.091389	14.557222	270.5597	178.2944	224.4271
121.096389	14.558333	267.6796	228.8049	248.2423
121.095833	14.556944	242.6110	183.9287	213.2699
121.088333	14.573056	210.8752	179.5334	195.2043
121.090000	14.570556	221.2939	218.7519	220.0229
121.086667	14.568889	251.8858	177.7872	214.8365
121.074167	14.551389	127.8181	191.9858	159.9020
121.072222	14.549444	140.2540	200.9078	170.5809
121.078333	14.548611	148.7133	191.8246	170.2690
121.084330	14.654390	381.3559	418.1792	399.7676
121.071258	14.630372	535.4813	580.2436	557.8625
121.070277	14.629718	470.1493	491.6489	480.8991
121.034987	14.613878	579.5455	628.1111	603.8283
121.020037	14.607088	345.1687	373.2866	359.2277
121.016781	14.603881	573.2177	628.6556	600.9367
121.018268	14.605372	620.6897	598.1252	609.4075
121.032119	14.612492	427.6473	442.5805	435.1139
121.031992	14.612651	626.5356	681.8182	654.1769
121.032601	14.612581	634.1030	700.0000	667.0515

Longitude	Latitude	V_{S30} (Lithology)	V_{s30} (SPT-N)	V_{S30} (Mean)
121.042340	14.618272	480.2590	498.8926	489.5758
121.042928	14.618779	606.3523	606.3523	606.3523
121.050675	14.621660	616.4384	681.8182	649.1283
121.051045	14.622074	560.1328	587.2965	573.7147
121.051404	14.621979	626.1268	626.1268	626.1268
121.057136	14.625008	562.5000	624.7570	593.6285
121.057247	14.624872	490.1445	496.0336	493.0891
121.057586	14.625061	567.0267	563.5683	565.2975
121.064638	14.627911	578.6062	613.4021	596.0042
121.064993	14.627950	655.1074	634.6372	644.8723
121.065239	14.628186	493.3211	531.1292	512.2252
121.073240	14.631417	634.1030	700.0000	667.0515
121.072478	14.632829	620.6897	593.7271	607.2084
121.029333	14.611692	468.1967	448.2830	458.2399
121.023381	14.609591	419.5640	380.7494	400.1567
121.021116	14.607891	372.6708	386.1811	379.4260
121.017432	14.604273	681.8182	681.8182	681.8182
121.025906	14.610568	673.0769	673.0769	673.0769
121.026421	14.610575	637.4735	611.2436	624.3586
121.093056	14.530556	177.7830	149.8251	163.8041
121.093611	14.531111	156.6646	144.0351	150.3499
121.092500	14.545833	172.5973	191.4602	182.0288
121.078611	14.543611	148.5647	247.3961	197.9804
121.081944	14.543056	140.8528	205.9038	173.3783
121.082222	14.544167	137.7944	176.8757	157.3351
121.084167	14.542778	136.8901	187.2466	162.0684
121.078889	14.521389	150.1250	138.9303	144.5277
121.080000	14.522500	165.6087	150.7357	158.1722
121.080000	14.541389	128.7992	175.8549	152.3271
121.062500	14.547778	155.9896	229.9297	192.9597
121.070000	14.529167	146.0757	168.2499	157.1628
121.072222	14.527222	151.5901	186.0190	168.8046
121.078611	14.536667	137.6402	166.5114	152.0758
121.078611	14.534722	121.8527	200.0709	160.9618
121.073333	14.526667	155.1210	164.2634	159.6922
121.053333	14.523333	351.0638	385.6319	368.3479
121.066389	14.508889	180.8766	195.4319	188.1543

Longitude	Latitude	V_{S30} (Lithology)	V_{s30} (SPT-N)	V_{S30} (Mean)
121.066667	14.510000	162.7576	170.8660	166.8118
121.064722	14.510278	132.0666	159.7978	145.9322
121.063333	14.510833	147.4852	159.2508	153.3680
121.074722	14.518333	134.9642	132.7045	133.8344
121.085278	14.525278	168.4004	193.5863	180.9934
121.088611	14.527500	123.8095	124.3900	124.0998
121.096944	14.533056	142.0114	193.2042	167.6078
121.103889	14.532500	163.7623	185.4987	174.6305
121.100833	14.535278	146.7294	152.2669	149.4982
121.101389	14.535833	152.2562	160.0100	156.1331

Appendix G - Preliminary Manual for Processing Ground-Motion Data

This code has been developed to do routine earthquake time history analysis. Modules within the code can be used and modified by users. The primary functions of the codes are:

1. Do instrument correction and write output time history
2. Calculate FFT and write output spectrum
3. Calculate and output 5% damped response spectrum
4. Convert to Wood-Anderson time history and calculate local magnitude
5. Fit Brune spectrum and calculate moment magnitude
6. Export to miniSEED format
7. Export to SAC format
8. Plot instrument response

The code currently reads the following formats:

1. eqWave text format
2. Nanometrics ASCII format
3. TSPAIR text format
4. SAC binary
5. miniSEED binary

G.1 Getting Started

These functions use the Python programming language for processing and plotting outputs. The primary modules required are:

1. Python 2.X
2. NumPy
3. SciPy
4. Matplotlib

Functions 6 & 7 above require the ObsPy module, which can be downloaded from http://www.obspy.org .

All Python modules can be downloaded an installed independently. However, there are other packages that can be downloaded which install all required packages.

G.1.1 For Mac OS

The easiest way to uses these codes is to install the ObsPy disk image file from http://www.github/obspy/wiki/Installation-on-Mac-OS-X .

This dmg file installs all the necessary packages required for these codes to work. Run the ObsPy application, and click on the iPython button. This will open the Python command line module required to use the codes.

In iPython, cd to the working directory where you have downloaded the process_waves modules. For example:

cd to_my/working/directory

G.1.2 For Windows

To install the standard Python packages, the best way s to download and install the Python XY application. The Python XY executable installs a number of Python-base applications. To run these codes, the best way is through the Spyder program. To start Spyder, go to the main Windows Start Menu, and select: Programs > Python XY > Spyder

This will automatically open the iPython command line window that we will use to run the codes. As in the Mac OS instructions, cd to the working directory:

cd to_my\working\directory

If windows users want to use the functions dependent on the ObsPy package, they must install it separately.

G.2 Instrument Calibration Information

By default, this code reads uncorrected waveform data. The necessary information to correct for instrument response:

STA	Station Code
TYPE	Instrument type: short period (E or S), broadband (H or B), accelerometer (N)
START	Start date of instrument configuration (YYYYMMDD)
STOP	Stop date of instrument configuration (YYYYMMDD)
LON	Station longitude
LAT	Station latitude
NETID	Network ID
NATFREQ	Natural frequency of sensor (= -12345 if poles and zeros file defined)
DAMPING	Damping of sensor (= -12345 if poles and zeros file defined)
SEN	Sensor sensitivity (in V/m/s for velocity or V/g for acceleration transducers)
RECSEN	Recorder sensitivity (in Counts/V)

GAIN	Recorder gain
COMPONENT	Instrument component (follows standard IRIS codes)
PAZFILE	Reference file to poles and zeros file (located in the *paz* directory)

The instrument calibration file *stationlist.dat* will be generated automatically on first use. An example format of this file is:

STA TYPE STARTSTOP LON LAT NETID NATFREQ DAMPING SEN RECSEN GAIN COMPONENT PAZFILE

PVCP B 00010101 25990101 124.1591 13.5966 PV -12345 -12345 1168.0 419430.4 1.0 BHE trillium-240-g2.paz

G.3 Using the codes

Now we will lead users through using the code showing the required user inputs and program outputs. Text in red is only seen by the user on the first use of a given instrument, or for inputting earthquake source parameters. These details are saved to the files stationlist.dat and eventlist.dat for subsequent use. These files can also be edited manually by the user if desired. Text indicated in blue provide user tips or describe idiosyncratic behavior of the code. Where indicated, text in [square] brackets are default values.

G.3.1 Option 1: Do instrument correction and save displacement, velocity and acceleration time histories

>>> run process_waves.py 'eqwave_data/2012-06-19 1053 00 JENM.txt'

Plot outputs ([y]/n)? >

Reading header info...

Reading data...

Select task:

1) Do instrument correction and write output time history

2) Calculate FFT and write output spectrum

3) Calculate and output 5% damped response spectrum

4) Convert to Wood-Anderson time history and calculate local magnitude

5) Fit Brune spectrum and calculate moment magnitude

6) Export to miniSEED format

7) Export to SAC format

8) Plot instrument response

Task number > 1

Enter site information for JENM Up Tran

Velocity sensor or accelerometer ([v]/a)? >

Open date of station (YYYYMMDD [00010101]) > 20070528

Close date of station (YYYYMMDD [25990101]) >

JENM network ID [PV] > MEL

Look-up station details here: http://www.isc.ac.uk/registries/listing/

JENM station latitude (decimal degrees) > 146.420

JENM station longitude (decimal degrees) > -38.351

Use poles and zeros file ([y]/n)? >

1) cmg-3esp-60s

2) cmg-3es

3) cmg-40t-1s

4) cmg-40t-30s

5) cmg-5t

6) geotech-23900

7) s-13j

8) ss-1

9) sts2-g3

10) titan

11) trillium-240-g1

12) trillium-240-g2

Select PAZ file > 3

Short Period or Broad Band instrument ([s]/b)? >

Enter seismometer sensitivity [1.0 V/m/s] > 2000

Enter recorder sensitivity [1.0 Count/V] > 314570.0

Enter recorder gain [1.0] >

In plot, trim wave by select desired time window.

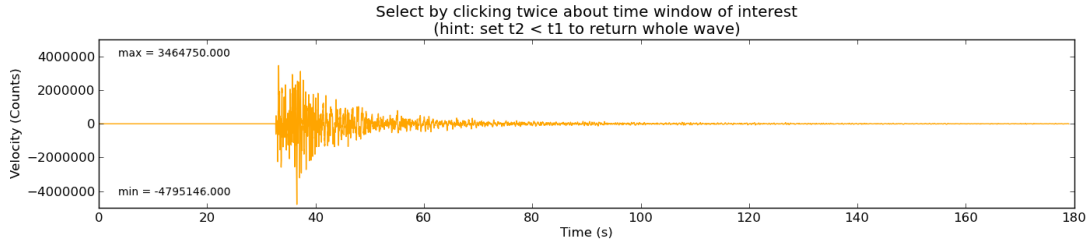

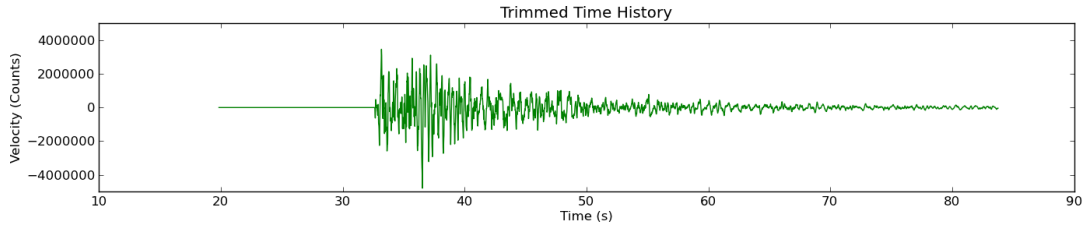

(Close figure)

High pass Butterworth corner [0.2 Hz] >

Low pass Butterworth corner [50.0 Hz] > 30

Enter earthquake latitude (decimal degrees) > -38.24

Enter earthquake longitude (decimal degrees) > 146.19

Enter earthquake depth (km) > 11

Enter earthquake magnitude (MW) > 5.0

The file “cor/ 201206191053.JENM.EHZ.cor” is written and following figure is displayed:

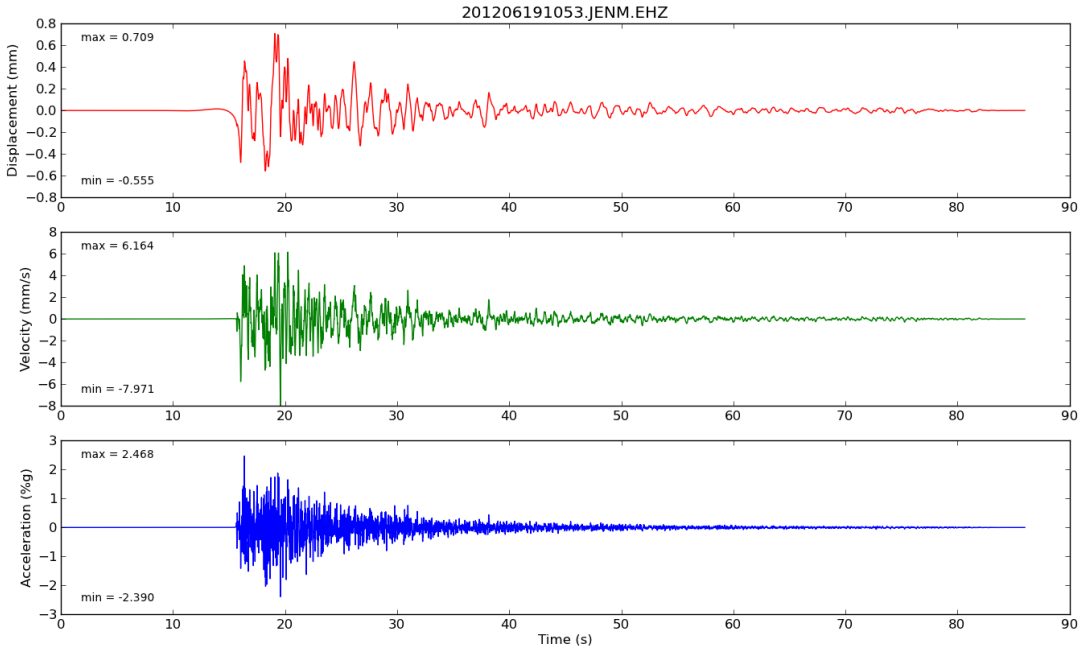

(Close figure)

Perform another task using wavefile: eqwave_data/2012-06-19 1053 00 JENM.txt (y/[n])? >

G.3.2 Option 2: Calculate FFT and write output spectrum

>>> run process_waves.py '../../EQ_DATA/2012-06-19.Moe/2012-06-19 1053 00 JENM.txt'

Plot outputs ([y]/n)? >

Reading header info...

Reading data...

Select task:

1) Do instrument correction and write output time history

2) Calculate FFT and write output spectrum

3) Calculate and output 5% damped response spectrum

4) Convert to Wood-Anderson time history and calculate local magnitude

5) Fit Brune spectrum and calculate moment magnitude

6) Export to miniSEED format

7) Export to SAC format

8) Plot instrument response

Task number > 2

In plot, trim wave by select desired time window. This window displays twice to allow the user to focus on a particular phase for frequency-domain processing if desired

High pass Butterworth corner [0.02 Hz] > 0.1

Low pass Butterworth corner [50.0 Hz] >

Select earthquake location from list...

DATETIME MW_MAG LON LAT DEP

1) 201206191053 5.0 146.19 -38.24 11.0

Automatically associating earthquake parameters above...

Modify 'eventlist.dat' manually if this is not what you want!

The file “fds/ 201206191053.JENM.EHZ.fds” is written and following figure is displayed:

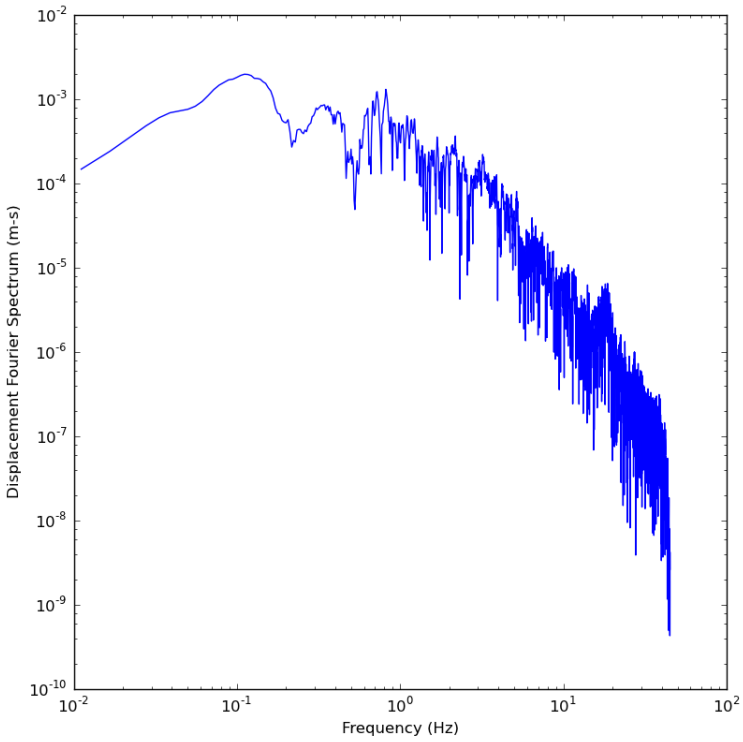

G.3.3 Option 3: Calculate and output 5% damped response spectrum

>>> run process_waves.py 'eqwave_data/2012-04-19 1909 RAW.txt'

Plot outputs ([y]/n)? >

Reading header info...

Reading data...

Select task:

1) Do instrument correction and write output time history

2) Calculate FFT and write output spectrum

3) Calculate and output 5% damped response spectrum

4) Convert to Wood-Anderson time history and calculate local magnitude

5) Fit Brune spectrum and calculate moment magnitude

6) Export to miniSEED format

7) Export to SAC format

8) Plot instrument response

Task number > 3

Select channel:

1) COTT EHE

2) COTT EHN

3) COTT EHZ

4) COTT HNE

5) COTT HNN

6) COTT HNZ

7) TPND EHE

8) TPND EHN

9) TPND EHZ

10) TPND HNE

11) TPND HNN

12) TPND HNZ

13) ...

Channel number > 3

In plot, trim wave by select desired time window. Note, this calculation can take up to 30 sec. Windowing a shorter time range will optimise this calculation.

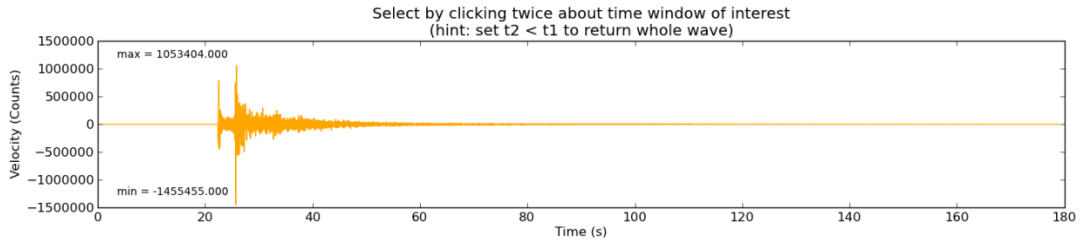

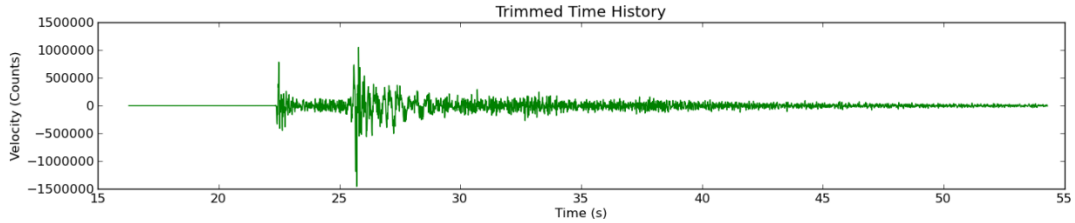

(Close figure)

High pass Butterworth corner [0.2 Hz] >

Low pass Butterworth corner [50.0 Hz] >

Select earthquake location from list...

DATETIME MW_MAG LON LAT DEP

1) 201204191909 3.5 148.603 -35.231 4.0

Automatically associating earthquake parameters above...

Modify 'eventlist.dat' manually if this is not what you want!

Calculating 5.0% damped response spectrum...

This process may take up to a minute to complete. The file "psa/ 201206191053.COTT.EHZ.psa" is written and following figure is displayed:

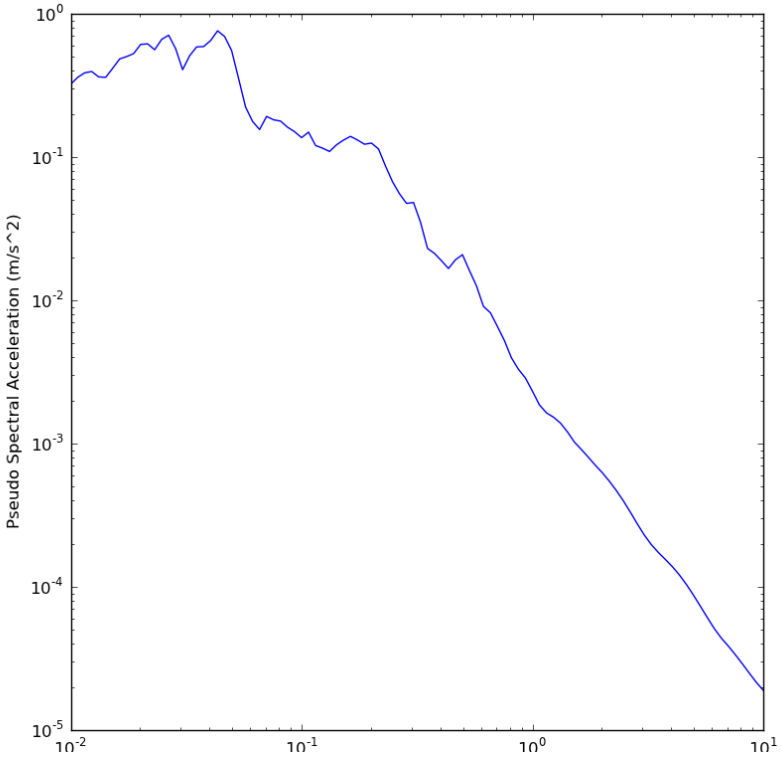

Perform another task using wavefile: eqwave_data/2012-04-19 1909 RAW.txt (y/[n])? >

G.3.4 Option 4: Convert to Wood-Anderson time history and calculate local magnitude

This option deconvolves response of instrument and then convolves the corrected time history with the response of a standard Wood-Anderson displacement torsion seismograph (i.e. amplification = 2080, natural frequency = 1.25 Hz and damping = 0.8). Local magnitude ML will then be calculated from the maximum zero to peak amplitude of the selected time window using:

1. R35: Richter (1935) for southern California
2. GS86: Greenhalgh & Singh (1986) for South Australia
3. HB87: Hutton & Boore (1987) for southern California
4. GG91: Gaull & Gregson (1991) for Western Australia
5. MLM92: Michael-Leiba & Malafant (1992) for eastern Australia
6. WGW96: Wilkie (1996) updated from Wilkie et al (1994) for SE Australia

7. A10: Allen (2010; unpublished) for SE Australia

>>> run process_waves.py '../../EQ_DATA/2012-06-19.Moe/2012-06-19 1053 00 JENM.txt'

Plot outputs ([y]/n)? >

Reading header info...

Reading data...

Select task:

1) Do instrument correction and write output time history

2) Calculate FFT and write output spectrum

3) Calculate and output 5% damped response spectrum

4) Convert to Wood-Anderson time history and calculate local magnitude

5) Fit Brune spectrum and calculate moment magnitude

6) Export to miniSEED format

7) Export to SAC format

8) Plot instrument response

Task number > 4

High pass Butterworth corner [0.2 Hz] >

Low pass Butterworth corner [50.0 Hz] >

Select earthquake location from list...

DATETIME MW_MAG LON LAT DEP

1) 201206191053 5.0 146.19 -38.24 11.0

Automatically associating earthquake parameters above...

Modify 'eventlist.dat' manually if this is not what you want!

In plot, trim unwanted phases (e.g. surface/Rg waves)

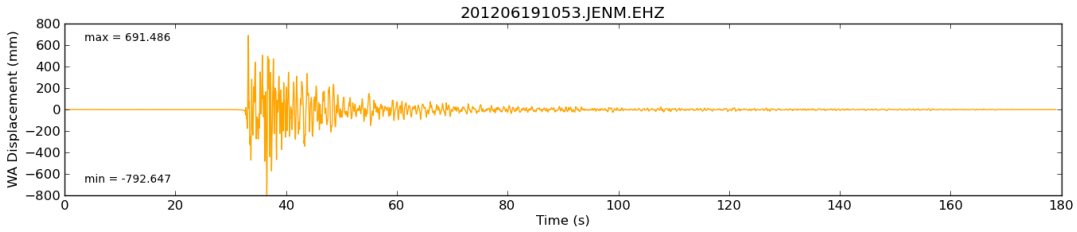

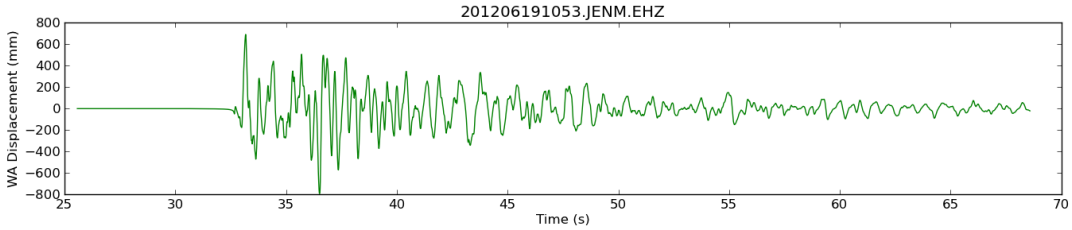

ML calculated from record: 201206191053.JENM.EHZ at Rhyp = 26.0 km

R35: 4.8*

GS86: 5.1

HB87: 5.1*

GG91: 5.2

MLM92: 5.2

WGW96: 5.2

A10: 5.0

* Does not use correct component

G.3.5 Option 5: Fit Brune spectrum and calculate moment magnitude

Not yet functional

G.3.6 Option 6: Export to miniSEED format

Not yet functional

G.3.7 Option 7: Export to SAC format

Exports file to instrument corrected SAC file format. Note, this must be run in an active obspy iPython window

G.3.8 Option 8: Plot instrument response

run process_waves.py 'phivolcs_data/YGUIM_HHZ_20120206_000000_20120206.030000.txt'

Plot outputs ([y]/n)? >

Reading header info...

Reading data...

Select task:

1) Do instrument correction and write output time history

2) Calculate FFT and write output spectrum

3) Calculate and output 5% damped response spectrum

4) Convert to Wood-Anderson time history and calculate local magnitude

5) Fit Brune spectrum and calculate moment magnitude

6) Export to miniSEED format

7) Export to SAC format

8) Plot instrument response

Task number > 8

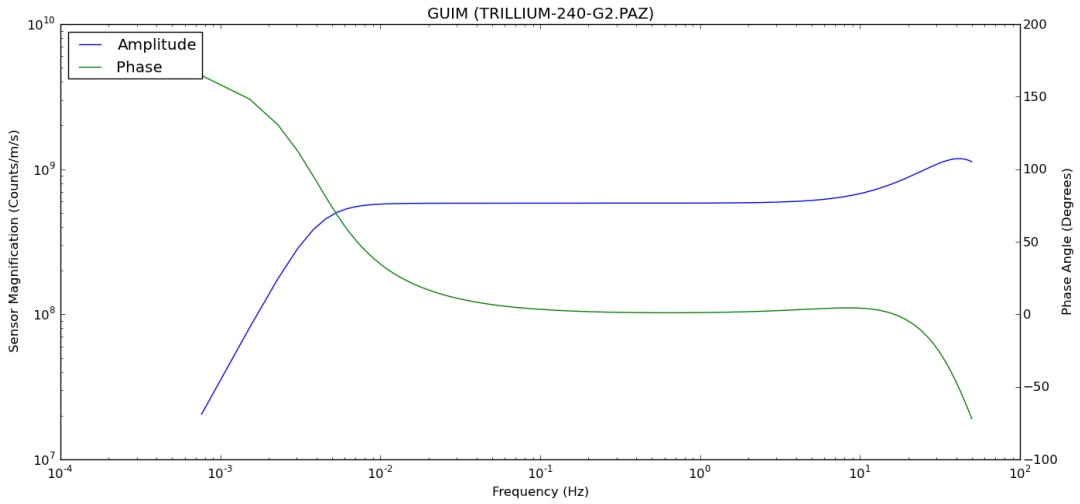
GUIM (TRILLIUM-240-G2.PAZ)
Amplitude
Phase
Sensor Magnification (Counts/m/s)
Phase Angle (Degrees)
Frequency (Hz)

Appendix H - Residuals of Ground Motion Prediction Equations Compared to Actual Data

Residual plots for PGA, RSA (natural periods of 0.2 s, 1 s, 2 s). Median of residuals is also plotted with corresponding error bars.

H.1 Peak Ground Acceleration (PGA)

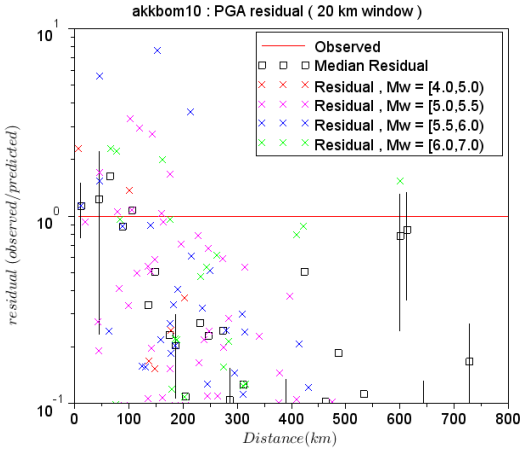

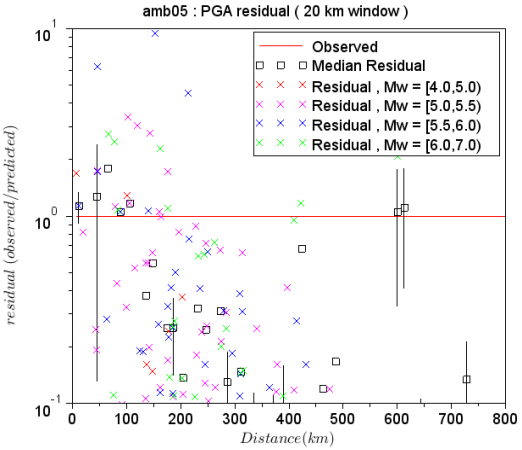

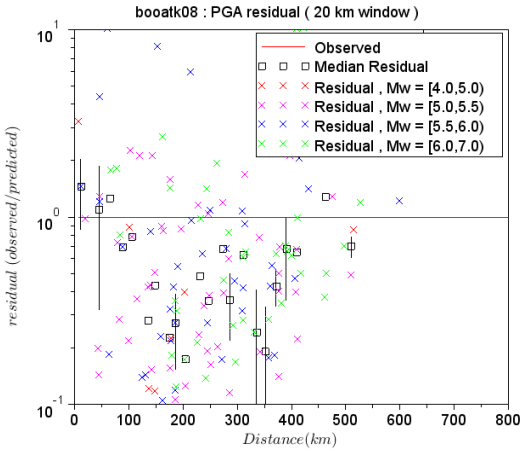

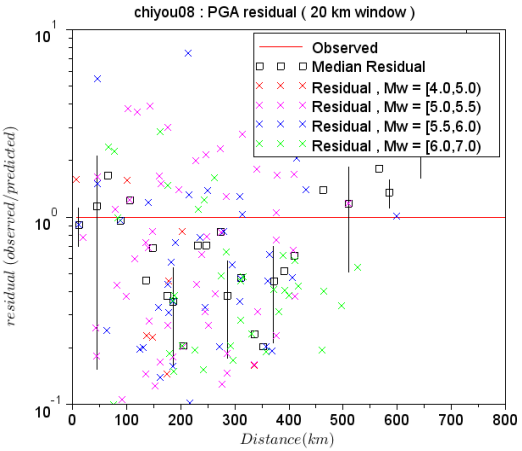

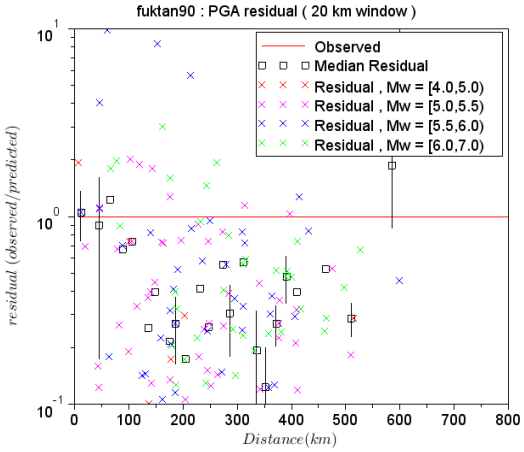
fuktan90 : PGA residual (20 km window)
Observed
Median Residual
Residual , Mw = [4.0,5.0)
Residual , Mw = [5.0,5.5)
Residual , Mw = [5.5,6.0)
Residual , Mw = [6.0,7.0)
residual (observed/predicted)
Distance(km)

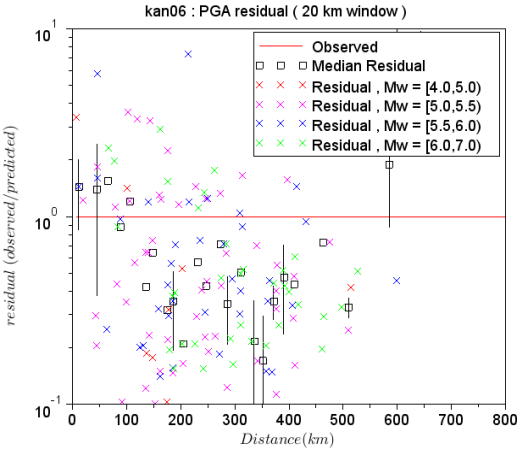
kan06 : PGA residual (20 km window)
Observed
Median Residual
Residual , Mw = [4.0,5.0)
Residual , Mw = [5.0,5.5)
Residual , Mw = [5.5,6.0)
Residual , Mw = [6.0,7.0)
residual (observed/predicted)
Distance(km)

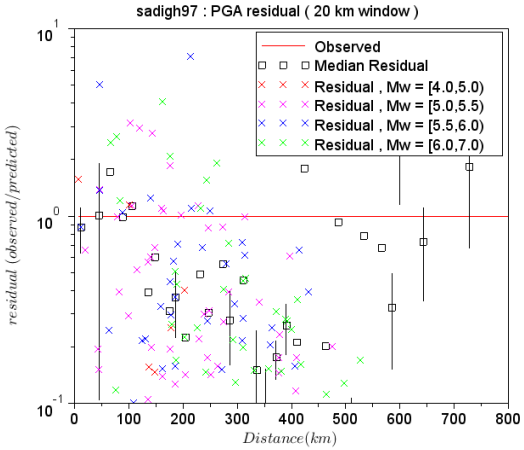
sadigh97 : PGA residual (20 km window)
Observed
Median Residual
Residual , Mw = [4.0,5.0)
Residual , Mw = [5.0,5.5)
Residual , Mw = [5.5,6.0)
Residual , Mw = [6.0,7.0)
residual (observed/predicted)
Distance(km)

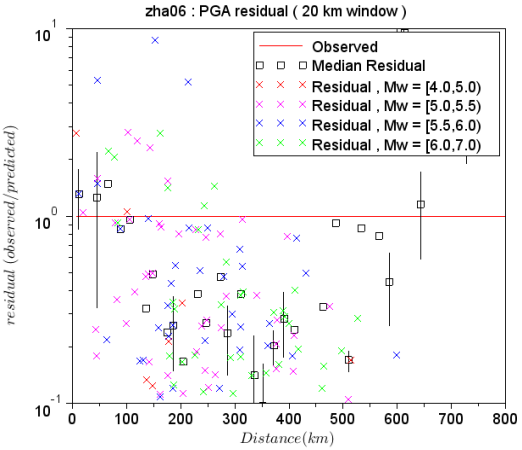
zha06 : PGA residual (20 km window)
Observed
Median Residual
Residual , Mw = [4.0,5.0)
Residual , Mw = [5.0,5.5)
Residual , Mw = [5.5,6.0)
Residual , Mw = [6.0,7.0)
residual (observed/predicted)
Distance(km)

H.2 Responds Spectral Acceleration (RSA), with natural period of 0.2 s.

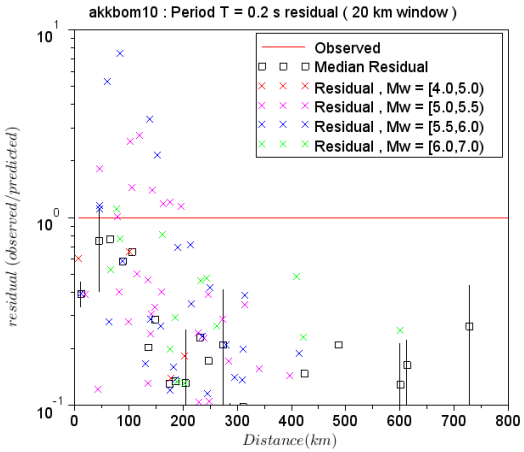

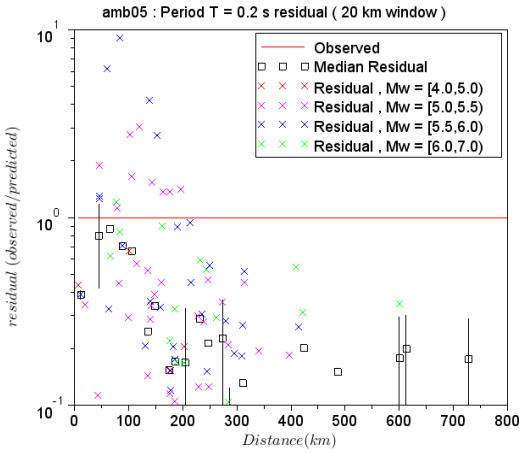

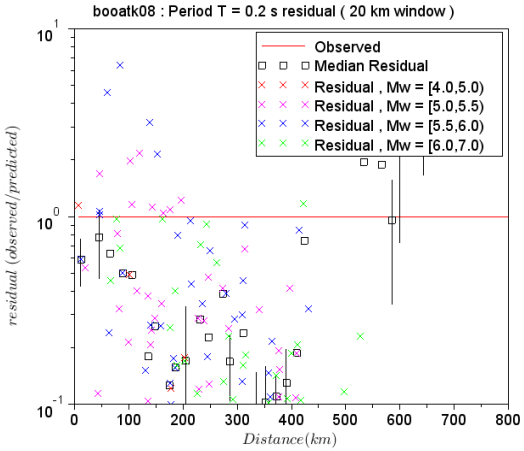

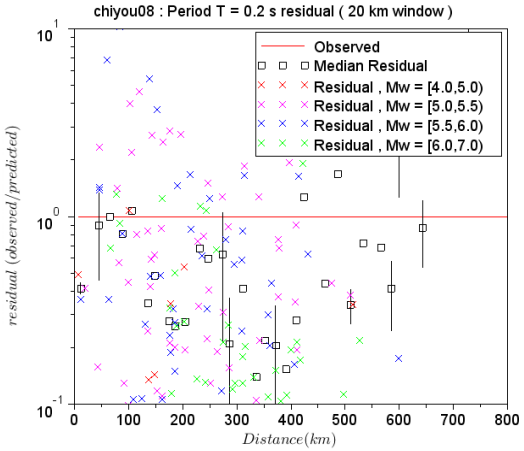

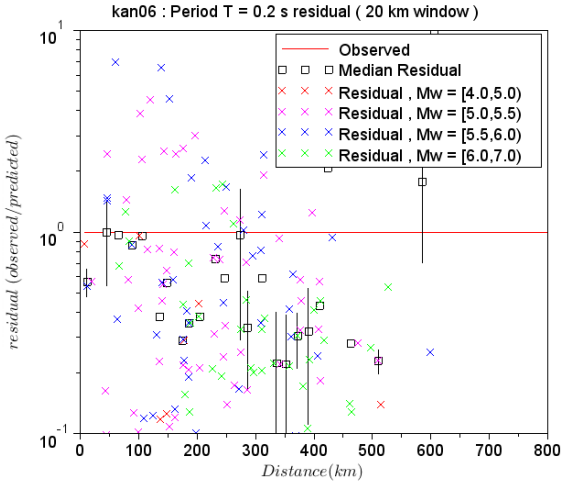

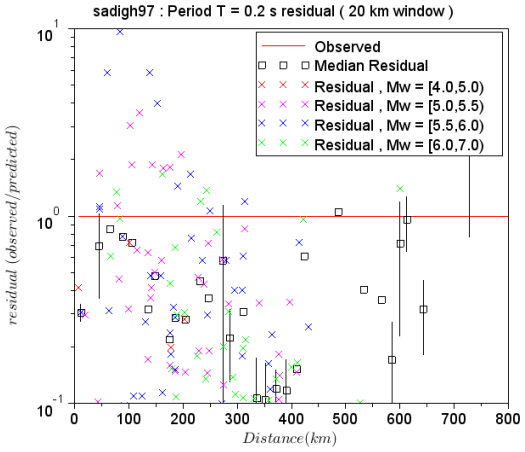

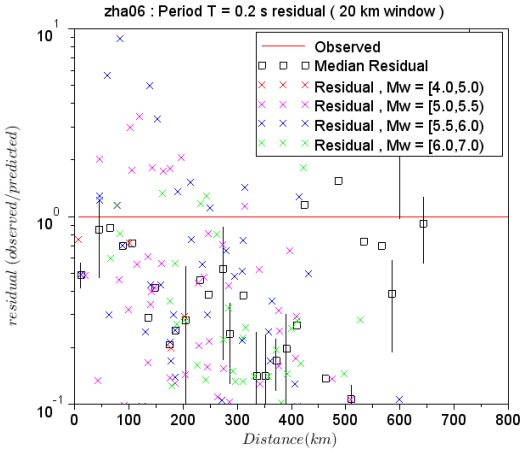

H.3 Responds Spectral Acceleration (RSA), with natural period of 1.0 s.

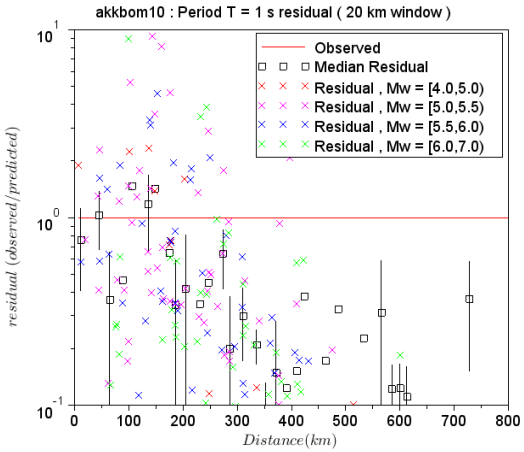

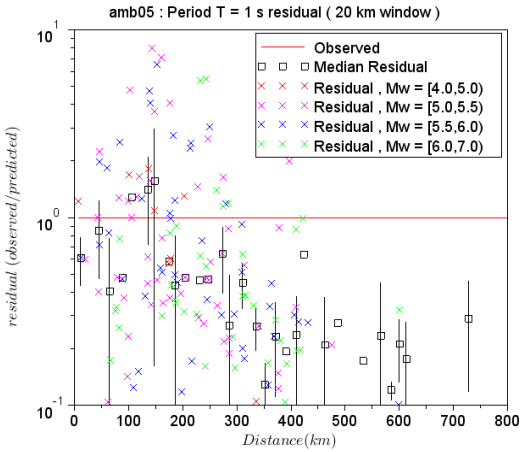

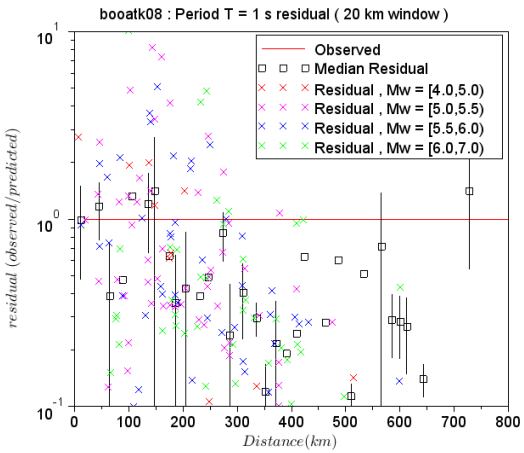

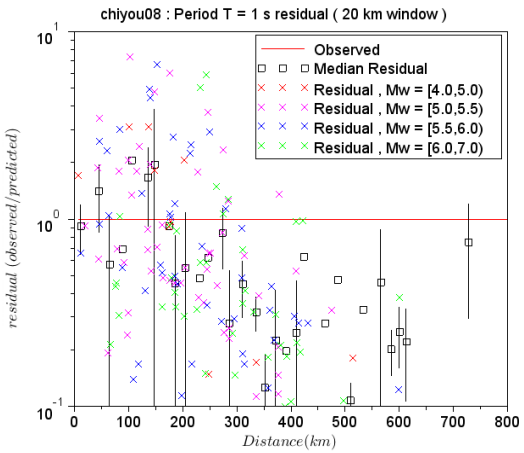

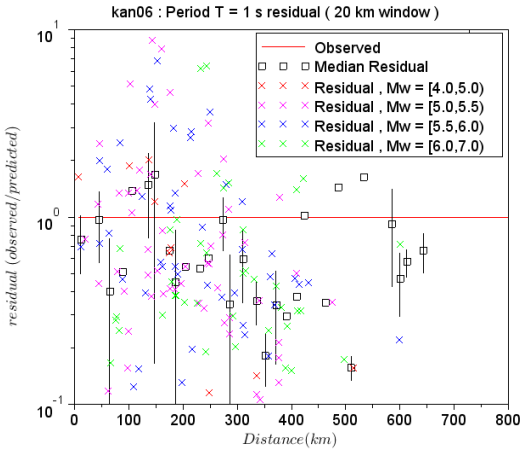
kan06 : Period T = 1 s residual (20 km window)
Observed
Median Residual
Residual , Mw = [4.0,5.0)
Residual , Mw = [5.0,5.5)
Residual , Mw = [5.5,6.0)
Residual , Mw = [6.0,7.0)
residual (observed/predicted)
Distance(km)

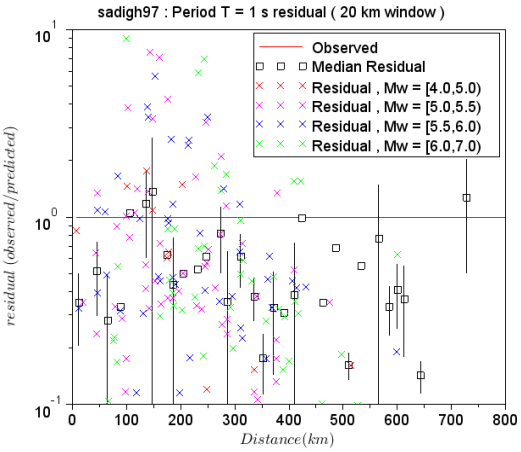
sadigh97 : Period T = 1 s residual (20 km window)
Observed
Median Residual
Residual , Mw = [4.0,5.0)
Residual , Mw = [5.0,5.5)
Residual , Mw = [5.5,6.0)
Residual , Mw = [6.0,7.0)
residual (observed/predicted)
Distance(km)

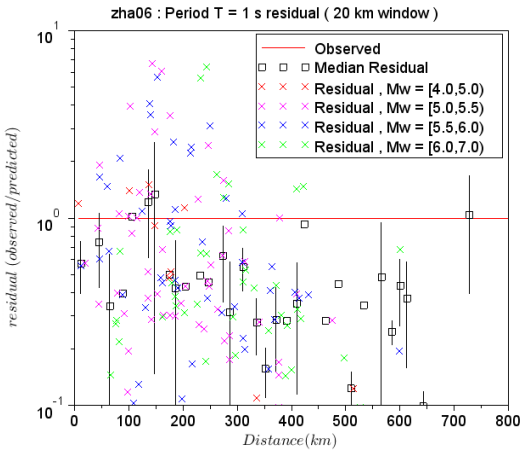
zha06 : Period T = 1 s residual (20 km window)
Observed
Median Residual
Residual , Mw = [4.0,5.0)
Residual , Mw = [5.0,5.5)
Residual , Mw = [5.5,6.0)
Residual , Mw = [6.0,7.0)
residual (observed/predicted)
Distance(km)

H.4 Responds Spectral Acceleration (RSA), with natural period of 2.0 s.

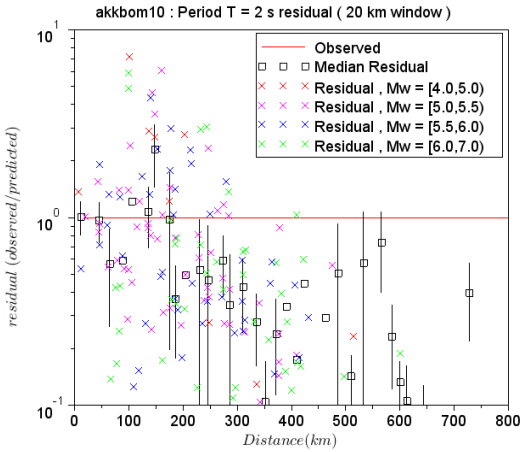

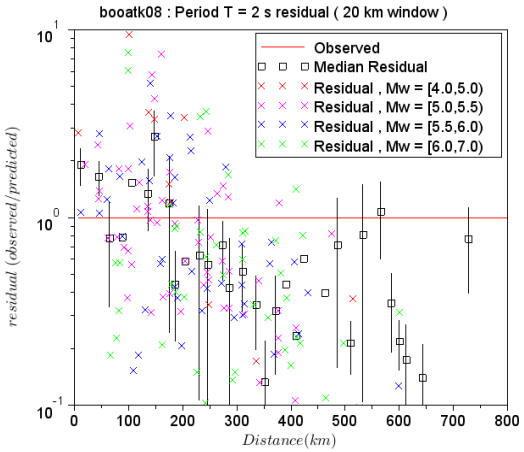

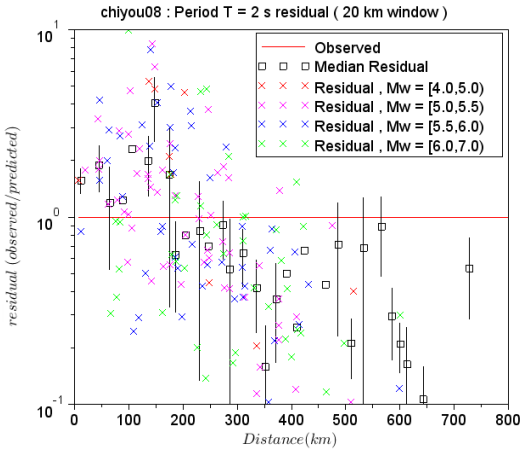

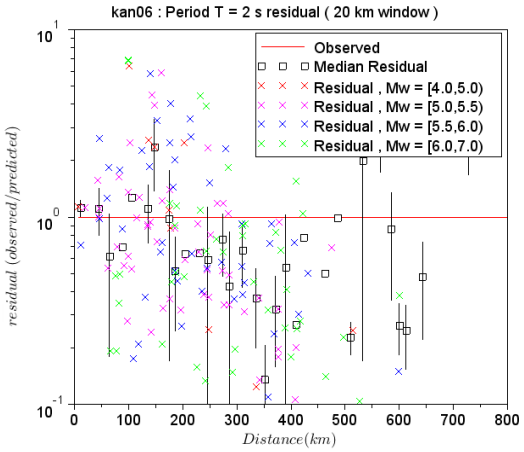

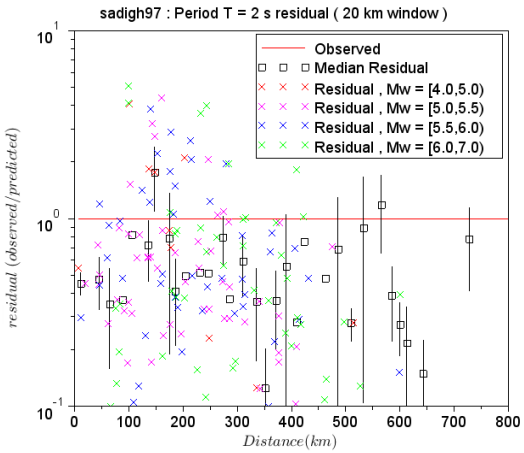

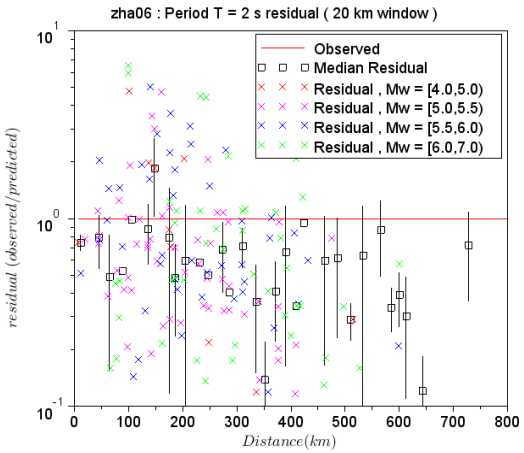

Appendix I - Building Types and Corresponding Building Vulnerability Models

Building type in exposure	Building type in vulnerability	Building type in exposure	Building type in vulnerability	Building type in exposure	Building type in vulnerability	Building type in exposure	Building type in vulnerability
W1_L_1	W1L	W1_L_2	W1L	W1_M	W1L	W1_H	W1L
W2_L_1	W1L	W2_L_2	W1L	W2_M	W1L	W2_H	W1L
W3_L_1	W3L	W3_L_2	W3L	W3_M	W3L	W3_H	W3L
N_L_1	NL	N_L_2	NL	N_M	NL	N_H	NL
CHB_L_1	CHBL	CHB_L_2	CHBL	CHB_M	CHBL	CHB_H	CHBL
URA_L_1	URAL	URA_L_2	URAL	URA_M	URAL	URA_H	URAL
URM_L_1	URML	URM_L_2	URML	URM_M	URML	URM_H	URML
RM1_L_1	URML	RM1_L_2	URML	RM1_M	URML	RM1_H	URML
RM2_L_1	URML	RM2_L_2	URML	RM2_M	URML	RM2_H	URML
MWS_L_1	MWSL	MWS_L_2	MWSL	MWS_M	MWSL	MWS_H	MWSL
CWS_L_1	CWSL	CWS_L_2	CWSL	CWS_M	CWSL	CWS_H	CWSL
C1_L_1	C1L	C1_L_2	C1L	C1_M	C1M	C1_H	C1M
C2_L_1	C1L	C2_L_2	C1L	C2_M	C1M	C2_H	C1M
C4_L_1	C4M	C4_L_2	C4M	C4_M	C4M	C4_H	C4H
PC1_L_1	PC2L	PC1_L_2	PC2L	PC1_M	PC2M	PC1_H	PC2M
PC2_L_1	PC2L	PC2_L_2	PC2L	PC2_M	PC2M	PC2_H	PC2M
S1_L_1	S1L	S1_L_2	S1L	S1_M	S1M	S1_H	S1M
S2_L_1	S1L	S2_L_2	S1L	S2_M	S1M	S2_H	S1M
S3_L_1	S3L	S3_L_2	S3L	S3_M	S3L	S3_H	S3L
S4_L_1	S4M	S4_L_2	S4M	S4_M	S4M	S4_H	S4M

Appendix J - Earthquake Impact Calculation Methods – A Worked Example

The impact calculations allow us to estimate the damages that hypothetical earthquake events could cause to buildings, and the number of people affected by the events. This document explains the calculations, and is partly based on the draft technical report for the earthquake component of the project. The calculation methods require three key inputs: the earthquake hazard model, the exposure data, and a vulnerability model.

J.1 Earthquake hazard model

The earthquake hazard model outputs take the form of ground shaking intensity grids. Each grid cell represents the Modified Mercalli Intensity (MMI) at that location (Figure J.1). For this example, the shaking intensity is expected MMI from magnitude 6.5 earthquake occurring at the Western Valley Fault. Notice that the ground shaking varies depending on distance from the earthquake source and soil condition.

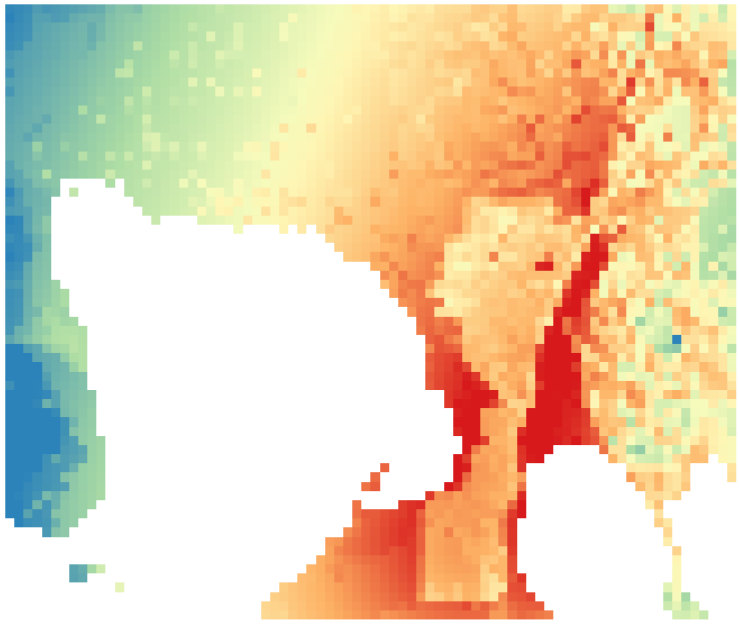

Figure J.1. Ground shaking intensity grid.

J.2 Exposure data

The exposure data describes the statistical properties of the building stock in each "exposure polygon." The exposure polygon boundaries are defined manually, based on land-use considerations (Figure J.2).

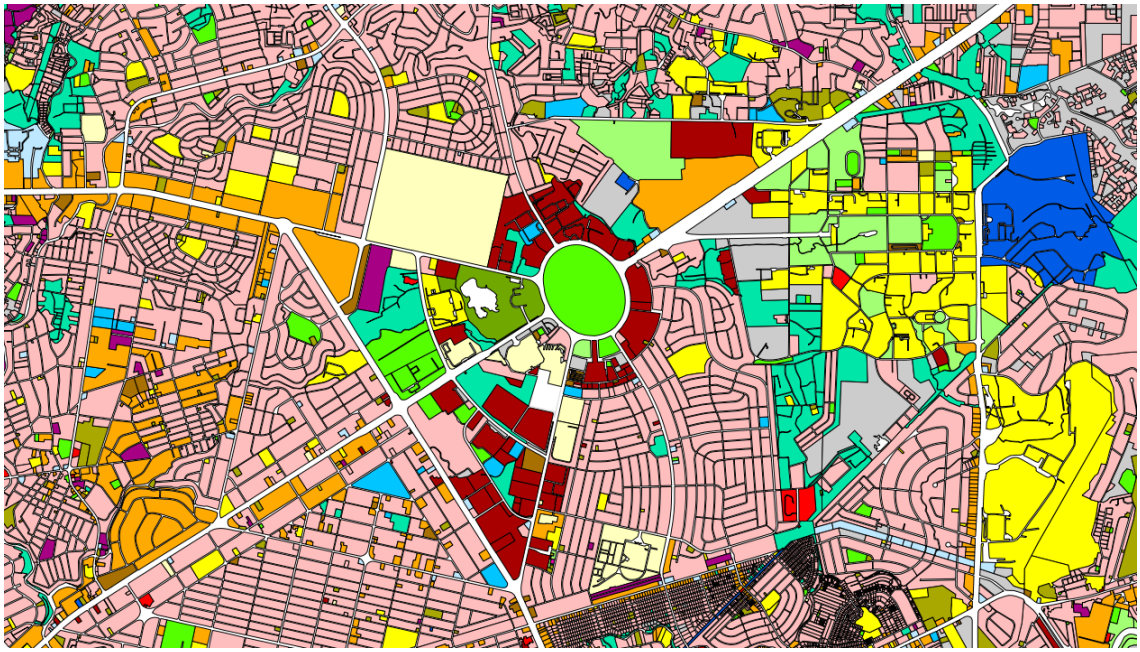

Figure J.2. An example of land-use polygons developed through the GMMA-RAP.

Each exposure polygon contains data describing a number of physical attributes of the land within the polygon, including:

1. The land use category (e.g. Residential, Major Commercial, etc.);
2. The fraction of the land area covered by buildings;
3. The total floor area of all buildings types;
4. The total footprint area (i.e. ground floor area) of the buildings;
5. The total floor area of different building types. The building categories are developed by engineering experts. They include: W1 (Wooden 1), W2 (Wooden 2), N (Makeshift/Informal), CHB (Concrete Hollow Block), CWS (Concrete with Steel), C1 (Concrete 1), C2 (Concrete 2), S1 (Steel 1), S2 (Steel 2), etc.;
6. The total floor area inside buildings with different numbers of storeys. The numbers-of-storeys are split into categories including: 1-storey, 2-storey, 3-8 storey, 9-16 storey, 16-25 storey etc.

In addition, we have information on:

1. Population - the information is used to compute number of casualties (i.e. injuries and fatalities).
2. The replacement costs of various building types, which is estimated from taxation data, as well as engineering guides on building construction costs in Manila. Replacement cost varies depending on the land-use of the exposure polygon
3. The Inter-Storey Height, which is an estimate of the typical vertical distance between consecutive storeys in a multi-storey building, and is important for assessing the impact of flooding on multi-storey buildings. The inter-storey height varies depending on the land-use in the exposure polygon (e.g. buildings in major commercial areas tend to have larger inter-storey heights than in residential areas).
4. Vintage of buildings, which is an estimate from analysis of a time-series of aerial imagery. Every building in a land use polygon is assumed to have the same vintage.

J.3 Vulnerability and fragility models

Vulnerability models consist of both fragility and vulnerability curves: fragility curves relate ground shaking intensity to the likelihood of physical damage, while vulnerability curves define economic loss as a fraction of replacement cost. Several curves have been developed by engineering experts, each of which is appropriate for a different building type (Figures J.2 and J.3).

Fragility curves describe the likelihood of physical damage (e.g. slight, moderate, extensive, or complete) for a range of different building types. Vulnerability curves describe the loss ratio (i.e. ratio of repair cost to building replacement value) as a function of the ground shaking, for a range of different building types. For example, a loss ratio of 0.5 means that the cost of repairing the damaged building is equal to 50% of its replacement cost.

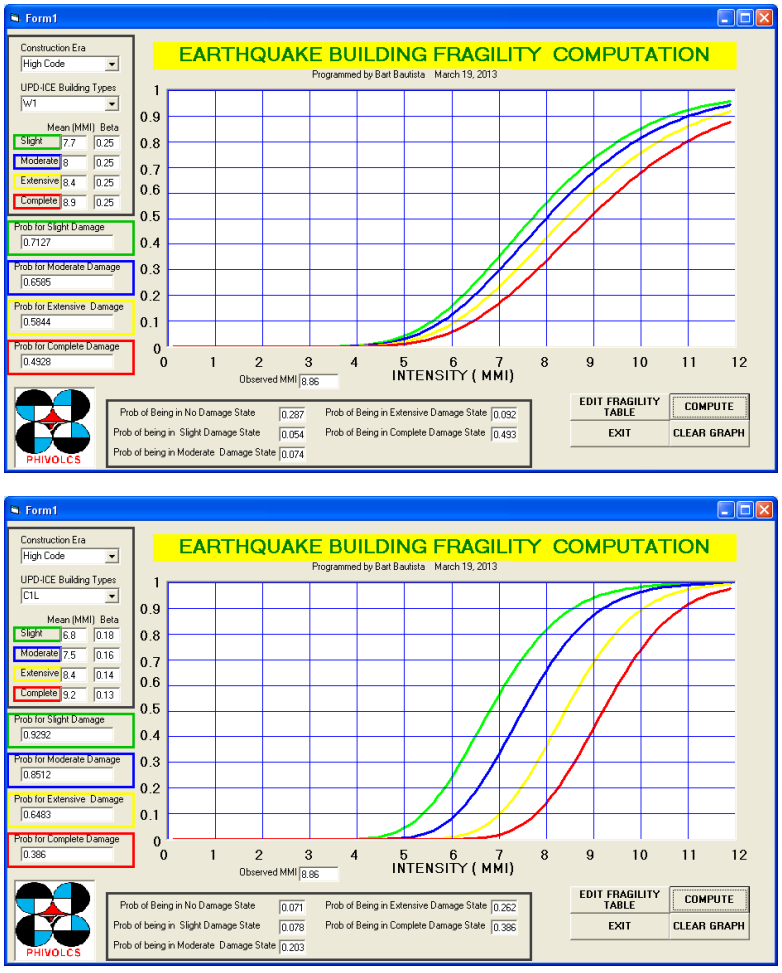

Figure J.3. Fragility curves of W1L (Low-rise wooden building) and C1L (Low-rise concrete frame building) developed by UPD-ICE for the present study.

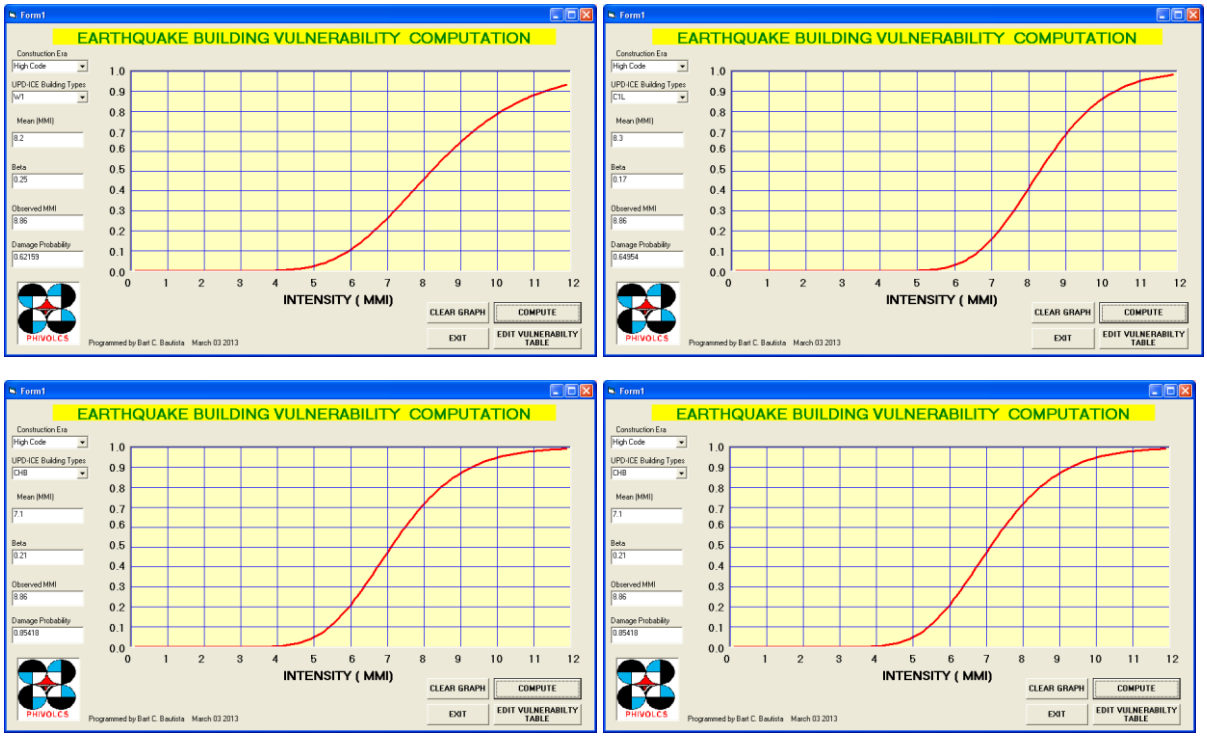

Figure J.4. Vulnerability curves for different building types developed by UPD-ICE for the present study.

A complication is that the building-type categories for these vulnerability curves do not exactly match the building-type categories in the exposure polygons. To overcome this issue, a simple mapping between the building types was developed (see Table 6 at the end of this document). This mapping largely groups low rise (i.e. one and two storey) buildings into the same vulnerability class.

J.4 Impact calculation

For simplicity, we will examine a single polygon, and assume the exposure polygon contains only one building type. In Figure J.1, we can see that the MMI across a single exposure polygon can vary due to the attenuation of ground motion with distance from the fault rupture and also from the soil conditions of the site (e.g. soft soil, hard rock, etc.). For our one polygon, we estimate the average MMI over the entire polygon (Figure J.3), a value of 8.86.

For this example, we have chosen a single polygon in the Taguig area. The polygon has the following attributes:

1. Formal Settlement, with Mixed Residential and Small Commercial land use;
2. Total area of 32,565 m²;
3. Total floor area of 18,767 m²;
4. Predominant year of construction is Pre-1972;
5. One-storey building area of 13,662 m²; two-storey building area of 4330 m², and medium rise buildings (3–8 storeys) 777 m²;
6. Population of 730.

J.5 Measures of damage

The measures of damage that we use are:

1. Damage probability: likelihood of being in or exceeding each damage state using fragility curves
2. Damaged floor area equivalent: floor area in each damage state, which is equal to the damage probability multiplied by the total floor area
3. Loss ratio: as defined above, this is the ratio of the cost of repairs to the cost of total replacement using the vulnerability curve
4. Building damage cost: This is equal to the loss ratio multiplied by the associated building replacement cost.
5. Number of casualties: This is estimated by multiplying number of people occupying a given building type in a given damage state by the HAZUS-MH casualty severity rate for that building and damage state.

J.6 Impact calculation process

The following outlines a step-by-step process for calculating the measure of damage for a single polygon.

1. Calculate a representative MMI value for the polygon. For our polygon of interest, this is 8.86.
2. Define the combinations of building type and storey categories from those available in the exposure database. These are populated in the exposure database, with an estimated floor area for each of the combinations and are governed by the land use category and predominant vintage of construction. In the polygon selected, there are 18 combinations of building type and storey category with floor area greater than zero (W1-L-1, N-L-1, CHB-L-1, URA-L-1, URM-L-1, C1-L-1, S1-L-1, S3-L-1, , , CHB-L-2, URA-L-2, URM-L-2, MWS-L-2, CWS-L-2, C1-L-2, S1-L-2, S3-L-2, C1-M and S1-M). Refer to the documentation for the exposure database for an explanation on how these values are calculated.
3. Using the building type, land use category and the building cost database, calculate the value of each building type/storey category class within the polygon. For each building type/storey category combination:

$$[\text{Building value}] = [\text{Floor area}] \times [\text{Construction cost}]$$

4. Add these to obtain the total value of built assets in the polygon (the total value is stored for future use). For the polygon chosen, there are **18769.1 m² of floor area**, with a total value of PHP 181,218,885. The largest contribution to this value is from 1-storey C1 buildings (C1-L-1), of which there are **6793 m²**, with a value **of PHP 89,667,600** (Table J.1).

Table J.1. Building type/storey category combinations, corresponding vulnerability model floor area of each combination (m²), construction cost (PHP /m²) and total value (PHP). Total floor area and total value for the polygon is given at the bottom.

Building type/storey category	Building type of vulnerability model	Floor area (m²)	Construction cost (Peso/sq. m)	Building value (Peso)
W1-L-1	W1L	3205.6	PHP 5,600.00	PHP 17,951,360.00
N-L-1	NL	256	PHP 1,200.00	PHP 307,200.00
CHB-L-1	CHBL	3348.5	PHP 6,500.00	PHP 21,765,250.00
URA-L-1	URAL	8.2	PHP 7,150.00	PHP 58,630.00
URM-L-1	URML	8.8	PHP 7,150.00	PHP 62,920.00
C1-L-1	C1L	6793	PHP 13,200.00	PHP 89,667,600.00
S1-L-1	S1L	22.3	PHP 30,000.00	PHP 669,000.00
S3-L-1	S3L	19.7	PHP 15,000.00	PHP 295,500.00
W1-L-2	W1L	770.5	PHP 5,600.00	PHP 4,314,800.00
N-L-2	NL	61.5	PHP 1,200.00	PHP 73,800.00
CHB-L-2	CHBL	804.9	PHP 6,500.00	PHP 5,231,850.00
URA-L-2	URAL	2	PHP 7,150.00	PHP 14,300.00
URM-L-2	URML	2.1	PHP 7,150.00	PHP 15,015.00
MWS-L-2	MWSL	235.7	PHP 6,000.00	PHP 1,414,200.00
CWS-L-2	CWSL	810.4	PHP 9,000.00	PHP 7,293,600.00
C1-L-2	C1L	1632.8	PHP 13,200.00	PHP 21,552,960.00
S1-L-2	S1L	5.4	PHP 30,000.00	PHP 162,000.00
S3-L-2	S3L	4.7	PHP 15,000.00	PHP 70,500.00
C1-M	C1M	774.5	PHP 13,200.00	PHP 10,223,400.00
S1-M	S1M	2.5	PHP 30,000.00	PHP 75,000.00
Total		18769.1		PHP 181,218,885.00

5. For each building type, use the MMI value and the corresponding fragility and vulnerability models to calculate the damage probability and loss ratio for each building type. The **CHBL** and **MWSL** building types experience the greatest damage per unit of floor area (Table J.2).

Table J.2. Damage fraction for each building type/storey category combination.

Building type	MMI value	Probability of being in slight damage state	Probability of being in moderate damage state	Probability of being in extensive damage state	Probability of being in complete damage state	Loss ratio
W1L	8.86	0.054	0.074	0.092	0.49	0.622
NL	8.86	0.04	0.06	0.08	0.59	0.702
CHBL	8.86	0.06	0.08	0.10	0.71	0.854

Building type	MMI value	Probability of being in slight damage state	Probability of being in moderate damage state	Probability of being in extensive damage state	Probability of being in complete damage state	Loss ratio
URAL	8.86	0.08	0.09	0.09	0.58	0.722
URML	8.86	0.08	0.09	0.09	0.57	0.713
C1L	8.86	0.08	0.20	0.26	0.39	0.650
S1L	8.86	0.10	0.10	0.10	0.45	0.612
S3L	8.86	0.06	0.06	0.05	0.38	0.469
MWSL	8.86	0.06	0.08	0.10	0.71	0.854
CWSL	8.86	0.07	0.07	0.13	0.53	0.695
C1M	8.86	0.06	0.15	0.30	0.25	0.552
S1M	8.86	0.21	0.40	0.11	0.13	0.521

6. For each building type:

$$[\text{Repair cost}] = [\text{Loss ratio}] \times [\text{building replacement cost}]$$

The building replacement is calculated at Step 4. The greatest cost of damage is incurred by the C1L building type, with a cost of PHP 72,241,679. This is due to the high cost of construction cost per square metre and the abundance of C1L construction in the polygon.

Table J.3. Damage fraction, building value and cost of damage.

Building type	Loss ratio	Building value (Peso)	Cost of damage
W1L	0.622	PHP 22,266,160.00	PHP 13,840,346.76
NL	0.702	PHP 381,000.00	PHP 267,303.33
CHBL	0.854	PHP 26,997,100.00	PHP 23,060,398.40
URAL	0.722	PHP 72,930.00	PHP 52,684.83
URML	0.713	PHP 77,935.00	PHP 55,544.70
C1L	0.650	PHP 111,220,560.00	PHP 72,241,679.77
S1L	0.612	PHP 831,000.00	PHP 508,361.68
S3L	0.469	PHP 366,000.00	PHP 171,565.90
MWSL	0.854	PHP 1,414,200.00	PHP 1,207,982.17
CWSL	0.695	PHP 7,293,600.00	PHP 5,068,077.68
C1M	0.552	PHP 10,223,400.00	PHP 5,641,107.14
S1M	0.521	PHP 75,000.00	PHP 39,063.23
Total		PHP 181,218,885.00	PHP 122,154,115.59

7. The cost of damage from all building types is summed to obtain the total cost of damage in the polygon. The total cost of damage for this polygon is **PHP 122,154,115.59**.
8. For the entire polygon:

$$[\text{Loss ratio}] = [\text{Total cost of damage}] \div [\text{Total building replacement cost}]$$

9. For this polygon, the damage fraction = 122,154,115.59 / 181,218,885.00 = **0.674**.
10. For each building type:

$$[\text{Damaged floor area equivalent}] = [[\text{Damage probability}] \times [\text{floor area}] \times 100] \div [\text{Land area of polygon}]$$

The result is expressed in units of ha/km².

Table J.4. Damaged floor area equivalent, and per square kilometre of land area by building type.

Building type	Floor area (m²)	Slightly damaged floor area equivalent	Moderately damaged floor area equivalent	Extensively damaged floor area equivalent	Completely damaged floor area equivalent
W1L	0.622	0.662	0.905	1.119	6.017
NL	0.702	0.044	0.061	0.079	0.574
CHBL	0.854	0.717	1.004	1.236	9.024
URAL	0.722	0.002	0.003	0.003	0.018
URML	0.713	0.003	0.003	0.003	0.019
C1L	0.650	2.020	5.249	6.787	9.988
S1L	0.612	0.008	0.009	0.008	0.039
S3L	0.469	0.004	0.004	0.004	0.029
MWSL	0.854	0.041	0.057	0.070	0.512
CWSL	0.695	0.165	0.179	0.322	1.317
C1M	0.552	0.136	0.367	0.723	0.599
S1M	0.521	0.002	0.003	0.001	0.001
Total		3.803	7.841	10.354	28.137

11. Add the damaged floor area equivalent values for all building types to obtain the total damaged floor area equivalent for each damage state for the polygon. For this polygon, the total damaged floor area equivalent for slight, moderate, extensive, and complete damage state is 3.803, 7.841, 10.354, 28.137 ha/km², respectively.
12. For each building type, calculate the population per building type:

$$[\text{Population}] = [(\text{Total Population}) \times (\text{Floor Area})] \div \text{Total Floor Area}$$

13. Compute probability of being in complete with and without collapse using probability of being in complete damage state (Table J.2) and collapse rate by building type (Table J.5).

Table J.5. Collapse rate and population for each building type.

Building type	Probability of being in complete damage state	Collapse rate	Probability of being in complete with collapse	Probability of being in complete with collapse	Population
W1L	0.49	0.03	0.478	0.0148	154.57
NL	0.59	0.03	0.57	0.02	12.34
CHBL	0.71	0.15	0.60	0.11	161.46
URAL	0.58	0.15	0.49	0.09	0.40
URML	0.57	0.15	0.48	0.08	0.42
C1L	0.39	0.13	0.34	0.05	327.55
S1L	0.45	0.08	0.42	0.04	1.08
S3L	0.38	0.03	0.37	0.01	0.95
MWSL	0.71	0.15	0.60	0.11	9.16
CWSL	0.53	0.15	0.45	0.08	31.50
C1M	0.25	0.10	0.23	0.03	30.11
S1M	0.13	0.05	0.13	0.01	0.10

14. For each building type, injury severity level (Table J.6), and damage state,

$$\begin{aligned}\text{No. of people in a certain injury severity level} &= \text{Indoor casualty rate (Table J. 7 through J. 12)} \\ &\times \text{Damage probablility (Table J. 2 and Table J. 5)} \times \text{Population (Table J. 5)}\end{aligned}$$

For each severity level and building type, the number of people from all damage states is summed to obtain the total number of people in a severity level and building type (Table J.12).

For example, number of people in severity 1 for W1L is computed as follows:

154.57*(0.0005*0.054+0.0025*0.074 +0.01*0.092 +0.05*0.478 +0.4*0.0148) = 4.78

15. Add the casualty for all building types to obtain the total casualty for the polygon. For this polygon, the total casualty from severity 1 to severity 4 (corresponding to fatality) is 39.62, 12.60, 2.02, 3.96 respectively.

Table J.6. Injury classification from HAZUS methodology.

Injury severity level	Description
1	Injuries requiring basic medical aid that could be administered by paraprofessionals. These types of injuries would require bandages or observation. Some examples are: a sprain, a severe cut requiring stitches, a minor burn (first degree or second degree on a small part of the body), or a bump on the head without loss of consciousness. Injuries of lesser severity that could be self treated are not estimated by HAZUS.
2	Injuries requiring a greater degree of medical care and use of medical technology such as x-rays or surgery, but not expected to progress to a life threatening status. Some

Injury severity level	Description
	examples are third degree burns or second degree burns over large parts of the body, a bump on the head that causes loss of consciousness, fractured bone, dehydration or exposure.
3	Injuries that pose an immediate life threatening condition if not treated adequately and expeditiously. Some examples are: uncontrolled bleeding, punctured organ, other internal injuries, spinal column injuries, or crush syndrome.
4	Instantaneously killed or mortally injured

Table J.7. Indoor casualty rates by building type for slight structural damage.

Building type	Severity 1	Severity 2	Severity 3	Severity 4
W1L	0.0005	0.0000	0.0000	0.0000
NL	0.0005	0.0000	0.0000	0.0000
CHBL	0.0005	0.0000	0.0000	0.0000
URAL	0.0005	0.0000	0.0000	0.0000
URML	0.0005	0.0000	0.0000	0.0000
C1L	0.0005	0.0000	0.0000	0.0000
S1L	0.0005	0.0000	0.0000	0.0000
S3L	0.0005	0.0000	0.0000	0.0000
MWSL	0.0005	0.0000	0.0000	0.0000
CWSL	0.0005	0.0000	0.0000	0.0000
C1M	0.0005	0.0000	0.0000	0.0000
S1M	0.0005	0.0000	0.0000	0.0000

Table J.8. Indoor casualty rates by building type for moderate structural damage.

Building type	Severity 1	Severity 2	Severity 3	Severity 4
W1L	0.0025	0.0003	0.0000	0.0000
NL	0.0025	0.0003	0.0000	0.0000
CHBL	0.0035	0.0004	0.0000	0.0000
URAL	0.0035	0.0004	0.0000	0.0000
URML	0.0035	0.0004	0.0000	0.0000
C1L	0.0025	0.0003	0.0000	0.0000
S1L	0.0020	0.0003	0.0000	0.0000
S3L	0.0020	0.0003	0.0000	0.0000
MWSL	0.0035	0.0004	0.0000	0.0000
CWSL	0.0035	0.0004	0.0000	0.0000
C1M	0.0025	0.0003	0.0000	0.0000
S1M	0.0020	0.0003	0.0000	0.0000

Table J.9. Indoor casualty rates by building type for extensive structural damage.

Building type	Severity 1	Severity 2	Severity 3	Severity 4
W1L	0.0100	0.0010	0.0000	0.0000
NL	0.0100	0.0010	0.0000	0.0000
CHBL	0.0200	0.0020	0.0000	0.0000
URAL	0.0200	0.0020	0.0000	0.0000
URML	0.0200	0.0020	0.0000	0.0000
C1L	0.0100	0.0010	0.0000	0.0000
S1L	0.0100	0.0010	0.0000	0.0000
S3L	0.0100	0.0010	0.0000	0.0000
MWSL	0.0200	0.0020	0.0000	0.0000
CWSL	0.0200	0.0020	0.0000	0.0000
C1M	0.0100	0.0010	0.0000	0.0000
S1M	0.0100	0.0010	0.0000	0.0000

Table J.10. Indoor casualty rates by building type for complete structural damage without collapse.

Building type	Severity 1	Severity 2	Severity 3	Severity 4
W1L	0.0500	0.0100	0.0001	0.0001
NL	0.0500	0.0100	0.0001	0.0001
CHBL	0.1000	0.0200	0.0002	0.0002
URAL	0.1000	0.0200	0.0002	0.0002
URML	0.1000	0.0200	0.0002	0.0002
C1L	0.0500	0.0100	0.0001	0.0001
S1L	0.0500	0.0100	0.0001	0.0001
S3L	0.0500	0.0100	0.0001	0.0001
MWSL	0.1000	0.0200	0.0002	0.0002
CWSL	0.1000	0.0200	0.0002	0.0002
C1M	0.0500	0.0100	0.0001	0.0001
S1M	0.0500	0.0100	0.0001	0.0001

Table J.11. Indoor casualty rates by building type for complete structural damage without collapse

Building type	Severity 1	Severity 2	Severity 3	Severity 4
W1L	0.4000	0.2000	0.0300	0.0500
NL	0.4000	0.2000	0.0300	0.0500
CHBL	0.4000	0.2000	0.0500	0.1000
URAL	0.4000	0.2000	0.0500	0.1000
URML	0.4000	0.2000	0.0500	0.1000

Building type	Severity 1	Severity 2	Severity 3	Severity 4
C1L	0.4000	0.2000	0.0500	0.1000
S1L	0.4000	0.2000	0.0500	0.1000
S3L	0.4000	0.2000	0.0300	0.0500
MWSL	0.4000	0.2000	0.0500	0.1000
CWSL	0.4000	0.2000	0.0500	0.1000
C1M	0.4000	0.2000	0.0500	0.1000
S1M	0.4000	0.2000	0.0500	0.1000

Table J.12. Indoor casualty by building type.

Building type	Severity 1	Severity 2	Severity 3	Severity 4
W1L	4.78	1.21	0.08	0.12
NL	0.45	0.12	0.01	0.01
CHBL	16.93	5.41	0.88	1.73
URAL	0.03	0.01	0.00	0.00
URML	0.04	0.01	0.00	0.00
C1L	13.11	4.49	0.83	1.66
S1L	0.04	0.01	0.00	0.00
S3L	0.02	0.01	0.00	0.00
MWSL	0.96	0.31	0.05	0.10
CWSL	2.51	0.79	0.13	0.25
C1M	0.75	0.23	0.04	0.08
S1M	0.00	0.00	0.00	0.00
Total	39.62	12.60	2.02	3.96

This process is repeated for all building types for all polygons.

J.7 Aggregation to Barangay and Municipality/City Level

For aggregating these measures to barangays or municipalities or city level (regions), a number of methods are used.

1. In the case of building damage costs, the cost from all exposure polygons within the region is summed to obtain the aggregated damage costs.
2. For loss ratio, the total building damage cost for the region is calculated (as above), then divided by the total building value in the region. i.e.

$$\text{Loss Ratio} = \text{Total Building Damage Costs} \div \text{Total Value of Buildings in Region}$$

3. The damaged floor area equivalent is:

$$\text{Damaged Floor Area Equivalent} = [\text{Total Damage Floor Area} \times \text{Floor Area within Region}] \div \text{Total Land Area Region}$$

4. The number of injuries and fatalities from all exposure polygons within the region are summed to obtain the aggregated number of injury and fatality for the area of interest.

These aggregations are independent of the region chosen.